MASTER THESIS

The Ameland Inlet during the Sinterklaas Storm: the role of flooding of watersheds

2DH model study in Delft3D-FLOW

Li, H. (Hua Zhi)

1/5/2018

Utrecht University

Front cover:

A view on the Corner Inlet, Victoria, Australia. In this picture, every morphological component of the tidal inlet system is well displayed.
*(Source: https://www.nature.com/scitable/knowledge/library/coastal-processes-and-beaches-26276621, Andrew D. Short © **2012 Nature Education**).*

Master Graduation Research

In partial fulfillment of the requirements for the degree of Master of Science in Earth Sciences

At Utrecht University

Thesis title:	*The Ameland Inlet during the Sinterklaas Storm: the role of flooding watersheds – 2DH model in DELFT3D-FLOW*
Date:	*May, 2018*
Author:	*Huazhi Li*
Student number:	*5960193*
Email address:	*h.li6@students.uu.nl*
Supervisors:	*Dr. Maarten van der Vegt*[1] *Klaas Lenstra MSc*[1]
Institute:	*Department of Physical Geography, Faculty of Geosciences, Utrecht University*

[1] Institute for Marine and Atmospheric Research, Utrecht University, Utrecht, Netherlands

Preface

This thesis concludes part of my Master study, the Master of Science in Earth Sciences at the Department of Physical Geography, Faculty of Geosciences, Utrecht University, The Netherlands. This research has been carried out in cooperation between Arcadis and Utrecht University.

I would like first to thank my thesis supervisors: Dr. Maarten van der Vegt and Klaas Lenstra MSc. Maarten is thanked for the opportunity he provided to work on this interesting thesis topic, the direction and guidance he gave to the project, and most importantly, his expertise on the tidal inlet systems he shared during the meeting. Moreover, I am so appreciated for attending your master course, *Morphodynamics of Tidal systems*, which made me extremelly interested in to tides and also gave me a huge motivation and inspiration to choose this thesis. Klaas is thanked for providing his in-depth knowledge on Delft3D and Matlab, his tremendous patience towards my 'silly' questions and his sharp comments on my writings. Thank you for your close attention on every phase of this thesis. Besides, I would also like to thank the model provider: Dr. Nathanaël Geleynse[2]. I am grateful for your perfect model, valuable suggestions you gave me on how to quickly get close to Delft3D and guiding me to complete model set-ups step by step. Working with you three on this project was really a great pleasure.

I would like to also thank my friends at Utrecht University. Thank you, Job van Beem and Jorick van der Heijden for sharing your opinions on my thesis. Besides, I would like to give thanks to Linxi Fu, another member of my research group, for sharing her thoughts and ideas on modelling and discussing Matlab scripts.

Finally, I must express my gratitude to my parents for supporting and encouraging me unfailingly and continuously during my broad study and thesis time.

[2] ARCADIS, Water and Environment Division, Zwolle, Netherlands

Abstract

A tidal inlet connects the back-barrier basin with the sea and is maintained by tidal currents. Inlet systems have great values for the local ecosystem, economy and community. In recent times, as a result of natural and anthropogenic impacts such as relative sea level rise and the construction of coastal protection measures, there has been an increasing shortage of sediments in the Dutch Wadden Sea. This master thesis focuses on the Ameland inlet. Classically, this system has been treated as being isolated. However, tidal watersheds are flooded during storms which facilitates exchange of water and sediment with the adjacent basins. This will affect the short-term water and sediment balance of the system.

The objective of this research is to study effects of flooding of watersheds and NW wind on the residual flow and sediment transport patterns in the tidal inlet system. This is done by employing 2DH process-based models in DELFT3D-FLOW to simulate the hydrodynamics and sediment transport at Ameland inlet during the Sinterklaas Storm (2013).

Results show that in the basin, flooding of watersheds has four main effects. Firstly, during surge rising, water enters into the system mainly over west watershed (99%) and via inlet (only 1%), and leaves entirely over east watershed. Secondly, during surge falling, water enters into the basin only over the west watershed and leaves via inlet (54%) and over the east watershed (46%). Thirdly, 90% of the total sediment import takes place via inlet with the rest over the west watersheds while all sediment is exported over the east watersheds. Lastly, around 4.8% more sediment (518 m^3) is imported owning to the connectivity of basins. Compared to flooding of watersheds, the NW wind is less significant in the basin. It inverts the direction of mean flows in the main channel (the Borndiep) and strengthens residual flows in the secondary channel (the Westgat). Moreover, it causes around 43% more sediment (3,100 m^3) imported into the basin.

There are l main effects of a passing storm, namely: 1) results in increased flood dominance 2) leading to a factor of 4 more sediment import compared to a natural storm.

Keywords: **Tidal inlet system, Ameland Inlet, Delft3D, Flooding watersheds, Winds, Sinterklaas Storm**

Table of Contents

1 Introduction

1.1 Background

The sea level rise during the Holocene caused the flooding of original dry continental shelves, leading to a complex pattern of sediment replacement. This reworking resulted in sediment accretion at topographic lows and erosion at high elevated areas, which finally contributed to the formation of sandy barrier islands (De Swart & Zimmerman, 2009). Around 15% of today's coastlines are owning to the relicts of the process of barrier coast formation (Beets & van der Spek, 2000; Woodroffe, 2003). Normally, these coasts are comprised of several offshore islands divided by tidal inlets which function as the connection between the ocean and the bay (Hayes, 1979; De Swart & Zimmerman, 2009). Tidal currents and wind waves are two major drivers with respect to the process of barrier coast and inlet formation while the barrier breaching and new inlet formation may be determined by storm surges (De Swart & Zimmerman, 2009). In principal, tides and waves dominate the orientation and amplitude of sediment transport, afterwards causing deposition and erosion occurring in different areas, which finally results in the system morphological changes. In the meanwhile, the system morphology also gives feedbacks on wave- and tidal-induced currents, and therefore modifies the process of sediment transport.

A typical barrier-inlet system features two barrier islands, an inlet with deep channels between two barriers and a back-barrier basin with channels and intertidal flats. At the seaward side, an ebb-tidal delta is found with a main ebb channel flanked by linear bars. At its seaward edge, a terminal sand lobe is located, indicating the transition from the shoal to the sea. The flood-tidal delta (shoal at the landward side) features bifurcating flood channels (Hayes, 1980).

Tidal inlet systems are important for the local ecosystem, economy and community. Most of them are rich in tidal flats which provide extensive and comfortable habitats for the local diverse flora and fauna (Dissanayake et al., 2012). Keeping this biodiversity is important for local economic development and therefore stimulates the population growth.

1.2 Problem description

Tidal inlet sediment dynamics are of great importance for barrier islands and back-barrier basins (Hayes, 1980). Field studies of Moslow & Heron (1978) and Hayes (1979) revealed that around one-third to two-thirds of sediments deposited in barrier islands come from the inlet throat. Besides, tidal inlet sediments are also transported and deposited in different areas, forming depositional sand units including shoals, swash bars, tidal flats and tidal deltas. At the seaward side, an ebb tidal delta forms due to waves and ebb-tidal currents, while a flood tidal delta is found at the landward side owning to flood currents. As an important morphological component of an inlet system, the ebb-tidal delta plays two important roles. The first one, filter function, is dissipating wave energy by increased bottom friction and wave breaking. Secondly, a large amount of sediment is stored at the ebb-tidal delta which can act as a temporary source of sediment for the barrier islands (feeder).

However, in recent times, natural and anthropogenic impacts such sea level rise, increasing population density, land subsidence and the construction of various coastal protecting structures (i.e. jetties, dykes and groins) have disturbed the natural dynamics of tidal inlet

systems (Elias et al., 2012). Typical examples are tidal inlet systems in the Dutch Wadden Sea. Relative sea level rise due to global warming has expanded the accommodation space, thus leading to an increasing amount of landward sediment transport (Elias et al., 2012). As a result, the Dutch Wadden Sea system calls for more sediment input. In principal, this increasing sediment demanding is satisfied by eroding the ebb-tidal delta and adjacent coasts of barrier islands. However, due to the implementation of coastal protection measures (e.g. alongshore dams, stone revetments and nourishments), barrier islands of Dutch Wadden Sea are kept in relatively fixed positions. Hence, ebb tidal deltas become the alternatively main provider for the increasing amount of sediment. Another consequence of the sea level rise is that it reduces the area of tidal flats which are valuable for local ecology and economy. Therefore, coastal management authorities are considering nourishments on ebb-tidal deltas. The question is whether these kinds of solutions are sustainable and whether this would result in an increased sediment transport into the basin. For this we need a better understanding of the sediment transport patterns in tidal inlet systems.

Classically, tidal inlet systems are regarded as being isolated, no interaction with other basins (De Forcket, 2008; Dissanayake et al., 2009; Jiao, 2014; Pluis, 2016). This means exchange of water and sediment only takes place via the inlet. However, Duran-Matute et al. (2014) quantified the residual tidal prisms via each inlet and over Terschelling watershed in Dutch Wadden Sea system. They found a net inflow occurring over the watershed, indicating that water exchange can also take place over the watersheds. Moreover, observations found that during storms, watersheds are flooded, facilitating water exchange locally. Although a lot of work and studies have been done on the hydrodynamics and morphodynamics of the tidal inlet system, the influence of flooding of watersheds on the water and sediment balance of tidal basins is new and has not been examined yet. Duran-Matute et al. (2014) only quantified the water balance but did not consider the sediment budget. However, whether sediment exchange will also take place with connected basins still remains questionable. Associated with storms, winds also have a big impact on the flow and sediment transport patterns. Effects of wind shear stress on them are well understood from previous studies (e.g. Duran-Matute et al., 2014; Herrling & Winter, 2014). However, effects of wind-induced surge changes on the flow and sediment transport patterns in the tidal inlet system have not been figured out.

1.3 Objectives

The objectives of this master thesis are to study the effects of flooding of watersheds and winds on the residual flow and sediment transport patterns in the Ameland inlet system during storms. In this research, answers to these objectives are presented based on results of 2DH models with varying boundary conditions and forcing types in DELFT3D-FLOW.

1.4 Reader guide

This thesis is structured as follows. The literature study (Chapter 2) summarizes the hydrodynamic and morphodynamic backgrounds of previous works starting from the large scale, Dutch Wadden Sea system, then to the Ameland Inlet system. The main research question with several specific sub-questions is formulated in Chapter 3. In next chapter, methods and materials are elaborated. Results of the patterns of flow and sediment transport are presented in Chapter 5 while comparisons with relevant papers are discussed in Chapter 6. Finally, main findings are concluded in Chapter 7.

2 Literature overview

2.1 Study area

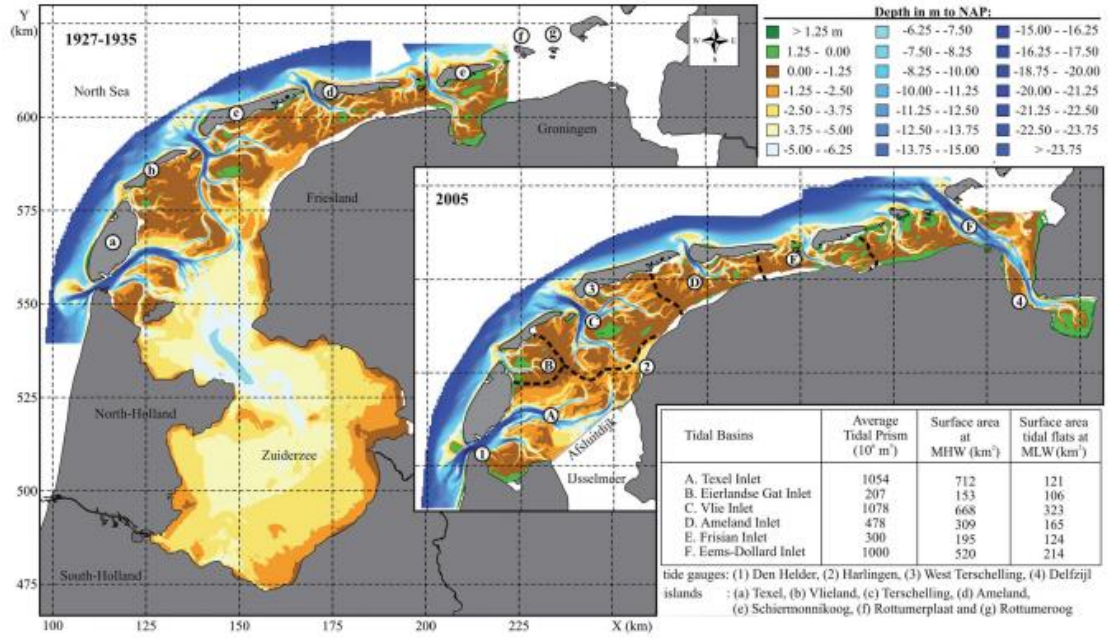

Figure 2.1 Representative maps displaying the configuration of the Dutch Wadden Sea from 1927 to 1935 (large figure) and 2005 (lower right). (Source: Elias et al., 2012)

From the Texel inlet in the west, the Dutch Wadden Sea extends to the Ems-Dollard estuary stretching northwardly with a distance of 135 km to the North Sea (Elias et al., 2012; Vroom & Wang, 2012). It consists of five barrier islands with a watershed behind each of them and a series of tidal basins separated by these watersheds (Oost et al., 2012). The configuration of the Dutch Wadden Sea system is shown in Figure 2.1 with black dashed lines marking the location of watersheds. Tidal watersheds are located at most high-elevated areas and are regarded as the separation of water flowing to channels and basins of different barrier systems (De Swart & Zimmerman, 2009). The western (Texel inlet, Vile inlet and Eierlandse Gat inlet) and eastern tidal inlet systems (Ameland inlet, Frisian inlet and Ems-Dollard estuary) differ in geometry. The first distinction lies in the orientation with regard to south-north for the western tidal inlet systems and to west-east for eastern ones (Elias et al., 2012). Secondly, in terms of back-barrier basins, those in the east are narrower and shallower featuring larger intertidal areas but smaller channels than those in the west (Elias et al., 2012).

The Ameland Inlet, located between two barrier islands of Terschelling in the west and Ameland in the east, provides for the exchange of water and sediment between Ameland basin and North Sea. Figure 1.2 indicates the topography of Ameland inlet system, which displays the most natural behaviors among the inlets of the Dutch Wadden Sea system. In Ameland system, there exist two deep channels at the ebb-tidal delta, Westgat and Akkepollengat, with north-western and northern directions, respectively. Akkepollengat, also regarded as the main ebb channel, features a swash bar (Bornrif) to its east and stretches into the basin connecting with the ebb channel, Borndiep. Similarly, the flood channel Westgat concatenates the basin channel Boschgat. Afterwards, these channels bifurcate into small and relatively shallow branches, making up part of the Wadden Sea, exhibiting a

drainage pattern. At the either edge of Ameland back-barrier basin, it features high-elevated tidal watersheds (marked in black dashed lines in Figure 2.1) which block water flowing into other adjacent basins. The western watershed (Terschelling watershed) is around twice the length of the eastern one (Ameland watershed). Besides, massive tidal flats and salt marshes are found around the borders of the basin (named Terschelling flat and Borndiep flat in Figure 2.2).

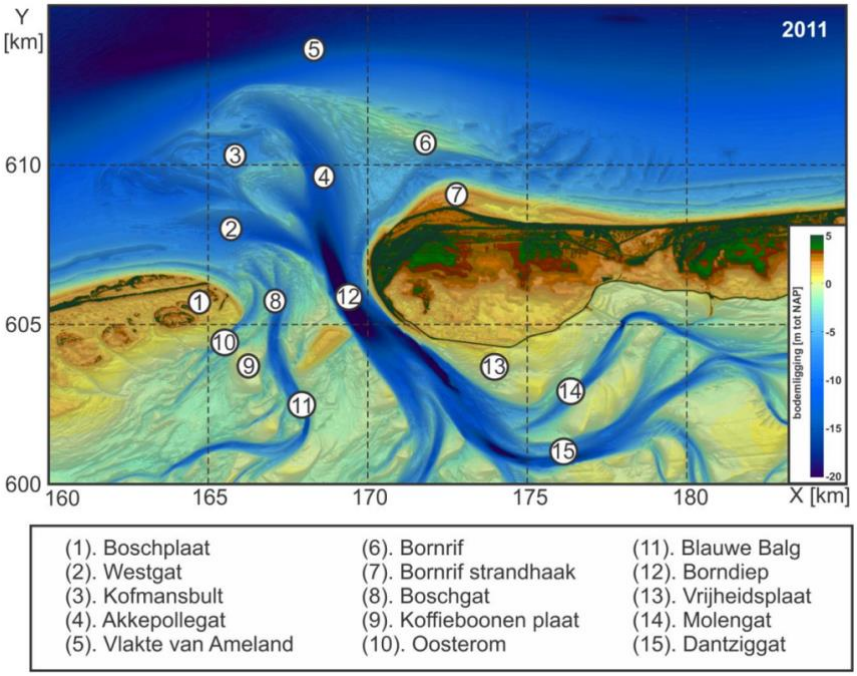

Figure 2.2 2011 topography of the Ameland Inlet system. (Source: Deltares, 2014)

2.2 Tidal inlet system

2.2.1 Morphological components

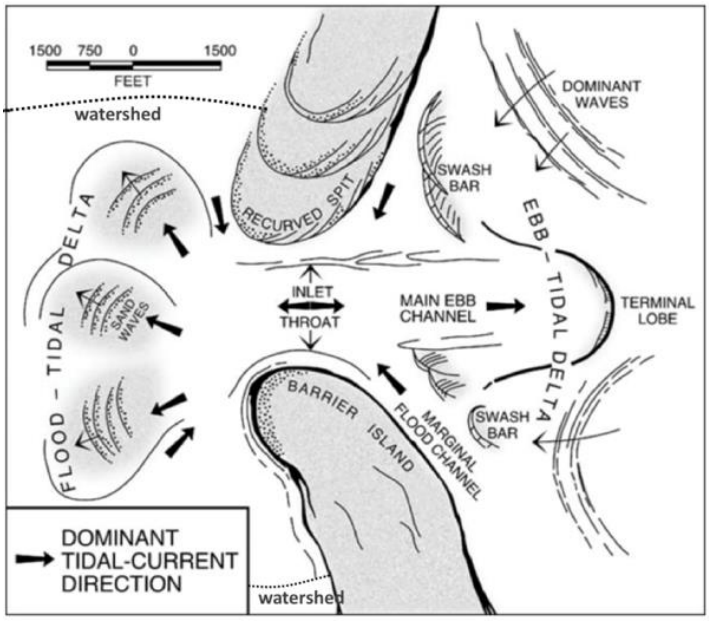

Figure 2.3 Morphological components of a typical tidal inlet system. (Source: Hayes & FitzGerald, 2013)

Figure 2.3 indicates main morphological units of a typical tidal inlet. It features a back-barrier basin with channels, an inlet maintained by tidal currents, an ebb-tidal delta and a flood-tidal delta (Hayes, 1975). There is a main ebb channel in which ebb currents are dominant, flowing seawardly through the inlet, flanked by swash bars at both sides and sometimes separated by flood channels at the margin (Hayes, 1980). Seaward end of the ebb channel, an ebb-tidal delta is found. At its front edge, the terminal lobe is located, indicating the steep transition from shoals to continental shelf (De Swart & Zimmerman, 2009). At the landside, a flood-tidal delta with bifurcating flood channels where flood flows and flood directed sand waves are dominant can be observed (Hayes, 1980).

2.2.2 Classification

It is well-accepted that waves and tides determine the morphodynamics of tidal inlets, and the different contributions of these two factors feature different morphological characteristics of tidal inlets (Hayes, 1979). Many works have been done to develop empirical and conceptual theories related to the classification of tidal inlet morphology (e.g. O'Brien, 1969; Jarrett, 1976; Hayes, 1979). The classification of Hayes (1979), which is the most widely used, relates inlet morphology to mean tidal range and mean wave height (see Figure 2.4). In this classification, three types of inlet systems are defined, namely wave dominated, tide dominated and mixed energy. Wave dominated inlets with micro tidal ranges (smaller than 2 m proposed by Davies [1964]) feature small ebb-tidal deltas (Hayes, 1980; Carr-Betts et al., 2012). These ebb-tidal deltas are expected to exhibit bypassing bars in the arcuate shape and a shoal at the offshore edge of the delta (Kraus, 2000). In tide dominated systems with tidal range between 2 m and 4 m, ebb-tidal deltas are well-developed featuring deep ebb channels. Often, there are two shore-normal parallel bars at channel margins of ebb-tidal deltas in tide dominated systems, while those of mixed energy inlets feature a linear bar at the updrift channel, a flood channel at the updrift part of the delta and a sand unit along the down-drift side.

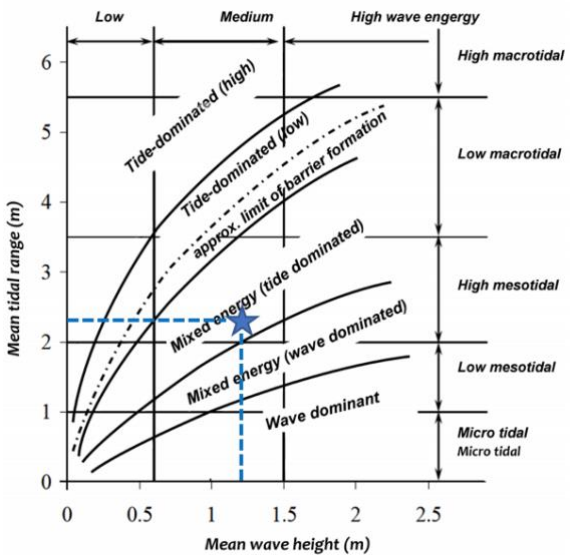

Figure 2.4 The Hayes (1979) classification of tidal inlet morphology by mean tidal range and mean wave height illustrating three major regimes: tide-dominated, mixed energy and wave dominant. The Ameland inlet is regarded as the type of mixed energy, marked by the blue star. (Source: redrawn from Hayes [1979])

The mean tidal range of the Ameland Inlet is approximately 2.15 m (based on the value of 2.4 m at Nes station) while the mean wave height is between 1.2m and 1.4 m. The Ameland inlet is thus a mixed energy system with tides being slightly more dominant according to the Hayes classification (1979).

In the following inlet morphology classification studies, more factors have been taken into consideration. Hayes (1980) stated that the tidal asymmetry, the size of back-barrier basin and tidal prism also determine the inlet morphology to a considerable extent. Besides, Sha (1989) and Sha & Van den Berg (1993) related the tidal prism to the area of the inlet cross-section (the PA relationship) by employing a process-based model. They suggested that the smallest cross-section area is dependent on the tidal prism. However, the cross-sections remain in almost constant conditions if there are no oblique waves approaching and breaking near the shore (Dissanayake et al., 2009). Moreover, Nahon et al. (2012) found that the theory of classical Hayes (1979) classification is too simple as it only considers two factors. Nevertheless, the results of Nahon et al. (2012) still posed a high agreement with the empirical theories, but other parameters i.e. grain size, wave forcing and geometry of lagoon and channel also affect the inlet morphology.

2.3 Dynamics and characteristics of tidal inlet systems

2.3.1 Hydrodynamic and sediment transport

Waves and tides are two dominant agents regarding to tidal inlet morphology (Hayes, 1980). The contribution of these two factors varies spatially. Seaward of the inlet, both are important (De Swart & Zimmerman, 2009). Shore-oblique waves drive longshore currents as they approach the shore and break afterwards. Together with tidal driven currents, they result in longshore sediment transport (represented as littoral drift in Figure 2.5). Part of the long-shore drift bypasses the ebb-tidal delta and attaches to the head of the downdrift barrier island by waves. The rest is transported to the inlet, causing local deposition. Then the inlet sediment is either imported into the basin by tidal flood currents or transported in the offshore direction to sustain the ebb-tidal delta and exported out to the next islands by ebb currents. In basin channels, tides are dominant and governing the sediment compared to waves.

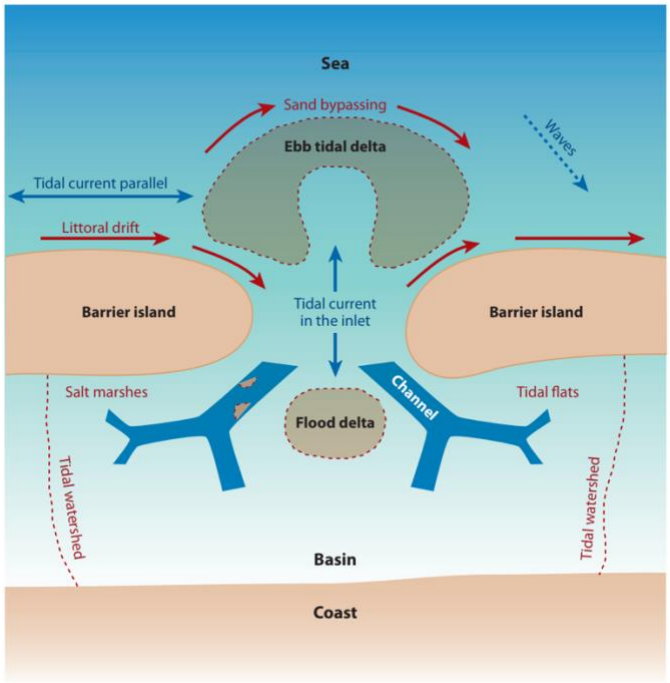

Figure 2.5 The generalized model of a barrier island system illustrating morphological features (not complete) and water motions. (Source: De Swart & Zimmerman, 2009)

In the Ameland inlet system, the semi-diurnal tides dominate and propagate from west to east (Duran-Matute et al., 2014) while waves approach to the shore in the dominant direction of northwest (Dissanayake et al., 2009). Tidal currents are responsible for sediment exchange inside the system among the basin, the two barrier islands and the ebb-tidal delta.

2.3.2 The sediment bypassing processes

Sediment bypassing process is of great importance on the morphological behaviors of not only barrier islands, but ebb-tidal deltas (Cheung et al., 2007). According to most studies, the bypassing mechanism is related to the type of the tidal inlet system. Bruun and Gerritsen (1959) proposed two main types of sediment bypassing. The first one is called bar bypassing which describes the wave-driven sand transport from the updrift island directly to the downdrift island, bypassing the ebb-tidal delta. This bypassing can be observed at wave-dominated barrier systems. The second bypassing, the tidal bypassing, describes sediment transport in channels as a result of tidal currents. This bypassing is more applicable in tide-dominated environments. Besides, FitzGerald (1982) found that the littoral drift causes sediment attachment directly from the ebb-tidal delta to the head of the downdrift barrier at mixed energy environments with slightly tide-dominated. Furthermore, FitzGerald et al. (2000) summarized that sand bypassing mechanisms are also dependent on inlet geometry, tidal prism, sediment balance, regional stratigraphy, the nearshore slope and the engineering works (more influencing recently). These sediment bypassing processes afterwards result in a cyclic behavior of ebb-tidal deltas.

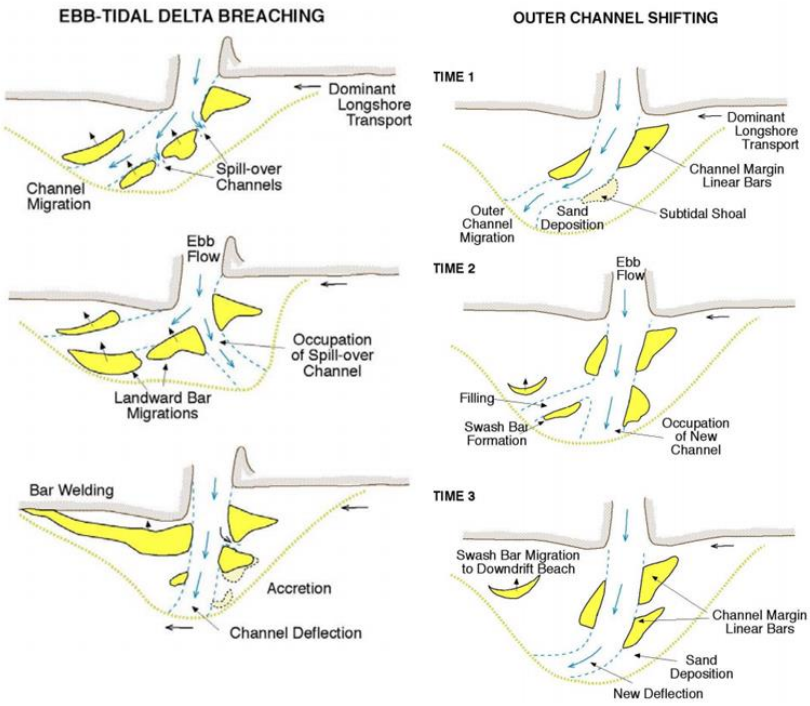

Figure 2.6 The schematic descriptions illustrating the processes of *ebb-tidal delta breaching* and *outer channel shifting* sand-bypassing mechanisms. (Source: Fitzgerald et al., 2000)

Recently, many works have focused on sand bypassing processes at the Dutch Wadden Sea inlets. Israël (1998) found that the Ameland inlet experiences cyclic morphological evolution featuring periodic channel migration and sediment supply fluctuation in an intermediate timescale of about 50 to 60 years. FitzGerald et al. (2000) specified six sand

bypassing models of natural barriers and three of jettied inlets. According to Israël and Dunsbergen (1999), the Ameland system characterizes *outer channel shifting* and *ebb-tidal delta breaching*, in terms of sediment bypassing mechanisms (schematic descriptions can be seen in Figure 2.4). The Ameland case is in between of these two mechanisms but closer to the breaching model as it features a large volume of sand in shoals, long period between shoals, and periodic channel dynamics close to inlet. In these processes, it is preferable for sediment driven by littoral drift to accumulate at the head of the ebb-tidal delta, leading to the deflected migration of the downdrift part of the main ebb channel, which therefore causes erosion at adjacent beaches. Since the flow generated by the deflected channel is insufficient, a new pathway forms allowing ebb discharges flowing seaward through the ebb-tidal delta. Gradually, the new channel conveys the majority of tidal prisms. As a result, the old channel is abandoned because part of sediment is deposited here due to both wave and tidal driven currents. The rest is remained at near areas forming bar complex, moving landward, and finally attaching to the beach. The Ameland system exhibits that the main ebb channel evolves with orientation shifting to right and bar complex e.g. swash bars forms and migrates to the updrift side of the island of Ameland.

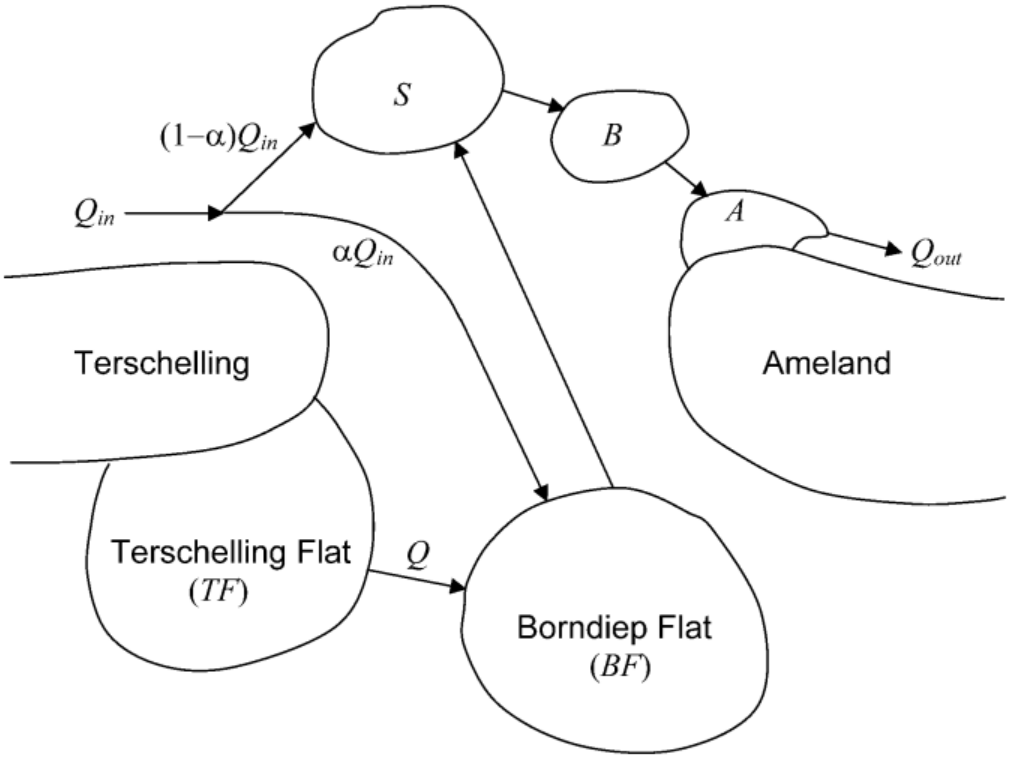

Figure 2.7 Schematic bypassing mechanisms at Ameland Inlet in the model of Cheung et al. (2007).

Cheung et al. (2007) employed an adapted model from the reservoir model of Kraus (2000) for the sake of bypassing process simulation at the intermediate timescale, like the Ameland case. It describes two pathways for the littoral sediment (Q_{in} in Figure 2.7) at the downdrift side of the island of Terschelling: (1) attaching to the outer edge of the shoal (*S*); (2) transported into the back-barrier basin (Borndiep Flat in this case) through the inlet by tidal flows. The results of Cheung et al. (2007) indicated that most sediment bypassing occurs through the second pathway, the tidal bypassing. The sediment of the shore is then transported, forming the swash bar (*B*) called Bornrif which migrates landward, and eventually attaches to the updrift side of the Ameland island in the form of an attenuating sandwave (*A*). Still, there is some sediment transported out (Q_{out}) the Ameland system. Cheung et al. (2007) estimated that around 85% to 90% of shore sediment is deposited at

the sandwave leading to the development of the Ameland island while the rest is exported out to the next tidal systems.

More recent studies found the importance of the formation of the spill-over channel at the ebb-tidal delta, where waves dominate the sediment bypassing (FitzGerald, 1988; Nahon et al., 2012; Pluis, 2016). A spill-over channel forms due to the deposition (a shoal forms) at the downdrift part of the main ebb channel by waves (Nahon et al., 2012). Then, the shoal moves landward under wave actions. This implies that waves strongly affect the attachment of these morphologic units, in accordance with FitzGerald (1982) and Sha (1990). Although Nahon et al. (2012) successfully modelled formation and movements of shoals, the underlying mechanisms were not discussed. Besides, in their models the ebb-tidal delta breaching occurred much quicker (around 18 weeks) while it takes around 50 to 60 years in the Ameland case. One of possible reasons suggested by Ridderinkhof et al. (2016) is that the tidal prism determines the duration between consecutive attachments of shoals to the next islands, which is an indicator of the period of this cyclic behavior. In general, a tidal inlet system with a larger tidal prism features a longer periodical evolution. Besides, the period of multi-channel systems is shorter than systems with a single channel.

According to Ranasinghe & Pattiaratchi (2003), the wave asymmetry is the main mechanism for shoal migration, leading to then the closure of the inlet. However, Bertin et al. (2009a) raised a different opinion. They stated that the imbalance pressure gradients and the onshore component of the wave radiation stress is the underlying cause. Ridderinkhof et al. (2016) employed a coupled model of Delft3D and SWAN to examine which physical mechanism is right. They concluded that although asymmetric waves do make some contributions, the growth and movement of shoals are resulted from the convergence of sediment transport toward the shoal. Thus, the process is dependent on the competence between the wave conditions and the morphology of the ebb-tidal delta which leads to the convergence or divergence of sediment transport. Especially during storms, this imbalance occurs since the energy of wave dissipation at shallow regions near the shore of the ebb-tidal delta is over the local bathymetry, which therefore causes landward residual currents due to gradients in radiation stresses. Thus, it leads to landward sediment transport which eventually results in the formation and migration of shoals. Nevertheless, Herrling & Winter (2014) found that the sediment also bypasses without forming coherent sand structures.

2.3.3 The cyclic behavior

The cyclic behavior of Ameland inlet is generally divided into four phases, shown in Figure 2.8. An inherent feature of the periodic evolution is the transition from a one-channel system to a two-channel system and back (Israël and Dunsbergen, 1999).

2.3.3.1 1st: the starting phase (one-channel system)

The first phase of the morphological cycle is defined as one-channel system in the inlet. This corresponds to the situations in 1903 and 1959. The ebb channel Borndiep, is connected with the western ebb channel Westgat, resulting in maximum discharge through Westgat. In the west of the basin, south of the island of Terschelling, the channel Boschgat which fills and drains this area directly discharges to Borndiep. The Boschgat migrates seaward across the tidal flat, Terschelling flat, and gradually connects to the sea due to the phase lag between tidal currents in the Boschgat and the Borndiep. The littoral sediment is deposited downdrift of Akkepollegat forming a shoal, and bypasses the inlet leading to the formation of

the swash bar to the east of the Akkepollegat and north of the Ameland barrier. The bar complex which is known as Bornrif undergoes landward migration.

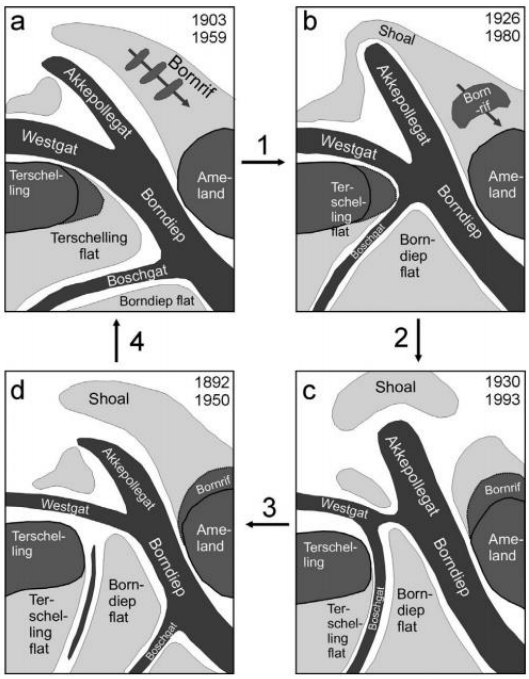

Figure 2.8 Schematic sketch illustrating four stages of the morphological cycle of the Ameland system: (a) One-channel system (b) Transition phase from one-channel to two-channel system (c) Two-channel system (d) Transition to the original state. (Source: Cheung et al., 2007)

2.3.3.2 2nd: the transition phase (from one-channel to two channel)

The configuration of the inlet in 1926 and 1980 illustrates that the Ameland inlet system is developing and transiting to two-channel system. As Boschgat moves in the northern direction connecting to the Westgat, the Borndiep Flat increases in areas. It indicates the beginning of the two-channel system at the inlet. Therefore, increasing amounts of water and sediment from the Borndiep are directed and transported through the Akkepollegat to the shoal. Due to the increase of incoming sediment at the shoal, the bar complex Bornrif develops and migrates to the updrift side of the Ameland barrier.

2.3.3.3 3rd: two-channel system (1930 and 1993)

In Figure 2.8c, it can be observed that a shortcut forms leading to the direct connection between the Boschgat and the Westgat. Therefore, discharges of the Akkepollegat come from the Borndiep. The Westgat becomes flood dominant as a result of the reduction of ebb flow from the Borndiep. This results in the offshore migration of the Borndiep flat and the landward migration of a part of the shoal, which subsequently leads to the eastward migration of the Borndiep and therefore erosion at the updift Ameland. At the same time, the bar complex combined with a part of the shoal attaches to the Ameland island.

2.3.3.4 4th: transition phase (from two-channel to original state)

In 1892 and 1950, the system is characterized by a breakthrough of the Borndiep resulting from phase lags of tidal currents between Westgat-Boschgat and Akkepollegat-Borndiep channel systems. This reduces the flow to the Akkepollegat but strengthens the flow to the Westgat. Thereby the sediment is transported and deposited at the transistion between the Boschgat and the Westgat, causing the gradual abandonment of the previous Boschgat

channel. Alternatively, there is a new Boschgat channel forming south of Terschelling, discharging into the Borndiep.

Table 2.1 Duration of each phase in 1892 and 1950 cyclic cycles.

Case	Phase 1	Phase 2	Phase 3	Phase 4	Period of one total cycle
1892	23 years	4 years	20 years	11 years	58 years
1950	21 years	13 years	15 years	9 years	58 years

2.4 Patterns of flow and sediment transport in the Dutch Wadden Sea

2.4.1 Residual circulation

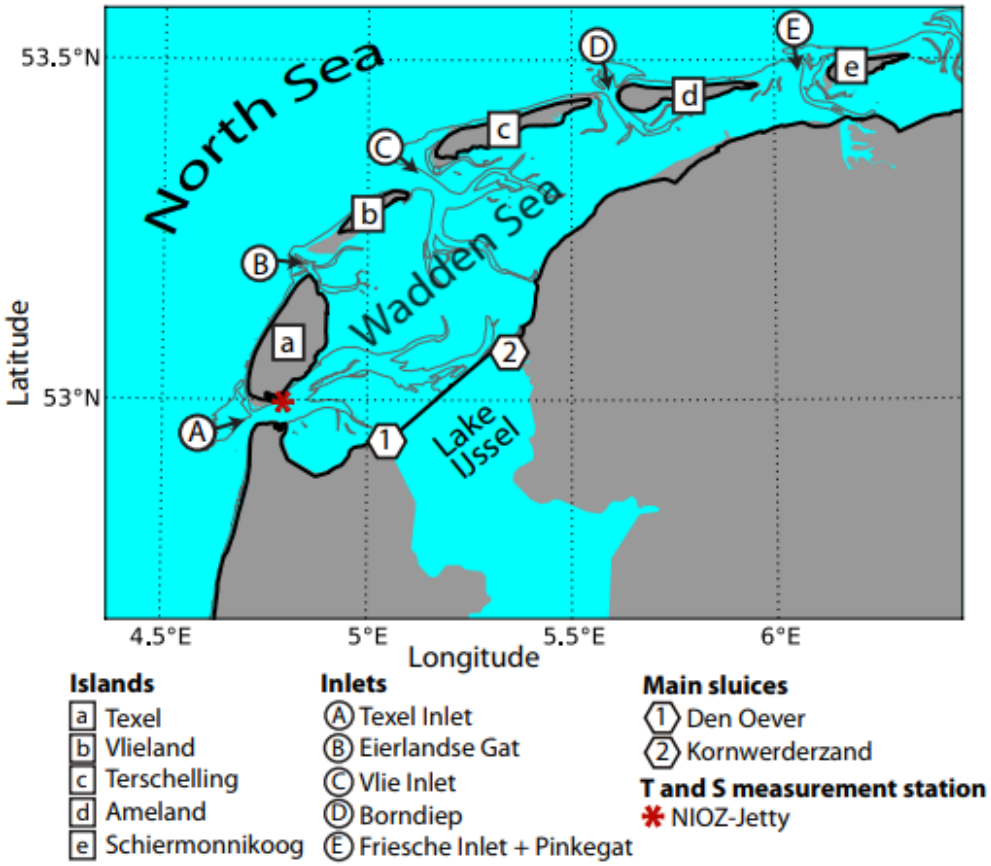

Figure 2.9 The map of the Dutch Wadden Sea system which marks important morphological units. (Source: Duran-Matute et al., 2014)

Residual circulation in the Dutch Wadden Sea has grabbed many researchers' intersets since 1970s. Figure 2.9 shows the distribution and location of tidal inlets, barriers, basins and main sluices of the Dutch Wadden Sea system. It has been investigated through numerical simulations as well as measurements. Ridderinkhof (1988a) employed a depth averaged numerical model to simulate water motions on the study area from the Texel Inlet to the Ameland watershed, only considering tides. Based on the model results, Ridderinkhof (1988a) concluded that the residual flow entered into the system through the Vlie Inlet with the discharge of 1145 m^3/s and left through the Texel Inlet (820 m^3/s), the Eierlandse Gat (250 m^3/s) and the Terschelling watershed (55 m^3/s). More recently, Buijsman & Ridderinkhof (2007) emphasized the importance of winds which can result in a large fluctuation of the magnitude and the alteration of the direction of residual transport. According to the

campaigns carried out by Dutch government Rijkswaterstaat in 2012 which measured net imports through two 13-hour transects at the Vlie Inlet, it exhibited an average inflow of 1300 m^3/s and 3900 m^3/s during two tidal cycles (Gerkema et al., 2014). The difference is explained by the variability of the local wind stresses which strongly supports the conclusion of Buijsman & Ridderinkhof (2007). This suggests that net exchange of water, but probably also sediment, strongly depends on the wind and the surge.

Duran-Matute et al. (2014) employed a 3D numerical model based on GETM (the General Estuarine Transport Model) to quantify the residual circulation in the Dutch Wadden Sea, considering tides, winds, fresh water discharges and meteorological forcing. They defined cross-sections at all inlets as well as the Terschelling watershed and then computed the mean tidal prism (the averaged value of tidal prisms for all tidal periods from 2009 to 2010). They differentiated the ebb and flood residual prisms where *flood* refer to the import into the system while *ebb* means the export. The outcome is shown in Figure 2.10.

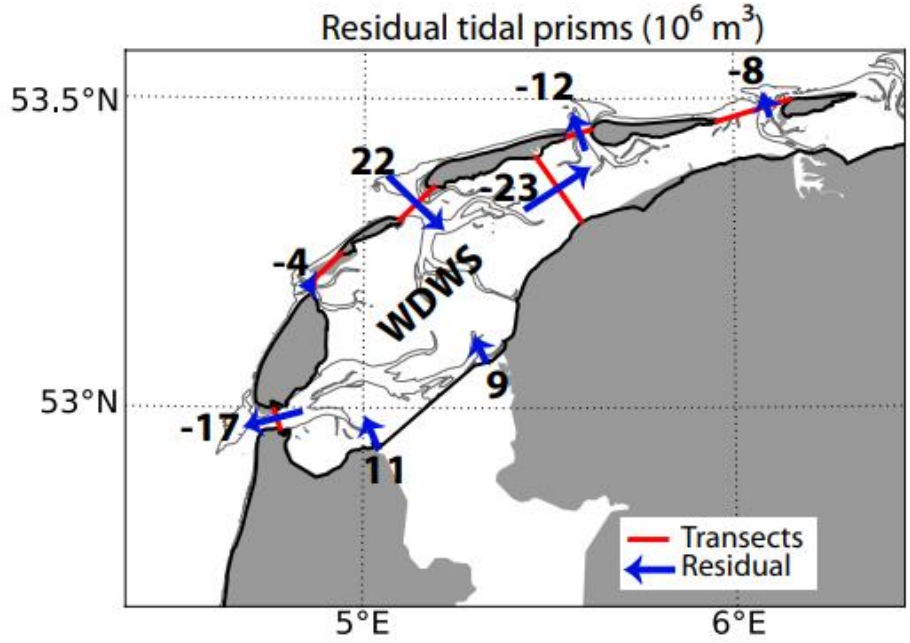

Figure 2.10 Average residual tidal prisms (calculated by flood - ebb) of the Dutch Wadden Sea system. The numbers (in Mm^3) and the length of blue arrows represent the magnitude of the residual tidal prism. The positive value means the import into the system. Transects of inlets and the Terschelling watershed are marked in red. (Source: Duran-Matute et al., 2014)

Duran-Matute et al. (2014) also calculated standard deviations for all transects to roughly show their variabilities. It was found that the standard deviation of Terschelling watershed is around 200% which is 10 times as those of inlets (in the order of 20%). Either the spring-neap cycle or wind effects can be reasons for the large variability of Terschelling watershed. After that, they listed the time-series residual discharges in year 2009 and 2010 at areas with significant flow exchange (the Texel Inlet, the Vlie Inlet and the Terschelling watershed). It was indicated that the residual flow entered into the system through the Vlie Inlet while left through the Texel Inlet with much smaller exchanges happening at the watershed at most of the time (shown in Fiugre 2.11 and 2.12), showing a high agreement with the results of Ridderinkhof (1988). However, some exceptions can be seen that the reverse situation happens (inflow through Texel while outflow through Vlie). They found that southwestern winds exceeding 15 m/s cause the inversion of the residual flow direction. This results in the negative volumetric flow rate at the Vlie inlet and Terschelling watershed. As a result, the wind speed and direction are the key factors on the residual flow patterns in the tidal inlet systems.

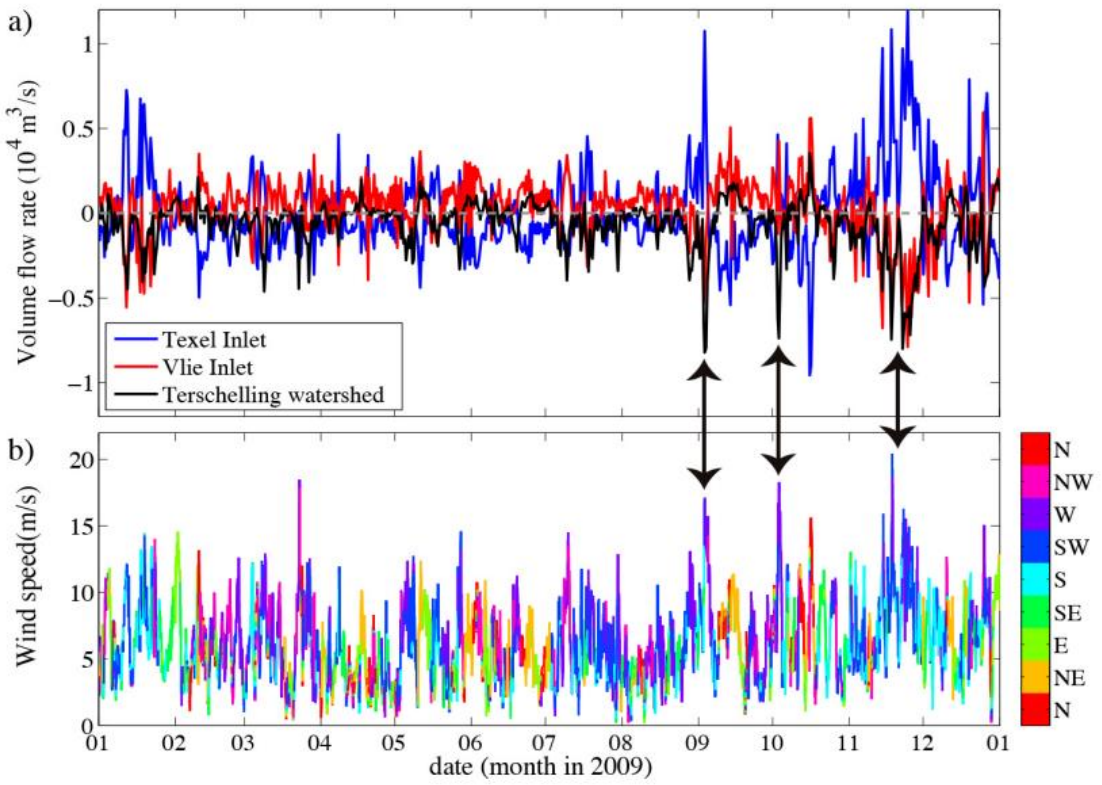

Figure 2.11 (a) Time-series residual discharge in the Texel Inlet, Vlie Inlet and Terschelling watershed in 2009 where positive means an inflow while the outflow is indicated by negative values. (b) Corresponding wind profile. The different wind directions are shown in different colour in correspondence with the colour bar on the right. The black arrows point out that the residual circulation is inverted and the corresponding wind events. (Source: Duran-Matute et al., 2014)

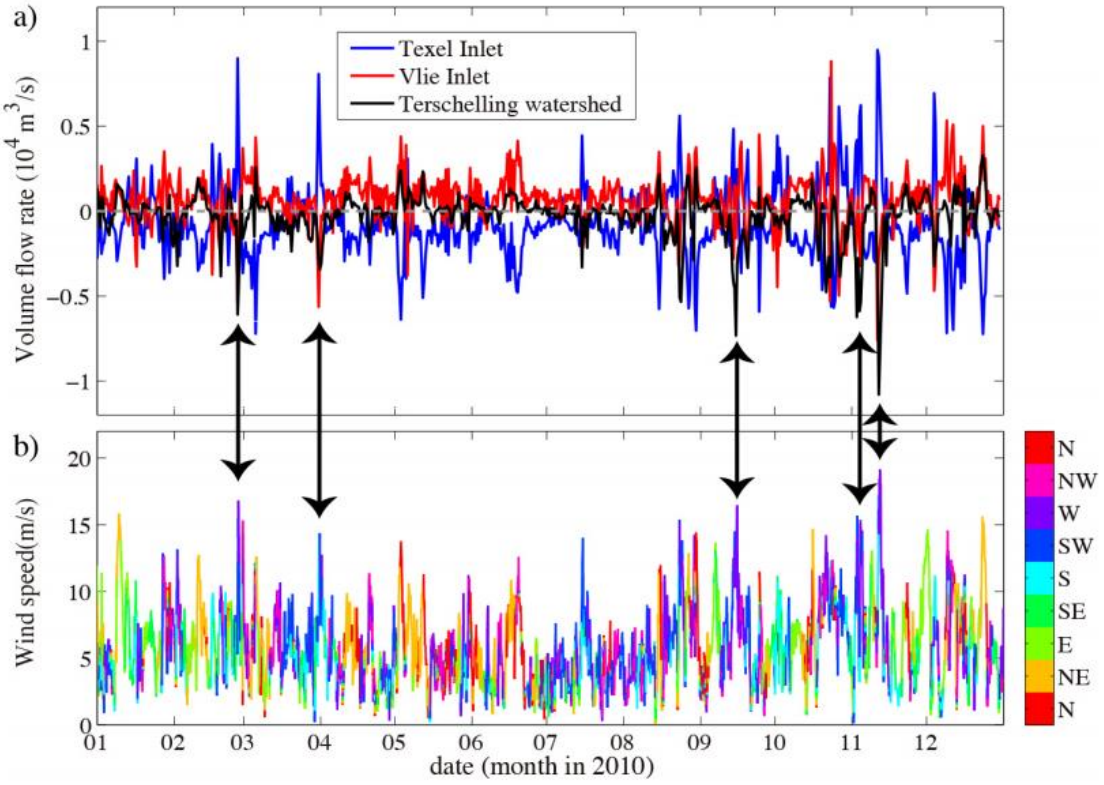

Figure 2.12 The same cases as Figure 2.12 but in year 2010. (Source: Duran-Matute et al., 2014)

With further studies, Duran-Matute et al. (2014) summarized three major effects of winds on the residual circulation in accordance with Li (2013): (1) wind-driven net flows are much larger than the tidal driven ones in terms of magnitude (2) the mean flows in the middle inlet are normally the weakest (3) wind can significantly invert the direction of residual flows where generally in the upwind inlet an inflow is found while the outflow can be observed in the downwind inlet.

Furthermore, Pluis (2016) investigated effects of tides, waves and the interaction of these two on the residual flow pattern in the Ameland inlet system during calm weathers (moderate waves) and storms. Figure 2.13 shows patterns of north-western wave driven residual flow under quiet and storm environments. It can be seen that at all conditions, waves generate (1) long-shore currents along the coasts of the island of Terschelling and Ameland (2) pronounced currents flowing over the ebb-tidal delta which are stronger at the shoal but relatively weak in the channels (3) a residual circulation in the north-western part of the ebb-tidal delta. Likewise, storms are considered to strengthen wave driven currents as they are 5 to 10 times larger during storms than those in the quite environments. In contrast, unlike wave conditions tidal driven currents are confined to the channels, see Figure 2.14. Flood currents can be observed in flood-dominant channel Westgat. The ebb flow diverges over the shoal at the downdrift part of the main ebb channel Akkepollengat. As a result, two gyres can be observed with one at the western part of the ebb-tidal delta and another at the eastern part of the inlet. Pluis (2016) also mentioned that the relative contribution of tides and waves on the residual flow differs under different conditions. During calm weathers, tides prevail over waves while storms enlarge the effects of waves especially enhancing wave driven flows in the flood channel, and thus waves are dominant in governing residual current patterns.

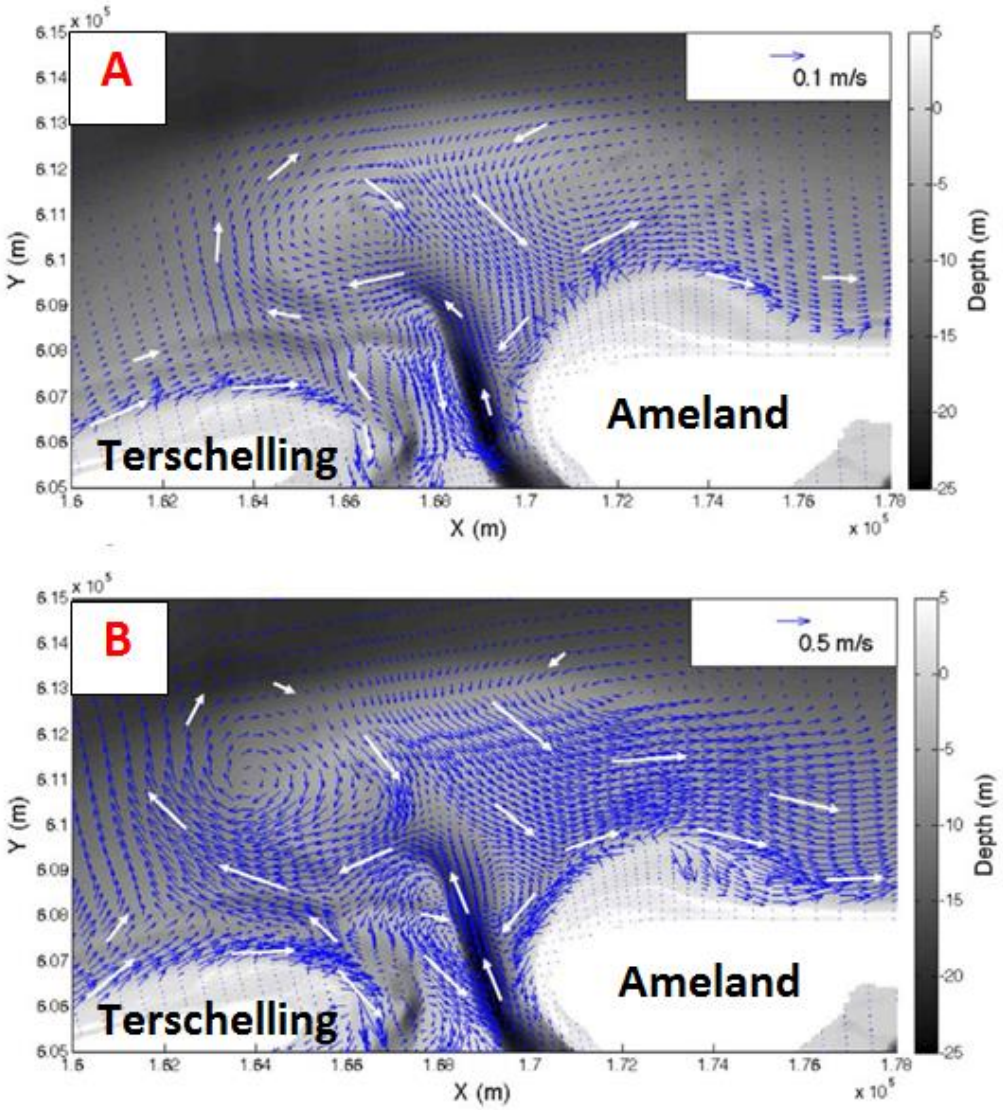

Figure 2.13 Patterns of wave-driven residual currents at the Ameland tidal inlet system during: (A) calm weathers, (B) storms. (Based on: Pluis, 2016)

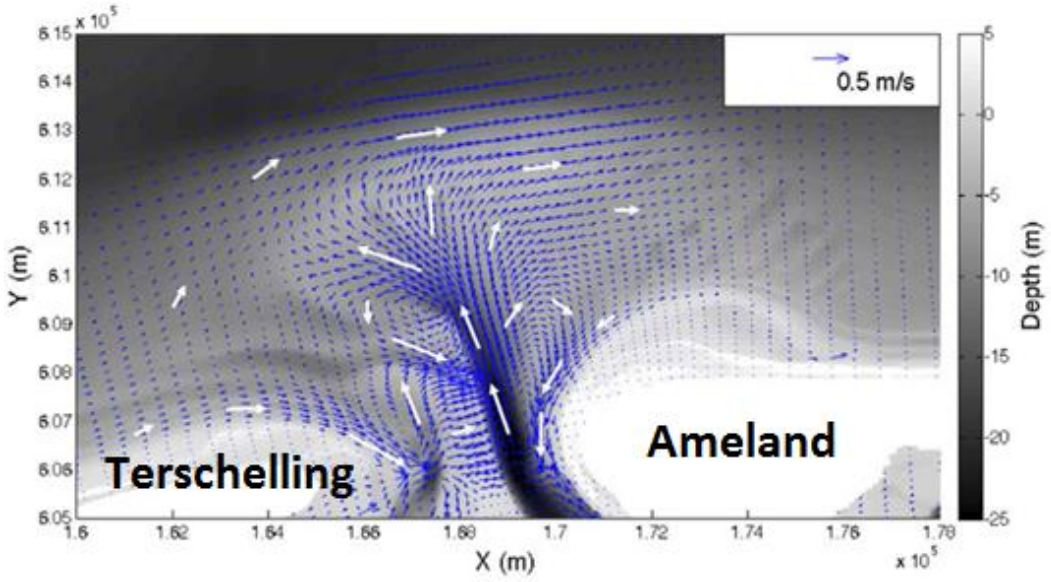

Figure 2.14 Patterns of tidal driven residual currents at the Amland tidal inlet system. (Based on: Pluis, 2016)

2.4.2 Sediment transport pattern

Herrling & Winter (2014) employed a numerical, process based and high-resolution model to study the morphological response of the Otzumer Balje inlet system to fair-weather conditions (tide dominant) and storm conditions (wave dominant). Figure 2.15 shows the modelled sediment transport under both conditions. During fair weathers, the effect tides on the sediment transport exceed that of waves. Significant transport takes place in the channels where sediment is delivered over the shoal and ebb-tidal delta through the main ebb channel and into the back-barrier basin through the flood channel. Relatively small eastward longshore transport can be observed along the coasts of two barrier islands.

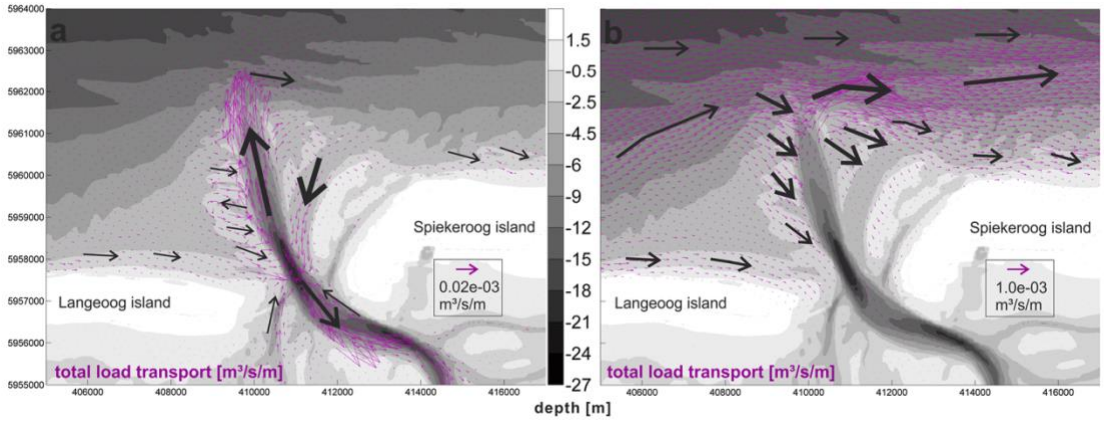

Figure 2.15 Patterns of sediment transport of the Otzumer Balje inlet system specified in the total sediment transport during fair weathers (left) and storms (right). (Source: Herrling & Winter, 2014)

During wave-dominance conditions, the magnitude of depth integrated sediment transport rate is estimated to be 0.001 $m^3/s/m$, which is 50 times larger than that of tidal-dominance conditions. It can be observed that strong littoral transport takes place along the island but decreases along the inlet. At the ebb-tidal delta, waves result in a land ward sediment transport. However, there is no clear transport in the basin channels.

Pluis (2016) studied the sediment transport pattern driven by tides, waves and combined action of the both in the Ameland inlet system, see Figure 2.16. He summarized during calm conditions, tides dominate the sediment transport pattern while waves prevail during storms, which agree with the results of Herrling & Winter (2014). During moderate wave condition, waves result in a landward sediment transport which is distributed nearshore and in the north of the ebb-tidal delta. Sediment is imported in the shallow part of the inlet while no clear transport can be observed in the deep part (the ebb channels Akkepollegat and Borndiep). Storms enhance the wave induced sediment transport. Therefore the system experiences the similar pattern with that of the moderate wave condition but a factor of 100 larger in the magnitude. In contrast, during tide-dominant condition the sediment transport is confined in channels. Sediment is exported in most channels. However, still small amounts of sediment import are found in the secondary channel Westgat and along the head of Ameland island.

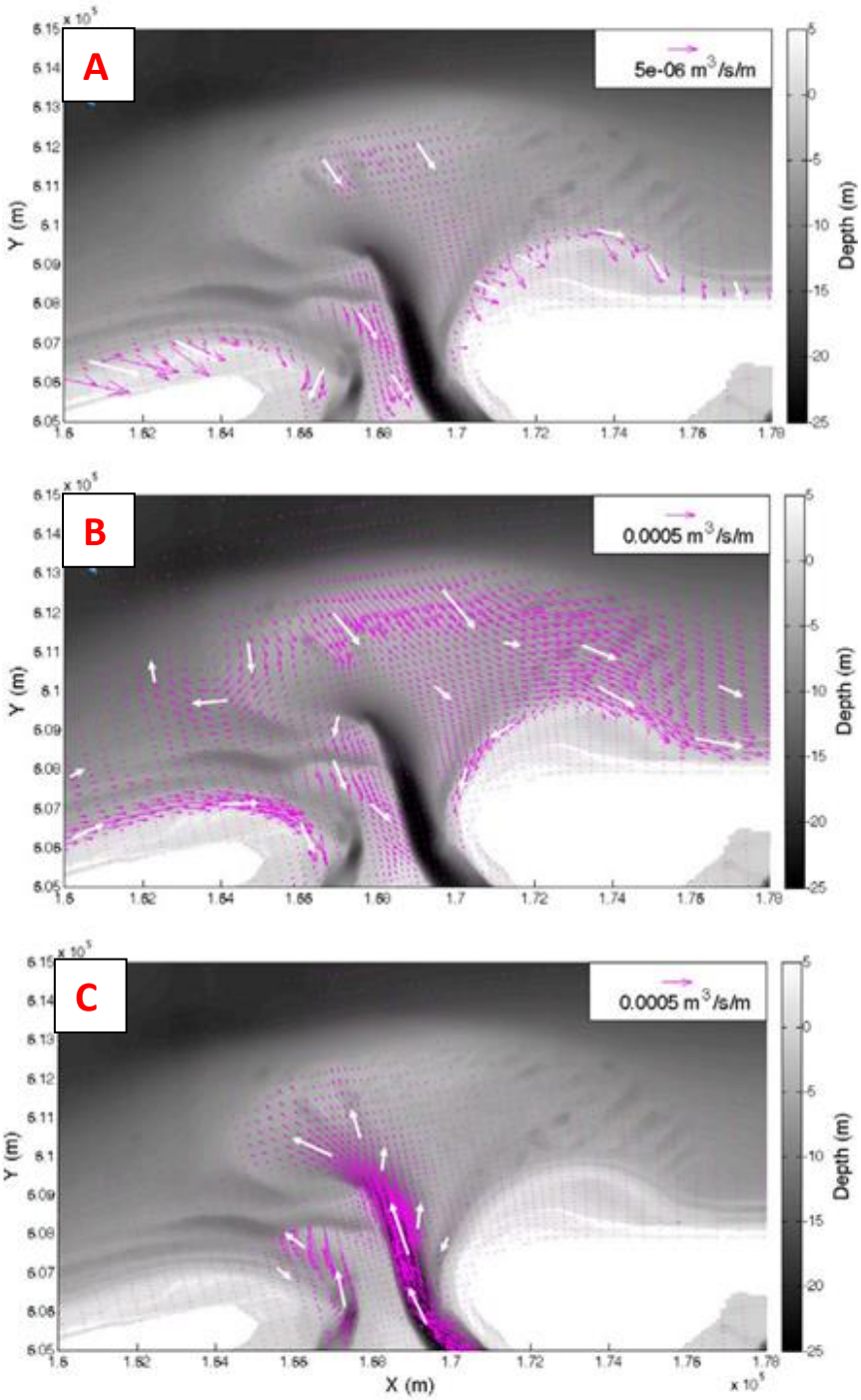

Figure 2.16 Total sediment transport under (a) moderate wave conditions (b) storm conditions (c) tide conditions. (Source: Pluis, 2016)

3 Synthesis and research questions

Previous studies and researches exhibit a large variety of knowledge and information on the tidal inlet system. Since 1980s, process-based numerical models have been widely used on the simulation of hydrodynamics and morphodynamics of tidal barrier system (e.g. Ridderinkhof, 1988; Dissanayake et al., 2012; Nahon et al., 2012; Ridderinkhof, 2016). Classically, numerical modelling studies on Ameland Inlet regarded it as an isolated system, with no interaction with other basins (e.g. De Forcket, 2008; Dissanayake et al., 2009; Jiao, 2014; Pluis, 2016). However, Duran-Matute et al. (2014) found a net inflow over the Terschelling watershed by quantifying residual tidal prisms at each inlet and over the watershed. This indicates the connectivity of basins. Moreover, recent observations found that watersheds of Ameland Inlet are flooded during storms, which might facilitate exchanges of water and sediment, affecting the short-term water and sediment balance of the system. Although Duran-Matute et al. (2014) found out that water exchange occurs over the watersheds, sediment exchange has not been quantified.

Only few studies examined how winds affect the flow and sediment transport patterns (Duran-Matute et al., 2014; Herrling & Winter, 2014). By comparing time-series residual discharges with corresponding wind data, Duran-Matute et al. (2014) concluded that NW winds with exceeding speed of 15 m/s would invert the direction of residual currents. However, the patterns of wind-driven residual flow and sediment transport were not shown in their results.

Due to all uncertainties and unknowns listed above, it is of prime importance to study how the Ameland Inlet responses to storms. This is why the main question of this research is formulated in this way:

'How does the Ameland Inlet behave in response to storms?'

Given that during storms, not only the flooding of watersheds affects the flow and sediment transport patterns, winds also have influences on them, it is necessary to separate these effects. As a result, sub-questions are made as follows:

1. *What are the effects of flooding watersheds on the flow and sediment transport patterns at the Ameland Inlet?*
2. *What are the effects of NW winds on the flow and sediment transport patterns at the Ameland Inlet?*
3. *What are the effects of surge height changes (storm comes and does not leave the system) on the flow and sediment transport patterns at the Ameland Inlet?*

4 Methodology

4.1 Modeling system

4.1.1 Hydrodynamic

This thesis employs several numerical and process-based models in DELFT3D-Flow to study the research questions. DELFT3D-FLOW is able to simulate water levels, tidal currents, wind-driven currents, sediment transport and morphological developments on a user-defined time and spatial scale (Deltares, 2014). Since margins of a river or a coastal region are normally not straight, the curvilinear grid system is thus adopted to reduce discretization errors. In order to save computational time, models in this research are set to depth-averaged mode (2DH) on a curvilinear boundary fitted grid under Spherical coordinate system (Deltares, 2014).

Spherical coordinate system is a special case of curvilinear system which is defined as:

$$\xi = \lambda \qquad 4.1(a)$$

$$\eta = \phi \qquad 4.1(b)$$

$$\sqrt{G_{\xi\xi}} = R\cos\phi \qquad 4.1(c)$$

$$\sqrt{G_{\eta\eta}} = R \qquad 4.1(d)$$

wherein ξ and η are Cartesian curvilinear coordinates [-], λ is the longitude [deg], ϕ is the latitude [deg], R is the radius of the Earth [m], $\sqrt{G_{\xi\xi}}$ and $\sqrt{G_{\eta\eta}}$ are coefficients used to transform curvilinear to rectangular coordinates [m].

The momentum equations in ξ- and η- directions the under Spherical coordinate system are:

$$\frac{\partial u}{\partial t} + \frac{u}{\sqrt{G_{\xi\xi}}}\frac{\partial u}{\partial \xi} + \frac{v}{\sqrt{G_{\eta\eta}}}\frac{\partial u}{\partial \eta} + \frac{\omega}{d+\zeta}\frac{\partial u}{\partial \sigma} - \frac{v^2}{\sqrt{G_{\xi\xi}}\sqrt{G_{\eta\eta}}}\frac{\partial \sqrt{G_{\eta\eta}}}{\partial \xi} + \frac{uv}{\sqrt{G_{\xi\xi}}\sqrt{G_{\eta\eta}}}\frac{\partial \sqrt{G_{\xi\xi}}}{\partial \eta} - fv = -\frac{1}{\rho_0\sqrt{G_{\xi\xi}}}P_\xi + F_\xi + \frac{1}{(d+\zeta)^2}\frac{\partial}{\partial \sigma}\left(\nu_V\frac{\partial u}{\partial \sigma}\right) + M_\xi \qquad 4.2(a)$$

and

$$\frac{\partial v}{\partial t} + \frac{u}{\sqrt{G_{\xi\xi}}}\frac{\partial v}{\partial \xi} + \frac{v}{\sqrt{G_{\eta\eta}}}\frac{\partial v}{\partial \eta} + \frac{\omega}{d+\zeta}\frac{\partial v}{\partial \sigma} + \frac{uv}{\sqrt{G_{\xi\xi}}\sqrt{G_{\eta\eta}}}\frac{\partial \sqrt{G_{\eta\eta}}}{\partial \xi} - \frac{u^2}{\sqrt{G_{\xi\xi}}\sqrt{G_{\eta\eta}}}\frac{\partial \sqrt{G_{\xi\xi}}}{\partial \eta} + fu = -\frac{1}{\rho_0\sqrt{G_{\eta\eta}}}P_\eta + F_\eta + \frac{1}{(d+\zeta)^2}\frac{\partial}{\partial \sigma}\left(\nu_V\frac{\partial v}{\partial \sigma}\right) + M_\eta \qquad 4.2(b)$$

In which σ is the scaled vertical co-ordinate (σ = 0 at the water surface; σ = −1 at the bed) [-],d is the depth below the reference level [m], ζ is the free surface elevation above the reference level [m], f is Coriolis parameter (inertial frequency) [1/s], ν_V refers to the vertical viscosity [m^2/s], P_ξ and P_η refer to the pressure gradients [kg/m^2s^2], and M_ξ and M_η represent the contributions due to external sources or sinks of momentum [m/s^2].

The Continuity equation is formulated as:

$$\frac{\partial \zeta}{\partial t} + \frac{1}{\sqrt{G_{\xi\xi}}\sqrt{G_{\eta\eta}}} \frac{\partial \left[(d+\zeta)U\sqrt{G_{\eta\eta}}\right]}{\partial \xi} + \frac{1}{\sqrt{G_{\xi\xi}}\sqrt{G_{\eta\eta}}} \frac{\partial \left[(d+\zeta)V\sqrt{G_{\xi\xi}}\right]}{\partial \xi} = (d+\zeta)Q \qquad 4.3$$

with U and V representing the depth average velocities in x- and y- directions:

$$U = \frac{1}{d+\zeta}\int_d^\zeta u dz \qquad 4.4(a)$$

$$V = \frac{1}{d+\zeta}\int_d^\zeta v dz \qquad 4.4(b)$$

with Q the contributions per unit area induced by discharge, precipitation and evaporation:

$$Q = \int_{-1}^{0} (q_{in} - q_{out}) d\sigma + P - E \qquad 4.5$$

where q_{in} and q_{out} are the local sources and sinks of water per unit of volume [1/s], P and E refer to precipitation and evaporation, respectively [m/s].

4.1.2 Sediment transport

The TRANSPOR2004 formulations (Van Rijn et al., 2004) are adopted with regard to sediment transport computation in this model. It differentiates between bed and suspended load transport mechanisms of which the summation is regarded as the total transport.

The total transport equation can be written as (Van Rijn et al., 2004):

$$q_{tot} = q_b + q_s \qquad 4.7(a)$$

where

$$q_b = q_{b,c} \qquad 4.7(b)$$

$$q_s = q_{s,c} \qquad 4.7(c)$$

wherein q_{tot}, q_b and q_s refer to the depth integrated total, bed load and suspended sediment transport, $q_{b,c}$ is current driven bed load transport while $q_{s,c}$ indicates current induced suspended sediment transport. Given the fact that this research does not take wave effect into consideration, wave induced sediment transport has been neglected. Besides, rather than to reconstruct the sediment transport exactly as the real situation, the aim of the research is to investigate the effects certain factors such as watersheds and storms by comparing the results of different scenarios, the model only picked up one sediment layer and set it to fine sand with a constant diameter of 250 μm as simple and general as possible. The complete expressions regarding to sediment transport are elaborated in Van Rijn et al. (2007a) and Van Rijn et al. (2007b).

4.1.2.1 Bed load transport

According to Van Rijn et al. (2004), the bed roughness predictor k is introduced to indicate local ripple height. This parameter is a function of the median grain size D_{50}, which then is used to calculate bottom friction through the Darcy-Weisbach equation. After that the bed shear stress can be computed. As a result, the bed load transport is dependent on the local

bottom slope S and the instantaneous velocity driven by l currents and waves $U_{CW,t}$ as:

$$q_b \propto U_{CW,t}^{2.5} \quad 4.8$$

4.1.2.2 Suspended sediment transport

The suspended sediment is calculated from:

$$q_{s,c} = \int_a^h ucdz \quad 4.9$$

wherein c and u indicate concentration and velocity.

The concentration profile can be determined by solving advection-diffusion equation (Van Rijn et al., 2007b) as:

$$\frac{\partial c}{\partial t} + \vec{\nabla} \cdot \vec{F} = 0 \quad 4.10$$

where $\vec{\nabla}$ = concentration gradient, $\vec{F}$ = flux of sediment by advection, settling particles and mixing.

4.2 Modelling philosophy

Three models are employed in this research: (1) the North Sea Model (version 6) from Zijl et al. (2013) (2) the Extended Wadden Sea model provided by Nathanaël Geleynse, (3) the Ameland model. Afterwards, a series of simulations based on these three models with different set-ups were performed to answer the corresponding research questions.

4.2.1 The North Sea Model

4.2.1.1 Model domain and bathymetry

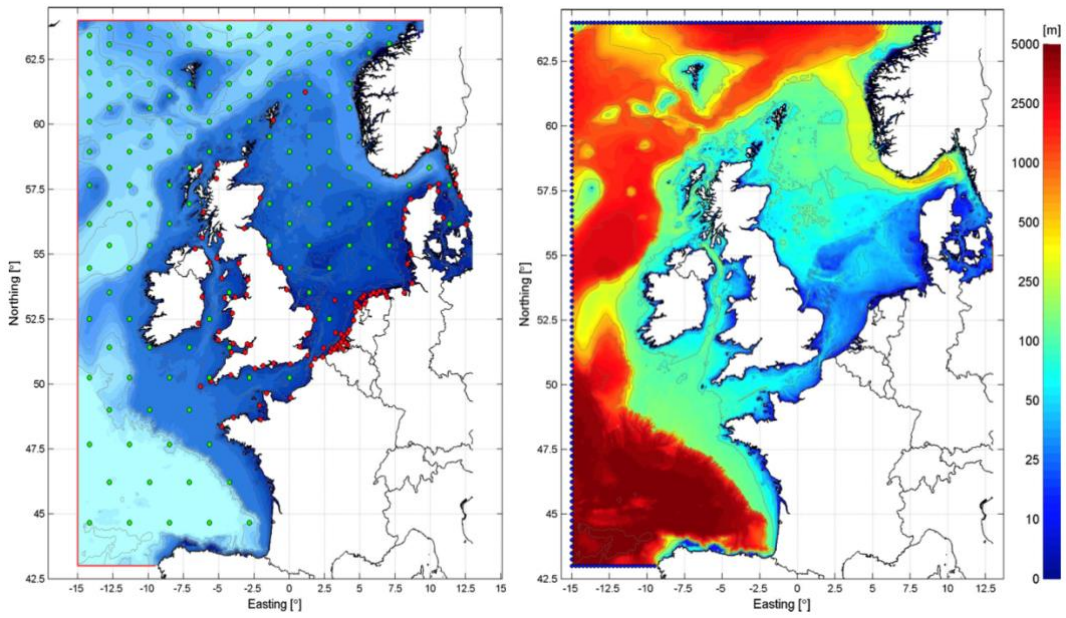

Figure 4.1 Left: the model domain of North Sea model with situ measurements (red) and radar locations (green); right: the latest bathymetry. (Source: Zijl et al., 2015)

The North Sea model was created in the 1980s and used to forecast water level accurately at the Dutch coast (Zijl et al., 2013). The model adopted in this research is the latest version improved by Zijl et al. (2015). It covers the northwest European coast from 15° W and 13° E and 43° N and 64° N, shown in Figure 4.1. The bathymetry of the North Sea model is applied from the NOOS dataset. Water depths are exceeding 2,000 m in the northern part while the south-west part features much higher water depths (over 5,000 m). The central part of the model domain is shallow (less than 100 m) with even shallower in the southern part (below 50 m).

4.2.1.2 Boundary forcing

Open boundaries with 205 sections are defined as 'Water-level type' in the north, west and south. At these sections, time-series water levels are imposed by applying 38 tidal constituents and surge (inverse barometer correction). At the surface, time- and spatial dependent wind speed and air pressure is applied from the Numerical Weather Prediction high-resolution limited area model (HiRLAM). The wind stress is calculated from the wind speed and drag coefficient at 10 m height from the surface using Charnock formulation (Charnock, 1955). Other forcing types such as tide generating forces and river discharges are also included.

4.2.2 The Extended Wadden Sea model

4.2.2.1 Grids

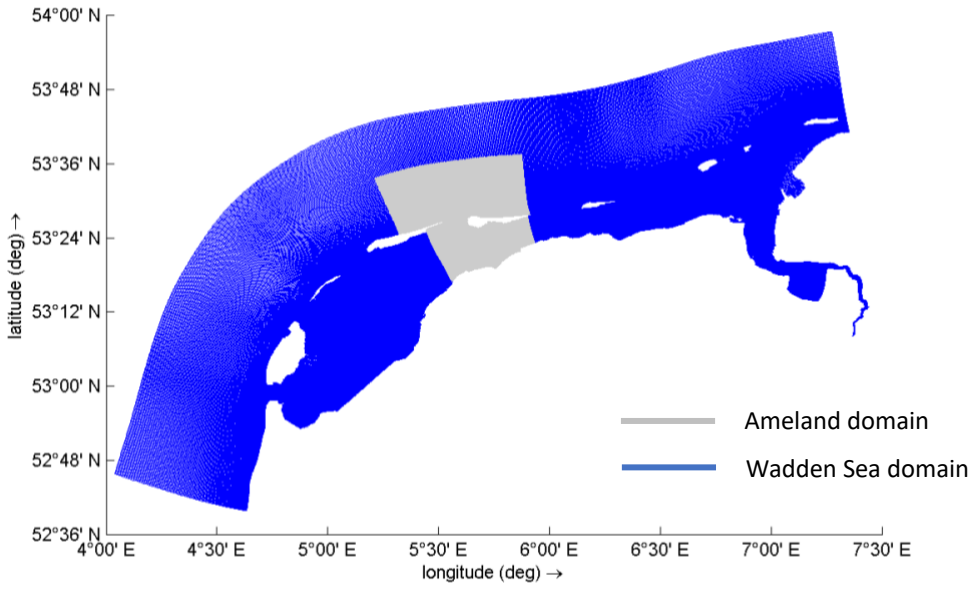

Figure 4.2 Hydrodynamic grid of the Extended Wadden (blue) Sea and Ameland basin (grey).

The Extended Wadden Sea model is a curvilinear model adapted from Kuststrook-fijn model (1999). There are two domains in this model, namely the entire Wadden Sea and Ameland. They are coupled using domain decomposition method, see Figure 4.2. The most important function of this method is to connect grids and generate communications among domains. In this case, the Ameland domain with finer grids allows for more detailed calculations on the flow and sediment motions.

The Wadden Sea domain covers the entire Dutch coast, bounded in the south by the

Belgian-Dutch border and by the German tidal basin of Norderney in the east. At the seaward side, it extends around 60 to 70 km to the North Sea (Deltares, 2009). Its resolution is spatially varying with the value of 400 to 500 m seaside and 100 to 180 m in the back-barrier basins, featuring 772 by 823 grid cells in shore-parallel and cross-shore directions, respectively. The Ameland region is separated from the entire domain and has undergone a factor 3 local refinement, featuring 362 by 956 grid cells. Its hydrodynamic grid includes Ameland back-barrier basin and spans a distance of 17 to 20 km seaward from the coast. In the shore-normal direction (almost West-East), it extends in total 37 km along Terschelling and Ameland islands up to the region with the water depth of 20 m. Likewise, the resolution is higher offshore, around 100 to 130 m and lower in the basin (30 to 50 m). Since calculations of hydrodynamics and morphodynamics are executed independently on each domain, *DD-boundaries* are generated for data communications and connections among domains (Deltares, 2014).

4.2.2.2 Bathymetry

Since 1965 when the project *National Morphological Monitoring Programme (MON*MORFOLOGIE)* operated by Rijkswaterstaat was implemented, the bathymetric data along the North Sea Coast has been monitored at several locations with the frequency of every year to every 6 years depending on area (EDMED, 2009). The bathymetries in this study are based on the latest measurement of Vaklodingen (2016), see Figure 4.3.

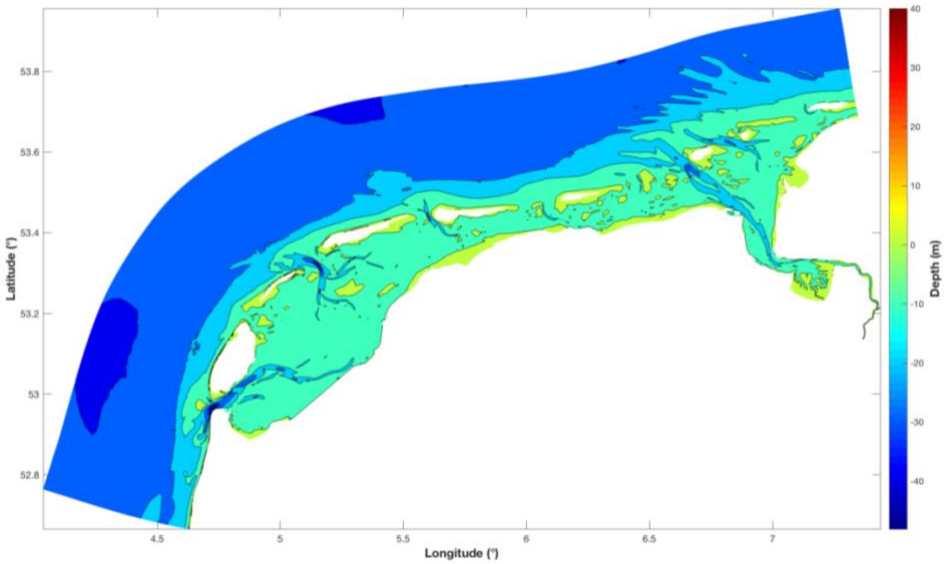

Figure 4.3 The 2016 bathymetry of the whole domain (Wadden Sea + Ameland).

4.2.2.3 Hydrodynamic settings

The data of boundary conditions is acquired from the North Sea model which aims at simulating and forecasting water levels along the Dutch coastline during storms (Zijl, 2013). The model employed the setup of boundary conditions including time and spatial dependent water level and velocity changes during one extreme storm, Sinterklaas Storm in 2013.

4.2.2.3.1 Tides

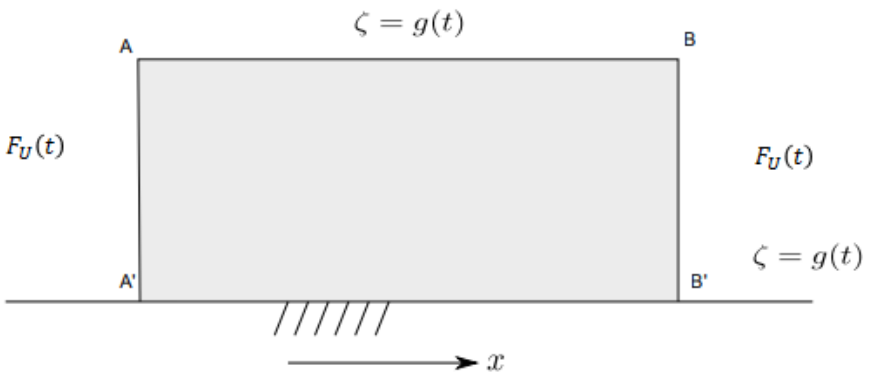

Figure 4.4 Simplified boundary conditions of the Extended Wadden Sea Model. The western boundary is set to Riemann boundary while Water Level boundary is carried out in the northern boundary. The tidal basin part of the eastern boundary implements 'Water-level' boundary but it is set to Riemann at the offshore part with the transition at islands. (Source: Deltares, 2011).

There are two types of boundary conditions defined in the east, north and west boundaries, namely 'Water-level' and 'Riemann' boundary. The generalized schematic of boundary conditions can be seen in Figure 4.4. The former describes the actual water levels at boundaries which vary in time and space. The 'Riemann' boundary is also called weakly reflective boundary where outgoing waves are able to cross it instead of being reflected back to the domain when the boundary reaches a certain level (Deltares, 2014). This type of boundary is employed to weaken the effect of reflective waves at open boundaries when the local water level or velocity is too large. Relevant equations are adjusted from the work of Engquist & Majda (1977, 1979), and Stelling (1984):

$$U + \alpha \frac{\partial}{\partial t}\{U \pm 2\sqrt{gH}\} = F_U(t) \qquad 4.6(a)$$

$$\alpha = T_d[s] \qquad 4.6(b)$$

where U, g and H refer to depth averaged velocity, gravitational acceleration and local water depth respectively, α is the reflection coefficient and T_d indicates how long it takes a surface wave to cross the model domain from left to right.

The west boundary (Belgian-Dutch border) is divided into 49 segments with all setting to 'Riemann boundary', see Figure 4.5. At the seaside, 'Water-level' boundary is applied to the north edge which consists of 154 sections of 5 grid cells each. However, the east boundary is a relatively complex case. Part of it covers the open sea while the rest features the basin land. As a result, 'Water-level' boundary is employed at 31 offshore sections and 'Riemann' boundary for the remaining 6 basin segments. Besides, the prescribed DD boundaries provide the communication and connection between Extended Wadden Sea and Ameland domains. During each computational time step (0.25 min in this research), the outer domain (Extended Wadden Sea model) will generate hydrodynamic conditions through DD boundaries to transfer and receive information and connections from the inner region.

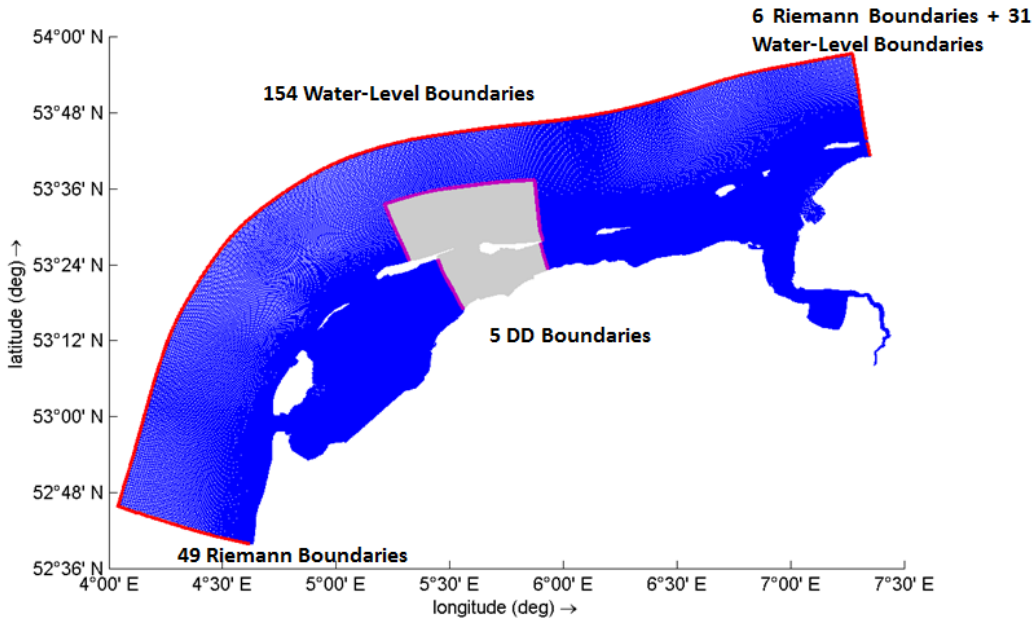

Figure 4.5 Segments and types of each boundary (open boundaries are marked in red while DD boundaries in purple).

In order to obtain accurate results, the time-series water levels from the North Sea model with an interval of 10 minutes from 1st Nov to 8th Dec 2013 are applied to all boundaries. The data of entire November provides the tidal information for the hydrodynamic of the Ameland inlet during the calm weather. The actual water levels from Dec 1st to Dec 8th prescribe the tidal movements during the Sinterklaas Storm, which is the core of the model.

4.2.2.3.2 Sinterklaas Storm: storm surge and winds

On 5th December 2013 the north-west Europe was confronted with a severe storm which lasted two days till the final hours of 7th December. Because it coincided with the date of the traditional Dutch holiday Sinterklaas, it hence was named, *'Sinterklaas Storm'*. In other countries, this heavy storm event was also known as *'Cyclone Xavier'*. It travelled from Greenland towards southern Scandinavia, causing high surges in the North Sea associated with strong north-eastern winds (Carrion, 2015). Figure 4.6 shows a) the path, and b) wind data of the Sinterklaas Storm.

As a part of Dutch government, Rijkswaterstaat (RWS) measured and recorded the data of Sinterklaas Storm passing. The water levels at open boundaries where surge changes are prescribed are from the large scale North Sea model. The wind data is derived from HIRLAM model which is aiming at the development of a short-range forecasting weather system. Then spatial and time varying wind data is applied in DELFT3D-Flow in the form of three input files: 1) air pressure, 2) wind speed in eastern direction, and 3) wind speed in northern direction. Besides, these files are stored in an independent co-ordinate system which is in this case, in an equidistant grid. The Extended Wadden Sea model starts to simulate the wind conditions from the bottom left of the grid extending to the whole domain with updating wind data every 3 hours.

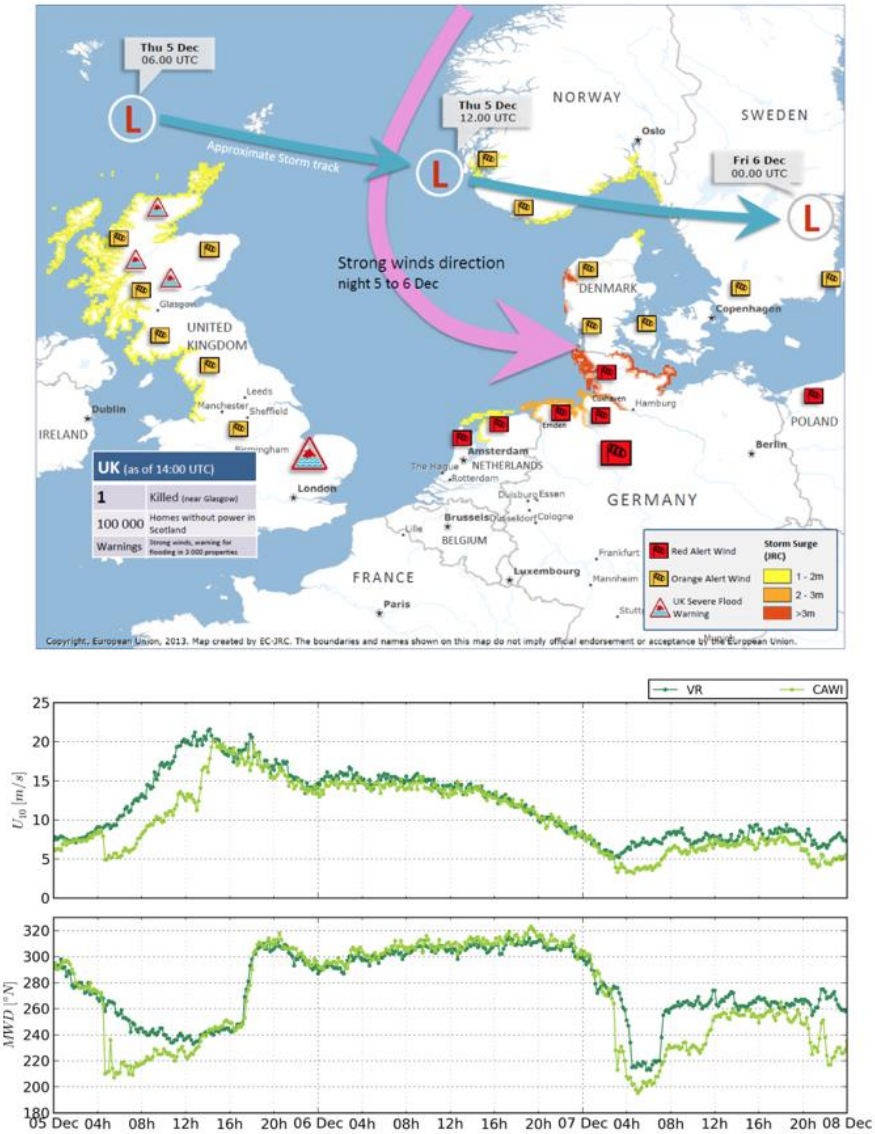

Figure 4.6 Upper: the path of Sinterklaas storm issued the 5th of December and its forecast till 6th of December; bottom: wind speed and directions. (Source: http://erccportal.jrc.ec.europa.eu/Maps; Carrion, 2015)

4.2.3 The Ameland model

The Ameland model is an independent model which has been widely used in previous studies on the Ameland inlet since it is classically regarded being isolated, with no interaction with other basins.

4.2.3.1 Grids

The computational grid of the Ameland model is from De Fockert (2008), based on the work of Steijn and Roelvink (1999), see Figure 4.7. It covers more or less the same area as the Ameland domain of the Extended Wadden Sea model does but is set under the curvilinear Cartesian coordinate system. In the West-East, the model domain stretches offshore from halfway the Terschelling Island to the middle part of the Ameland Island, whilst from the Terschelling watershed to the Ameland watershed at the Wadden Sea. It is bounded in the north by the offshore region of -20m water depth and by the Frisian dikes in the south. There are 348 by 324 grid cells in respectively x- and y- direction, featuring the resolution of 300 m

to 500 m offshore and 30 m to 40 m in the inlet. The model of De Fockert (2008) also considers the wave forcing which is neglected in this research.

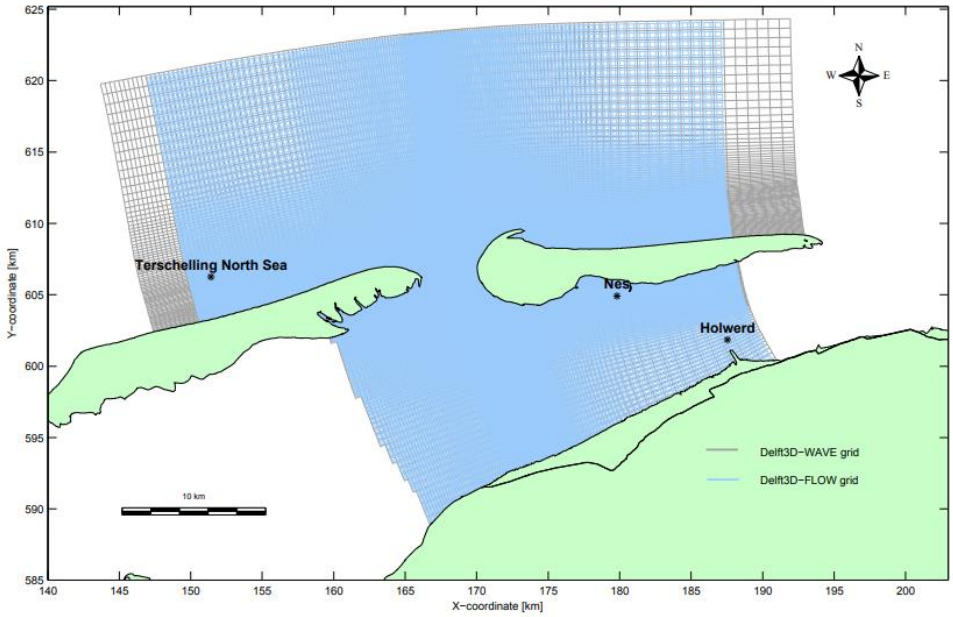

Figure 4.7 The computational grids in the Ameland model (Blue: hydrodynamic grid; Grey: wave grid which is ignored in this reseach). (Source: De Fockert, 2008)

4.2.3.2 Bathymetry

The bathymetric data of the Ameland model is consistent with that of the Extended Wadden Sea model by triangular interpolation from the most recent measurements using QUICKIN in DELFT3D, as shown in Figure 4.8.

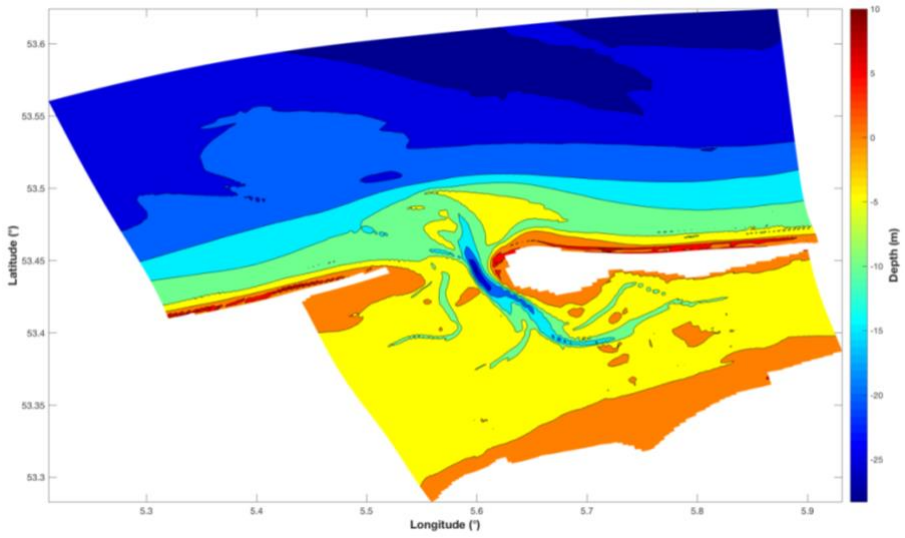

Figure 4.8 The 2016 bathymetry of the Ameland model.

4.2.3.3 Boundary conditions

Same as the Extended Wadden Sea model, the north boundary which is divided into 8 sections, employs 'Water-level' boundary, see Figure 4.9. However, only offshore grids in the west and east edges are selected as open boundaries (5 segments each), where 'Neumann'

boundary is applied. This type of boundary describes the water level gradient in time but does not consider the reflection influencing (Delatres, 2014).

The tidal boundary data (water levels and water level gradients) are derived from the outputs of the Extended Wadden Sea model. The water level slopes are calculated by the difference of water levels at the marginal grids of the Extended Wadden Sea and Ameland domain, divided by the corresponding distances. These water levels are acquired directly from those grid points at the offshore boundary of the Ameland domain.

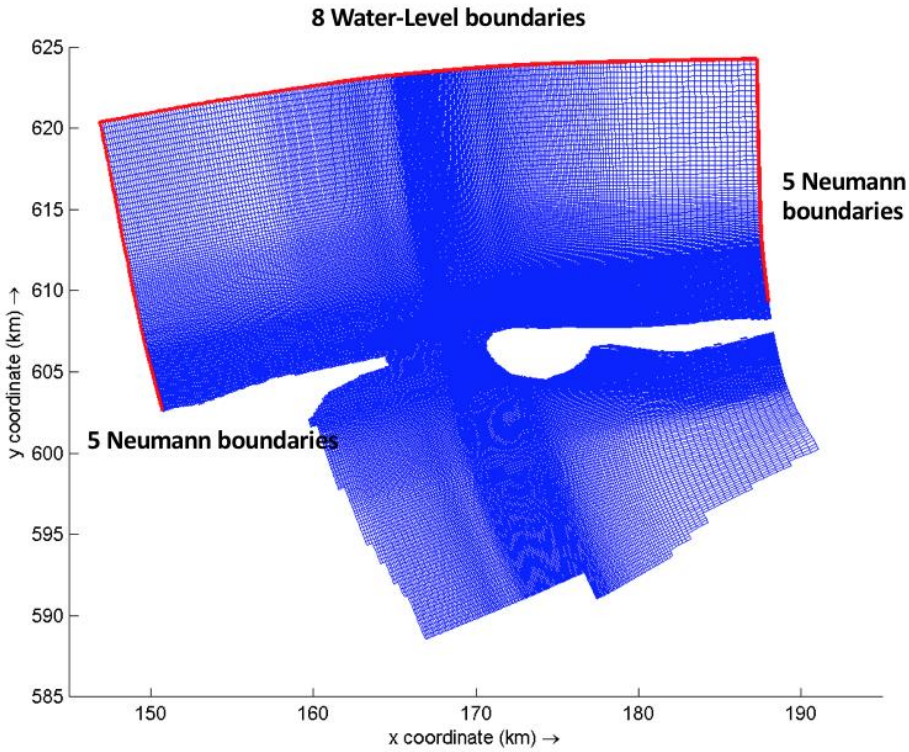

Figure 4.9 Segments and types of each boundary (open boundaries are marked in red).

4.3 Model scenarios

4.3.1 Model simulations

In order to separate the sole effect of flooding of watersheds, dams are introduced to be placed at the locations of watersheds. Hence, no water and mass exchange would take place over watersheds and thus the effect of flooding of watersheds can be studied by comparing model runs with and without dams. Similarly, the sole NW wind effect can be investigated by comparison between runs including NW wind and not. The sole effect of the passing storm can be studied by setting a constant surge height which means storms only come in but do not go out.

Several model simulations with different set-ups are carried out to solve research questions. Table 4.1 describes the general information of each model simulation. The first four are based on the Extended Wadden Sea model while the Ameland model is employed by the last run.

Research questions are solved by result comparisons of model runs: EXT02 and EXT03 (research question 1), EXT03 and EXT04 (research question 2), EXT02 and RIF401 (research question 3).

Table 4.1 Display of set-ups for each model simulation carried out in Delft3D Flow models.

Simulations	Model	Duration	Condition	Forcing types	Watersheds
EXT01	The Extended Wadden Sea model	01/11/2013-31/11/2013	Calm	Tides	n.a.
EXT02		01/12/2013-08/12/2013	Sinterklaas Storm	Tides + winds	n.a.
EXT03				Tides + winds	Dams placed
EXT04				Tides	Dams placed
RIF401	The Ameland model		Constant storm surge level of 1.745 m	Tides + winds	n.a.

4.3.1.1 1st simulation: EXT01

The first model (EXT01) is used to provide initial conditions for the storm simulation (EXT02) and dams placement simulation (EXT03) including water level, depth averaged velocity and bottom depth in the form of restart files (.rst). The simulating period is from 1st November to 31st November in 2013 which is the month before Sinterklaas Storm.

4.3.1.2 2nd simulation: EXT02

Compared to EXT01, the second run EXT02 is responsible for simulating hydrodynamic and sediment transport including the amount of water and sediment exchange during Sinterklaas Storm. The model runs from 1st Dec to 8th Dec of 2013. Except for tidal forcing, the spatial

and time varied wind forcing was applied in EXT02. As a result, this run simulates the tides, surge and wind-driven flows and water levels.

4.3.1.3 3rd simulation: EXT03

The aim of EXT03 is to investigate the effect of watersheds at Ameland inlet (Research question 1) by comparing results with those of EXT02. Hence, thin dams were placed on all watersheds of the Dutch Wadden Sea system (Figure 4.10), resulting in cutting off the water and sediment exchange among basins. Thin dams in Delft3D-FLOW are infinitely high and are following the grid orientation. There are two types of setting dams, called U and V dams where the exchange of water between two neighbor grid points is prohibited in M- and N-directions, respectively.

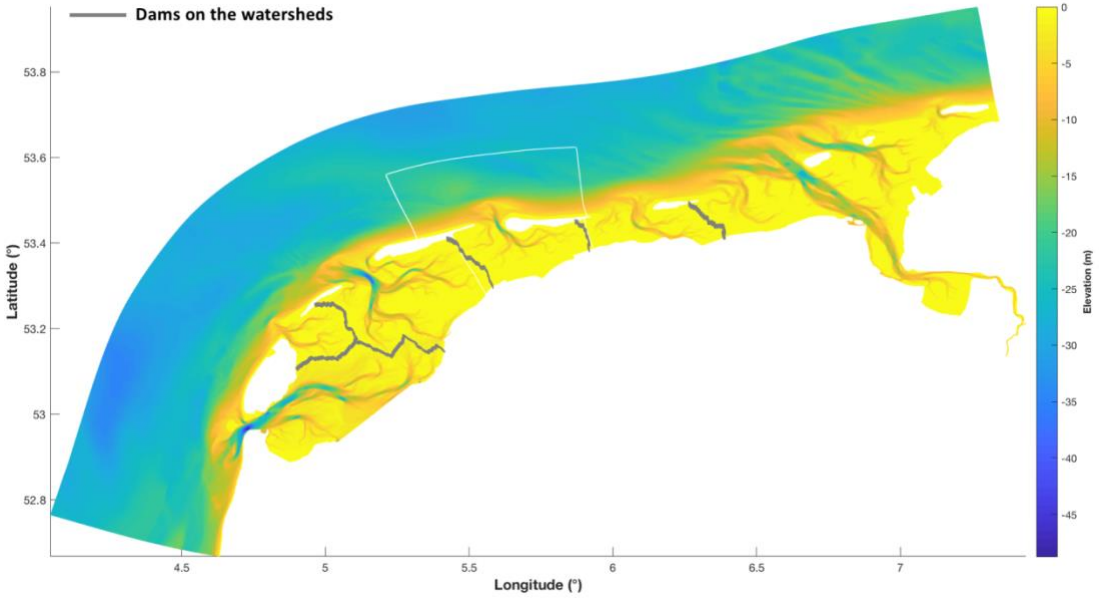

Figure 4.10 Location of infinite high dams placed on the watersheds.

4.3.1.4 4th simulation: EXT04

This simulation excludes wind data but keeps other set-ups same as EXT03. As a result, EXT04 is able to study patterns of wind-driven currents and sediment transport (research question 2) through the comparison with EXT03.

4.3.1.5 5th simulation: RIF401

Unlike the first three model simulations, RIF401 focuses on hydrodynamics and sediment transport of Ameland system. This means Ameland basin is considered as an independent system where thus the flow and sediment motions are constrained in the Ameland domain. It aims at studying how incoming and outgoing of storms affects local water and sediment patterns (research question 3). For this, storms are introduced as a constant increase of 1.745 m in water level. This can be fulfilled as following equations:

$$\eta_i = H_i - \overline{H}_i \tag{4.11}$$

$$H_i' = \eta_i + H_c \tag{4.12}$$

wherein, i is the i^{th} section of boundaries, η is the tidal induced water levels [m], H is

the local water level [m], $\overline{H}$ is the mean component of water level [m], H' refers to the new water level applied in the boundary conditions [m], H_c is the constant surge height (1.745 m in this case) [m].

4.3.2 Analyzing methods

4.3.2.1 Godin tidal filter

The Godin tidal filter is a low-pass filter to remove tidal variations from diurnal, semi-diurnal and short-period constituents (Walters & Heston, 1982). In other words, it is employed to obtain the mean component of time-series data such as water surface elevations and flow velocities. In this research, residual flow and sediment transport are derived by applying the Godin tidal filter. This filter successively uses running means of three shifting windows 24-, again 24- and 25-hour lengths, respectively (Shirahata et al, 2016).

4.3.2.2 Quantitative analysis: water and sediment discharges

In order to quantify the amount of exchanges of water and sediment between the Ameland barrier system and other basins or the North Sea, three cross-sections were defined which are the Ameland inlet, the west watershed and the east watershed, see Figure 4.9. Besides, the cross-section of the inlet throat is divided into two parts: the shallow and deep channels, corresponding to the Westgat and Borndiep respectively.

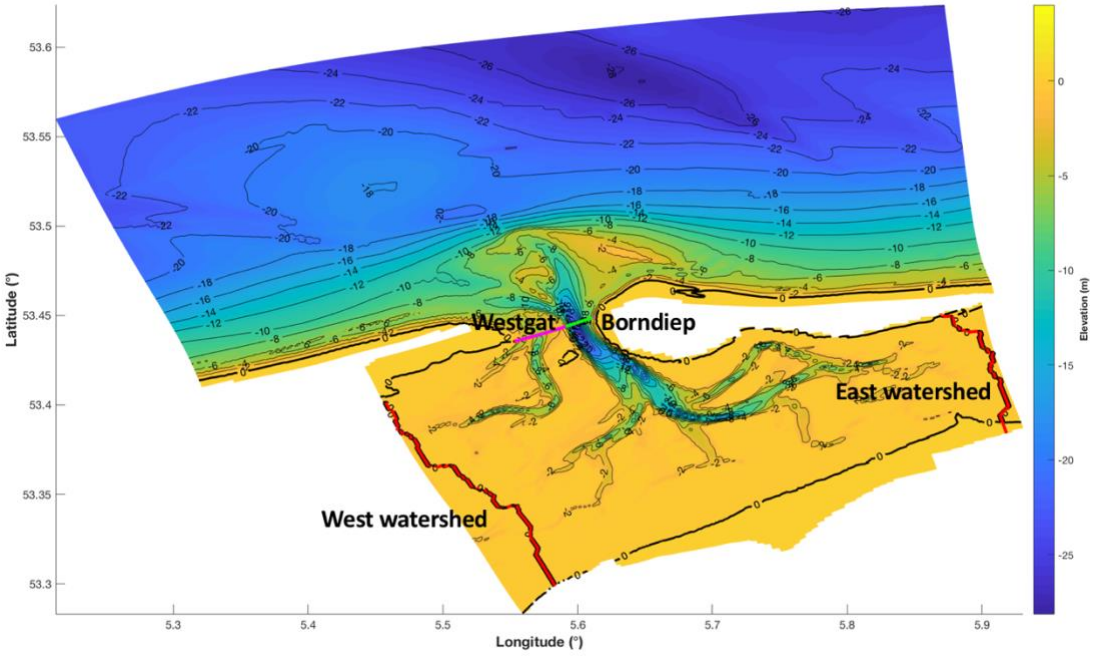

Figure 4.11 Cross-sections defined at the west watershed and the east watershed marked in red. The Ameland Inlet is divided into two parts: the shallow channel Westgat (in magenta) and deep channel Borndiep (in green).

These cross-sections are generated at the grid points of the inlet throat and watersheds. The depth averaged velocity and total transport vectors are extracted and decomposed in *M*- and *N*- directions which refer to the components along and cross the local grid point. With regard to the calculation of the water discharge, it is written as follow:

$$Q_{inlet} = \sum_{i=1}^{n} V_{i,t} \times H_{i,t} \times W_i \qquad 4.13(a)$$

$$Q_{watershed} = \sum_{i=1}^{n} U_{i,t} \times H_{i,t} \times W_i \qquad 4.13(b)$$

in which, n is the number of grid points of the cross-section, V_t and V_t are the cross- and along-grid components of time varied depth averaged velocity (m/s), H is the local time varied water depth (m) and W is the cell width (m).

Given that the sediment transport vector of model outputs is depth integrated, the amount of sediment flux is then calculated by:

$$Q_{s,inlet} = \sum_{i=1}^{n} Q_{s,v,i} \times W_i \qquad 4.14(a)$$

$$Q_{s,watershed} = \sum_{i=1}^{n} Q_{s,u,i} \times W_i \qquad 4.14(b)$$

Where, $Q_{s,v,i}$ and $Q_{s,u,i}$ refer to the the cross- and along-grid components of time-dependent depth integrated total sediment transport ($m^3/s/m$).

5 Results

The first section will describe general patterns of residual flow and sediment transport during calm, storm, dam placement, no-wind and constant storm surge height conditions. After that, comparisons will be generated among model simulations to study the effects of flooding watersheds (EXT02 and EXT03), NW winds (EXT03 and EXT04) and a passing storm (EXT03 and RIF401). Besides, to understand how Ameland Inlet responds to different conditions, time-series discharges and sediment transport will be displayed afterwards. In the second part, overall statistics will be listed to indicate the amount of water and sediment exchange before the storm, during surge rising and during the surge dropping for each model run. This is to illustrate how the tidal prism and the amount of sediment import in the Ameland system in response to different conditions.

5.1 General patterns of residual flow and sediment transport

5.1.1 Calm condition

This section shows the results of model run EXT01. It reveals the residual flow and sediment transport patterns during calm weathers.

5.1.1.1 Residual flow

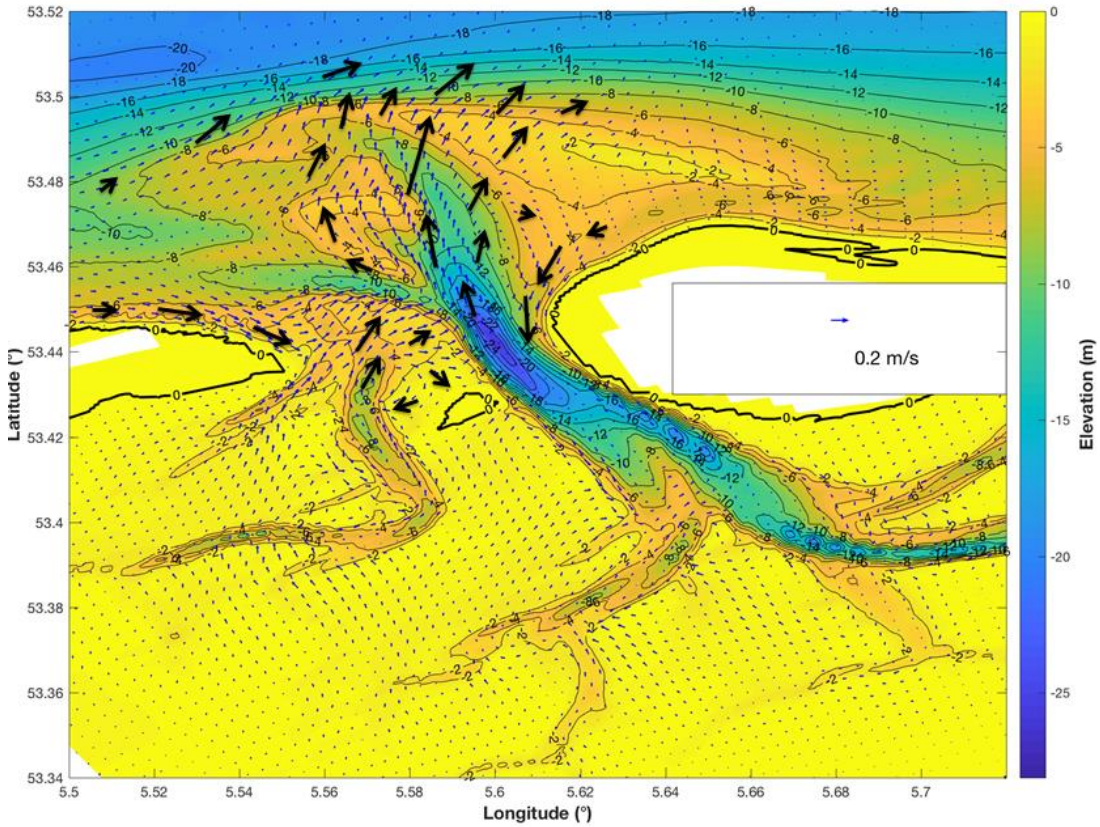

Figure 5.1 Depth-averaged residual flow pattern during the whole November in 2013.

Figure 5.1 shows the depth averaged residual flow pattern by averaging the actual flows of the last two tidal cycles during quite weather. Ebb-oriented residual flows can be observed in the ebb channels and flood-directed mean flows in the flood dominated channels. As a result,

a flow circulation exists at the area of swash bar complex Bornrif while another one is located at the end of the channel Boschgat. At the uplift side of the island of Terschelling, tides and winds drive residual currents flowing along the coast into the inlet, but then encountering with ebb-directed mean currents in two ebb channels Boschgat (the small one near the Terschelling island; the other is located to the south-east of Borndiep flat), and eventually forming ebb-directed mean flows in the channel Westgat and Akkepollegat. Magnitudes of these flows are up to 0.18 m/s in channels Westgat and Boschgat and only 0.05 m/s in the deepest channel Borndiep. Seaward the inlet, ebb-oriented residual currents are significant (0.22 m/s) in the main ebb channel Akkepollegat, and over the ebb-tidal delta (0.2 m/s). These flows join the along-shore currents along the terminal lobe and contribute to the overall eastward currents in the north, amounted to be 0.13 m/s. Over the watersheds, no clear residual flows can be observed.

5.1.1.2 Residual sediment transport

Figure 5.2 indicates the depth integrated residual total sediment transport. It follows the flow pattern. The strong flood-oriented mean currents at the downdrift part of Terschelling Island and the updrift part of Ameland Island result in landward sediment transport into the back-barrier basin through flood channels. Further landward, these channels have flood-directed sediment transport, leading to sediment import into the Ameland inlet system. However, at the seaward end of Borndiep, sediments are transported offshore to the ebb-tidal delta through the main ebb channel Akkepollegat, and eventually to the North Sea. In accordance with the flow pattern, no sediment exchange can be observed at the watersheds.

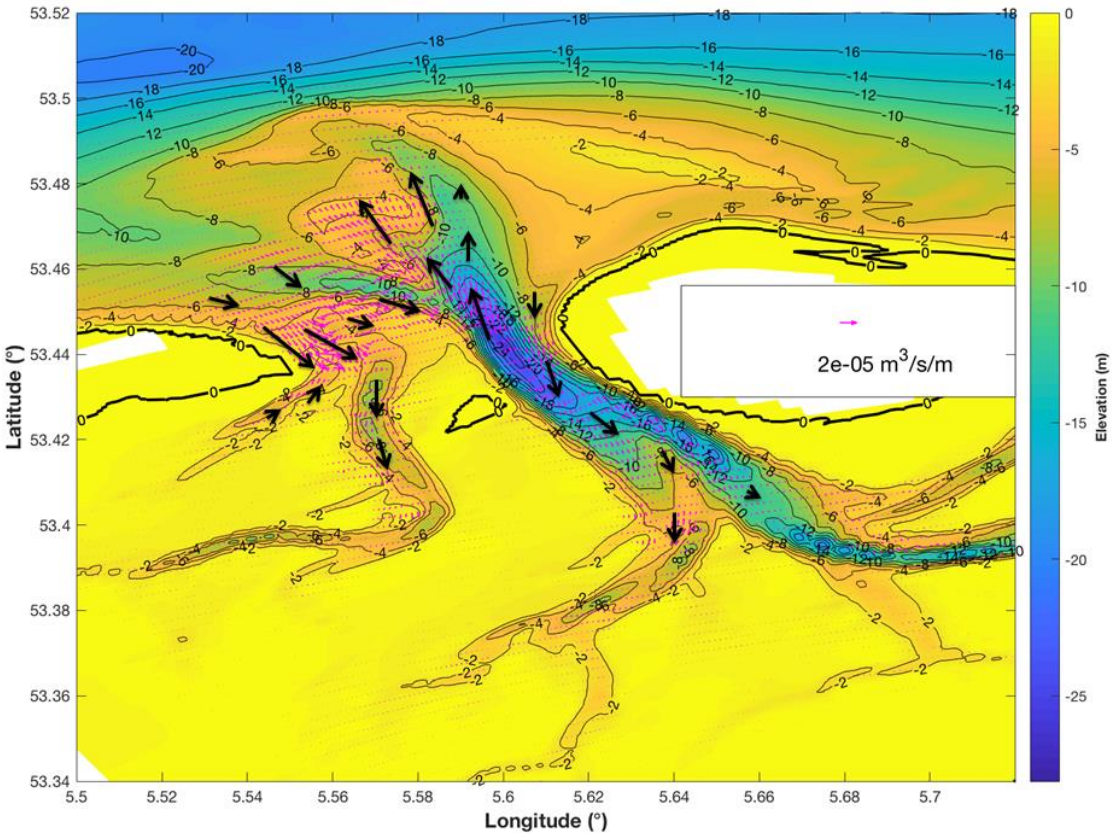

Figure 5.2 Residual sediment transport pattern during the whole November in 2013.

5.1.2 Transport patterns during storms

During a storm event, water level changes in the tidal inlet system can be divided into three stages. At the first phase (surge rising), the local water level increases rapidly and drastically in which a large amount of water and sediment are imported into the basin. Then, it reaches its maximum surge height indicating the transition from rising phase to falling phase. Finally, water is leaving the system with sediment exported. The water level decreases back to the value before the storm. Therefore, the residual flow and sediment transport patterns with rising surges are shown in following figures. Besides, situations with water leaving the system are also indicated to reveal how the Ameland system adjusts itself in response to the Sinterklaas Storm.

5.1.2.1 Residual flow

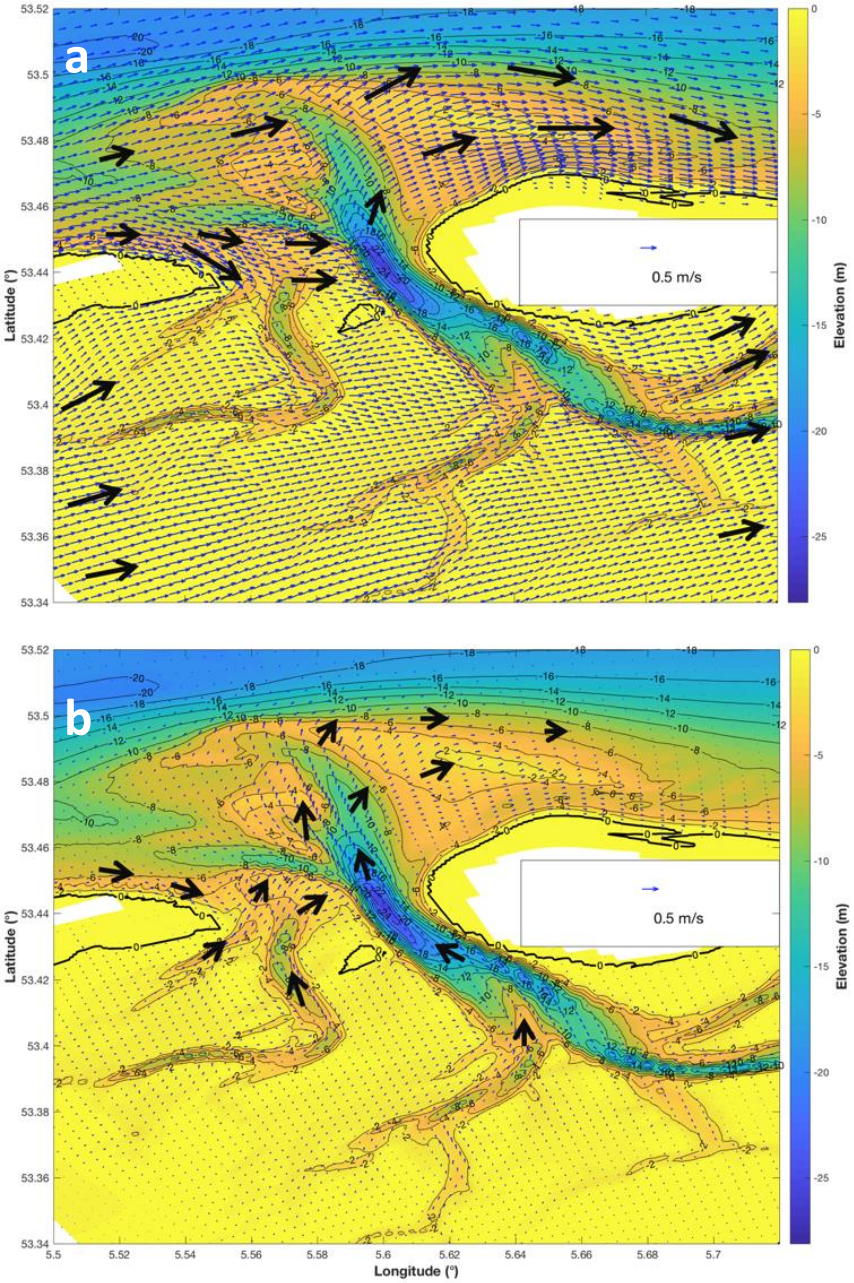

Figure 5.3 Residual flow pattern during a) uplifting phase, b) falling phase.

It can be seen in Figure 5.3(a) that the storm generates the overall eastward residual currents (around 0.5 m/s) which enter the back-barrier basin through the west watershed and then leave through the east watershed, crossing and flooding the whole basin. At the downdrift side of Terschelling, strong wind-driven longshore currents together with tidal currents are flowing in the flood direction in the channel Westgat. These currents mainly flow to the east watershed together with basin eastward currents. The rest flows to the inlet, and then groups with ebb-oriented mean currents in the ebb channel Akkepollegat. The strong offshore residual currents flow eastward over the ebb-tidal delta and then join the residual currents in Akkepollegat, resulting in strong longshore currents along the coast of Ameland island.

After the storm, the system exhibits an overall drainage pattern with a much smaller flow magnitude (about 0.2 m/s), see Figure 5.3(b). Residual currents are confined to the channels in which water are drained out the system, except for Westgat where the longshore currents are observed entering into the system but then being quickly converted to the outflow due to the combination with ebb-oriented currents in two channels Boschgat. Different from the situation during the storm, ebb-directed residual currents at the inlet throat flow over the ebb-tidal delta and rotate nearly 90 ° at the lobe of the delta due to offshore eastward currents. Weak residual currents (0.002 m/s) can be found flowing eastward at two watersheds.

5.1.2.2 Residual sediment transport

Figure 5.4 shows the sediment transport patterns during rising and falling phases. Sediment transport during the storm can be observed not only in the channels but also in the basin, while it is confined to the channels after the storm. During the storm, winds and tides impose eastward longshore currents along Terschelling coast. These currents stir and transport sediment over the western margin of the ebb-tidal delta to the inlet. In the deep part of inlet throat, a small amount of sediment is transported to the ebb-tidal delta through the main ebb channel Akkepollegat. In contrast, a moderate amount of sediment is imported to the basin through the channel Borndiep. Besides, due to the low water depth, a large amount of sediment is stirred at the shallow area of the inlet (to the east of Terschelling island) and then transported into the back-barrier basin through two channels Boschgat. It can be found that sediment is also imported into the basin through the west watershed but in a relatively small magnitude while no clear sediment exchanges can be observed at the east watershed. After the storm, the magnitude of sediment transport is largely reduced. Sediment is transported out the system through all basin channels whilst only a small sediment import can be found at the shallow area of the inlet.

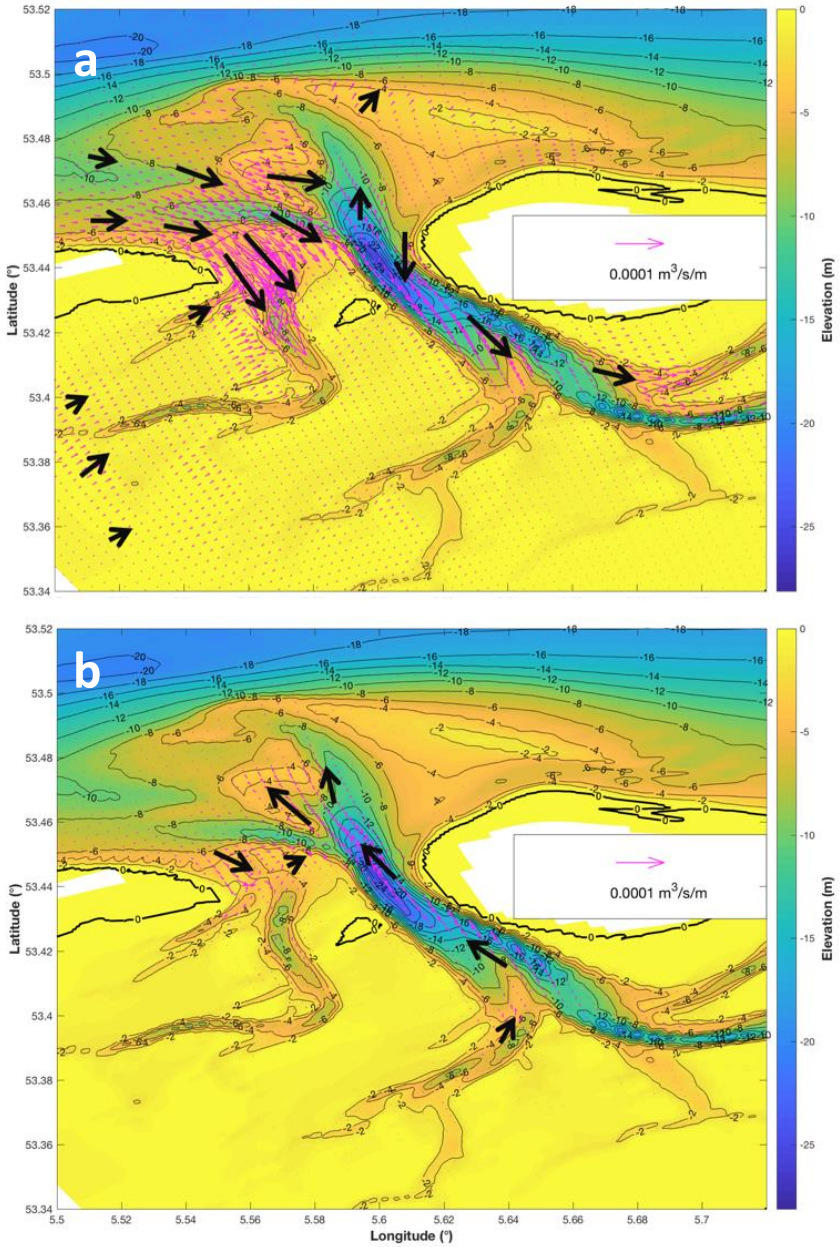

Figure 5.4 Residual transport patterns during a) the uplifting phase, b) falling phase.

5.1.2.3 Water and mass balance of the Ameland system

Figure 5.5 shows the time-series exchange of water and sediment of the Ameland Inlet during the Sinterklaas storm and the water level change at the Borndiep. Before surge rising (around the mid-day of Dec 4th), water comes into and leaves the system mainly via the inlet (2,000 m^3/s) with a very small inflow over the west watershed and outflow over the east watershed. During the uplifting phase (from the mid-day of Dec 4th to the first several hours of Dec 6th), a large amount of water enters into the system over the west watershed and simultaneously leaves over the eastern watershed. However, more water comes in the west (peak discharge of 14,000 m^3/s) than leaves in the east (peak discharge of 7,000 m^3/s). This leads to an outflow at the inlet. During the falling phase (till the mid-day of 7th Dec), the remaining water keeps being flushed out via inlet while little exchange can be found over the watersheds.

With regard to sediment exchange, the inlet starts to import sediment around 1.5 tidal cycle before the storm, of which the peak transport rate is amounted to be 0.058 m^3/s. When surge is rising, consistent sediment import through inlet is found with peak values of 0.11 m^3/s. However, export is found directly when surge is falling, which coincides with the outflow of water. Similarly, sediment enters into the basin over the west watershed and leaves over the east watershed during the rising phase. Before and after the surge rising, no clear sediment exchanges can be observed over the watersheds.

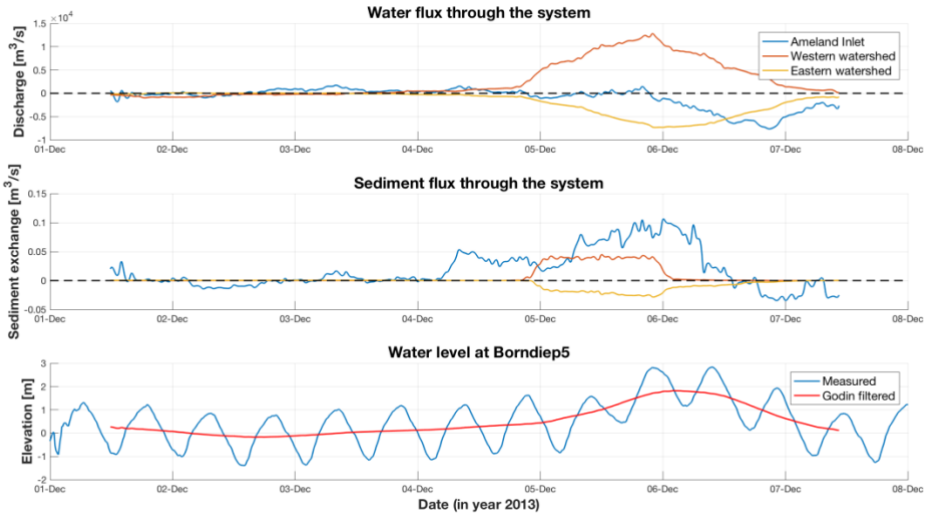

Figure 5.5 Time-series from 1st Dec to 8th Dec in 2013 of water (top) and sediment (middle) discharge through cross-sections in the Ameland Inlet system during storms in which positive means mass import into the system. The Ameland inlet, western watershed and eastern watershed are marked in blue, orange and yellow, respectively. The bottom plot shows the water level change in the same period where measured water levels are marked in blue while Godin filtered (mean water level) in red.

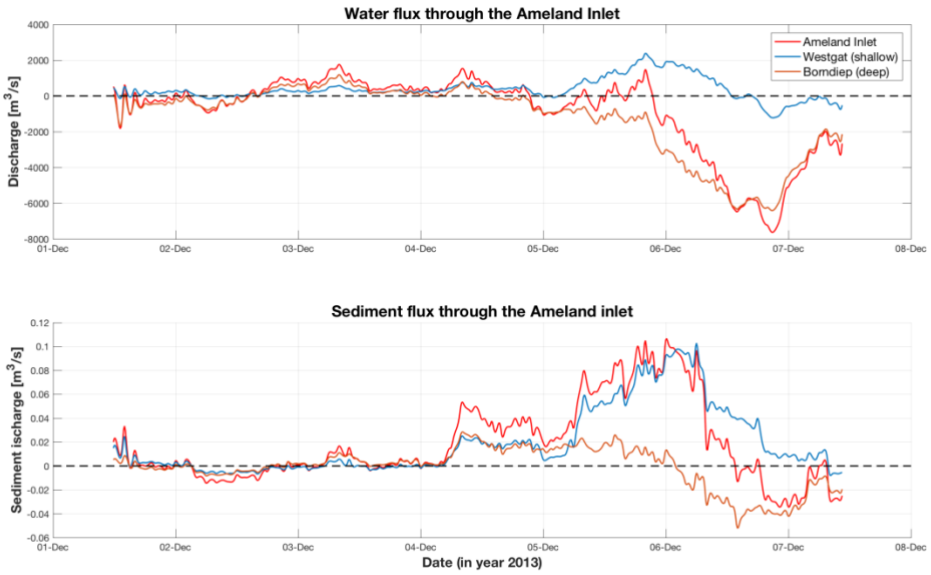

Figure 5.6 Time-series from 1st Dec to 8th Dec in 2013 of water (top) and sediment (bottom) discharge through Ameland inlet during storms in which positive means mass import into the system. The whole inlet, shallow part (Westgat) and deep channel (Borndiep) are marked in red, blue and yellow respectively.

Before surge rising, water and sediment are imported into the system at both the shallow part (Westgat) and deep channel (Borndiep) of the inlet. However, the Borndiep facilitates a small (1500 m^3/s) outflow of water during the uplifting phase, whereas initially stronger

inflow is found at the Westgat. Rising water levels in the basin accelerate the outflow through Borndiep up to 6200 m^3/s and cause a transition from inflow to outflow of water at Westgat on Dec 7th. However, sediment import is found at the Westgat both during the surge rising and falling phases. Only one-sixth of sediment import takes place at the Borndiep during the rising phase while afterwards sediment is exported locally.

5.1.3 Effect of closing off of watersheds

5.1.3.1 Residual flow

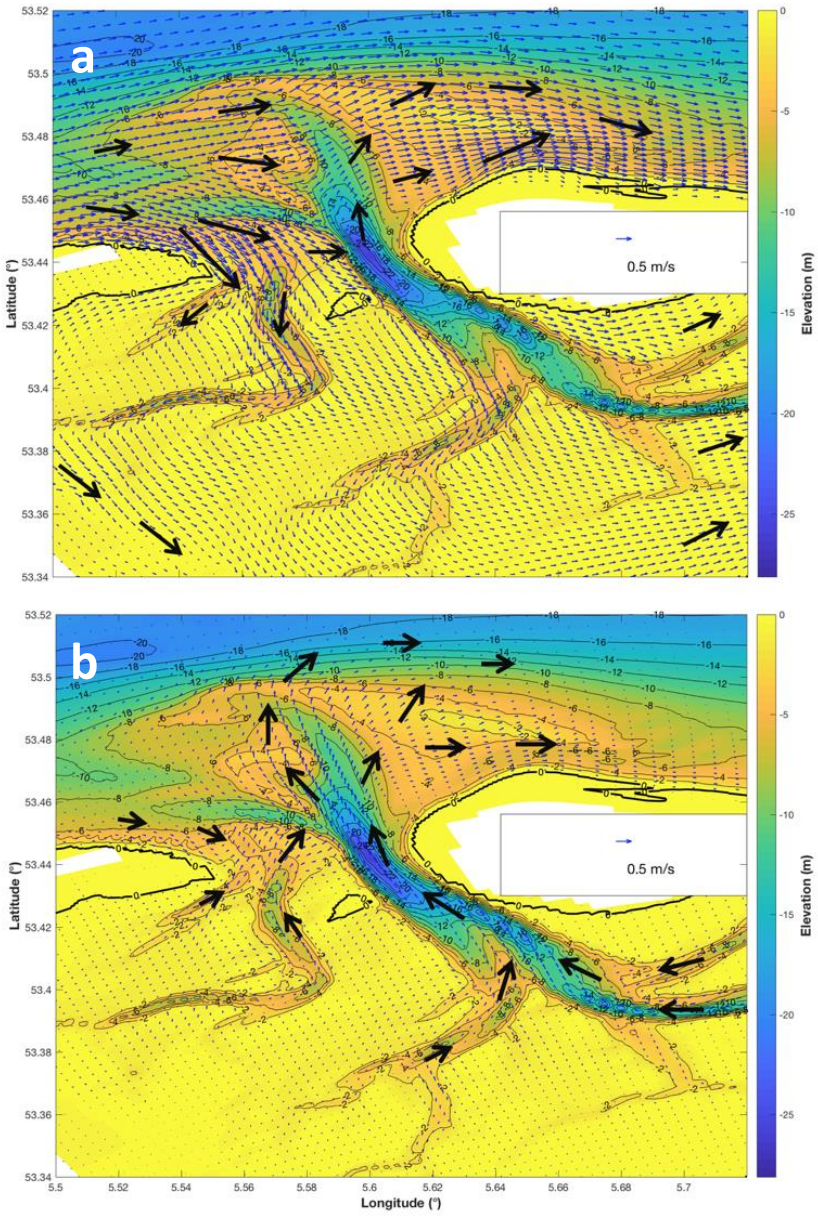

Figure 5.7 Residual flow patterns during a) the uplifting phase, b) falling phase, with dams placed on the watersheds.

Water and sediment exchange over the watersheds is blocked by placing infinitely high dams on the watersheds. The entire exchange between the North Sea and Ameland basin is via inlet. It can be seen in Figure 5.7 that Ameland Inlet features stronger residual flows compared to the previous condition (transport during storms). At both watersheds, mean

currents flow along the watersheds instead of over them. Similarly, the channel Westgat exhibits significant inflows (around 0.8 m/s) from longshore currents along Terschelling. Part of them flow into the basin through channel Boschgat while the rest flows into the main ebb channel Akkepollegat via the inlet. These ebb-directed mean currents flow over the ebb-tidal delta and encounter with offshore eastward currents at the terminal lobe, eventually leading to strong longshore eastward currents (1.0 m/s) along Ameland coast. During the falling phase, residual flow is largely reduced (around 0.1 m/s). Residual flows at all channels are in the ebb direction except for Westgat. Relatively strong ebb-directed currents (0.2-0.3 m/s) diverge at the seaward end of Akkepollegat, flow over the ebb-tidal delta and together with offshore eastward currents at the terminal lobe, forming longshore flows along the Ameland island.

5.1.3.2 Residual sediment transport

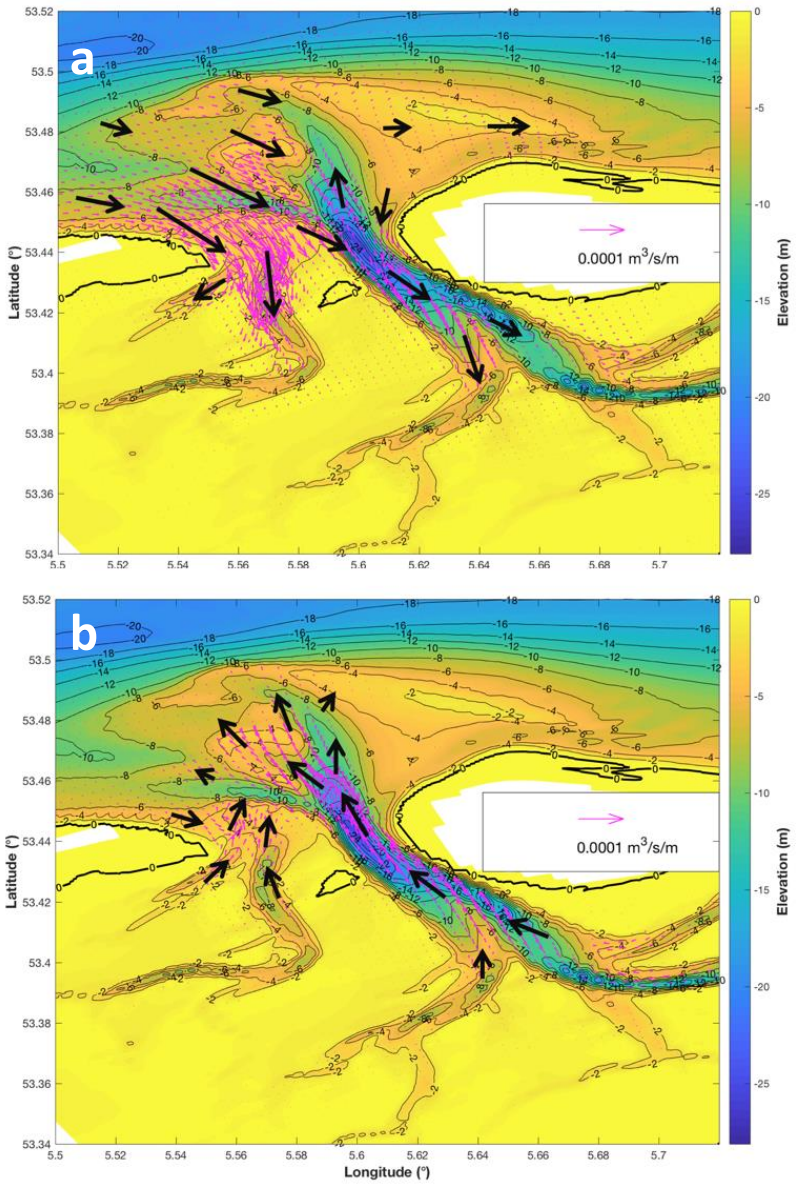

Figure 5.8 Residual sediment transport patterns during a) the uplifting phase, b) falling phase, with dams placed on the watersheds.

The total sediment transport with dams at both main and secondary channels during the rising phase is stronger than that without dams, shown in Figure 5.8 (a). Except for the main ebb channel Akkepollegat where sediment is transported out of the system, each channel is characterized by flood-directed sediment transport, causing a large amount of sediment imported into the basin. The most significant sediment input takes place at the channel Westgat (amount to 0.0003 $m^3/s/m$). Besides, NW winds result in south-eastward sediment transport at the ebb-tidal delta. After the storm, sediment is transported out of the system through all channels except for Westgat which is consistent with flow patterns.

5.1.3.3 Water and mass balance in the Ameland system

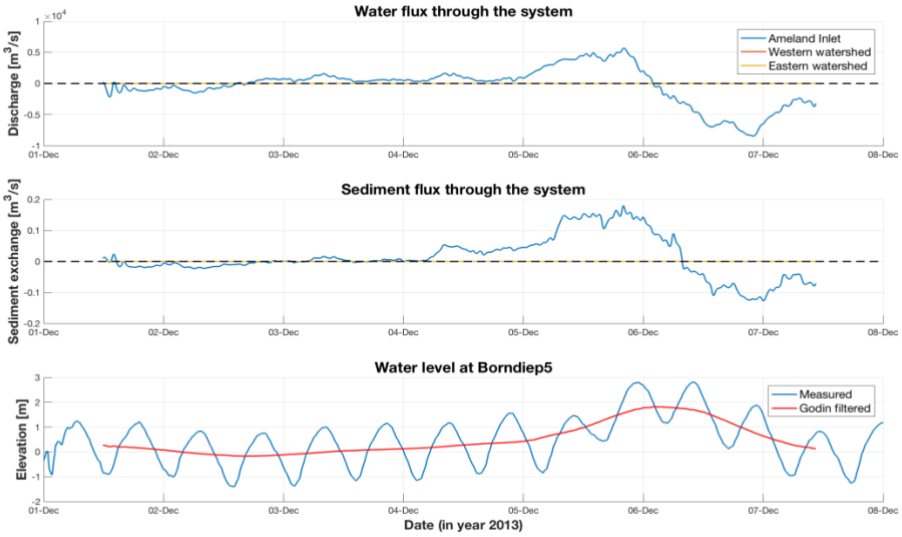

Figure 5.9 Time-series from 1st Dec to 8th Dec in 2013 of water (top) and sediment (middle) discharge through cross-sections in the Ameland Inlet system when closing off watersheds in which positive means mass import into the system. The Ameland inlet, western watershed and eastern watershed are marked in blue, orange and yellow, respectively. The bottom plot shows the water level change in the same period where measured water levels are marked in blue while Godin filtered (mean water level) in red.

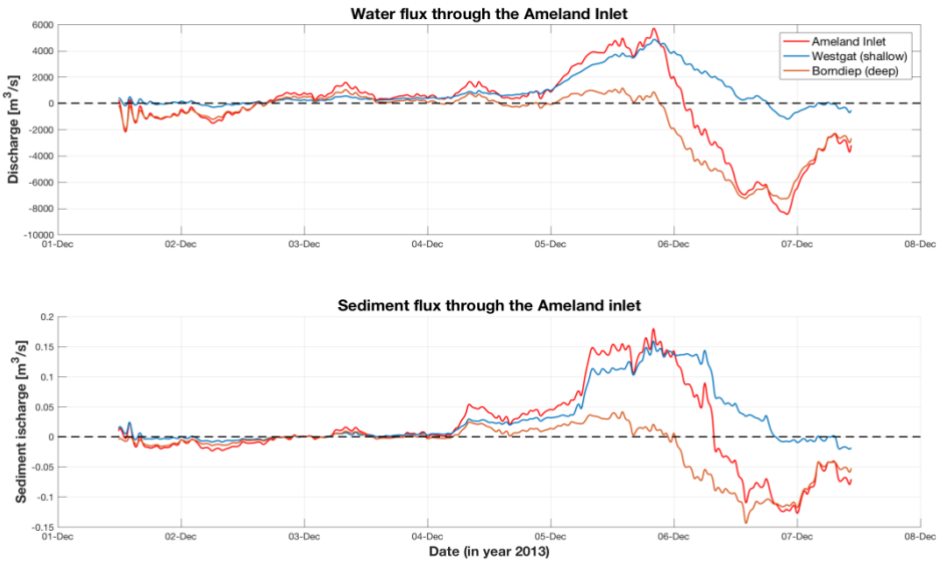

Figure 5.10 Time-series from 1st Dec to 8th Dec in 2013 of water (top) and sediment (bottom) discharge through Ameland inlet when closing off watersheds in which positive means mass import into the system. The whole inlet, shallow part (Westgat) and deep channel (Borndiep) are marked in red, blue and yellow respectively.

The placement of infinite high dams at the location of the watersheds limits the exchange of water and sediment to the inlet (see Figure 5.9). Before surge rising, small amounts of water and sediment are imported into the Ameland system. During the uplifting phase, there is a sharp increase in both water and sediment discharges up to 6000 m^3/s and 0.18 m^3/s respectively. Water leaves the basin through the inlet as the local water level drops, which accelerates the discharge to around 8000 m^3/s. The sediment exchange has the similar trend. However, the peak value of sediment import exceeds the peak value of export, resulting in a net sediment input (0.06 m^3/s). Figure 5.10 shows that most of the import of water and sediment during the storm is via the Westgat, while the Borndiep facilitates the export of water and sediment.

5.1.4 Condition of no-wind and no exchange over watersheds

5.1.4.1 Residual flow

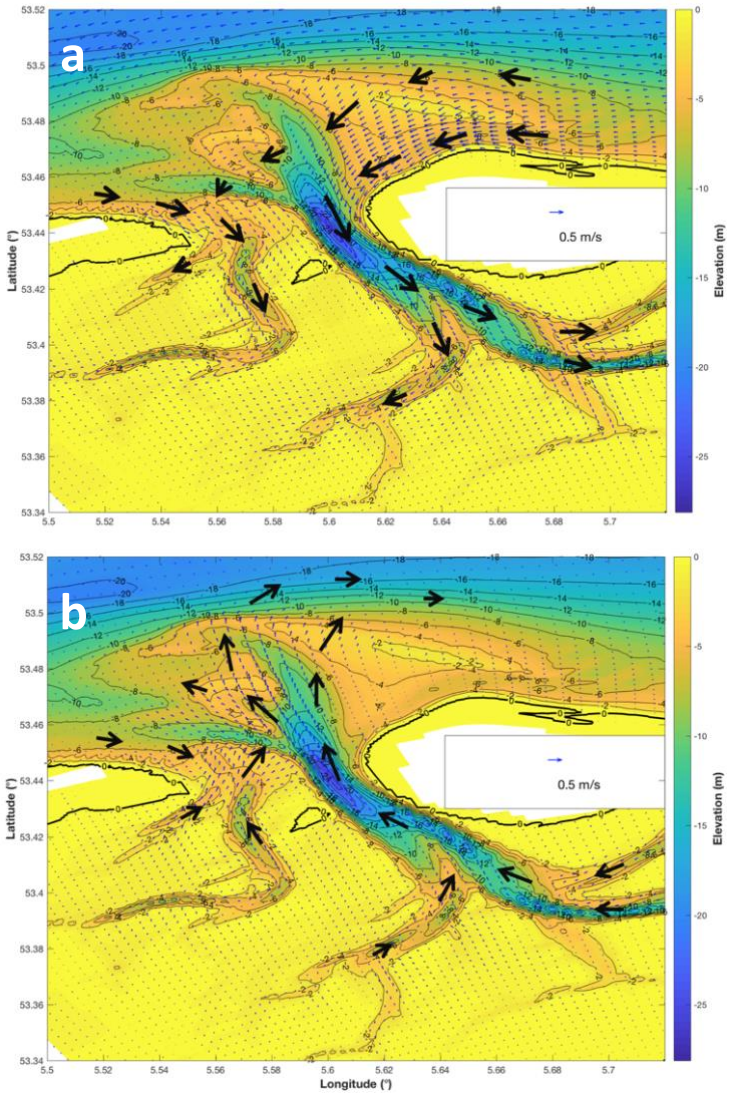

Figure 5.11 Residual flow patterns of no-wind conditions during a) the uplifting phase, b) falling phase.

Figure 5.11 shows the residual flow patterns of no-wind condition (EXT04). It can be seen that the flow patterns are totally different from previous conditions. Firstly, the magnitude of residual flows is much smaller than that of model runs EXT02 and EXT03. This reveals that

wind prevails over tides in generating residual currents. Besides, residual currents are generally stronger at the offshore region (the ebb-tidal delta and sea). It can be also observed that there is a strong inflow (0.5 m/s) through the Borndiep while the inflow through the Westgat is relative weak (0.2 m/s). Moreover, winds invert the direction of residual flows. At the offshore area, residual currents are flowing westwardly from the island of Ameland, over the ebb-tidal delta and to the Terschelling island. However, these flows are in the opposite direction (eastward) during the dam-placement condition (EXT03). The residual flow pattern of no-wind condition as water levels drop is similar with previous conditions. The water is drained through all channels except for the Westgat.

5.1.4.2 Residual sediment transport

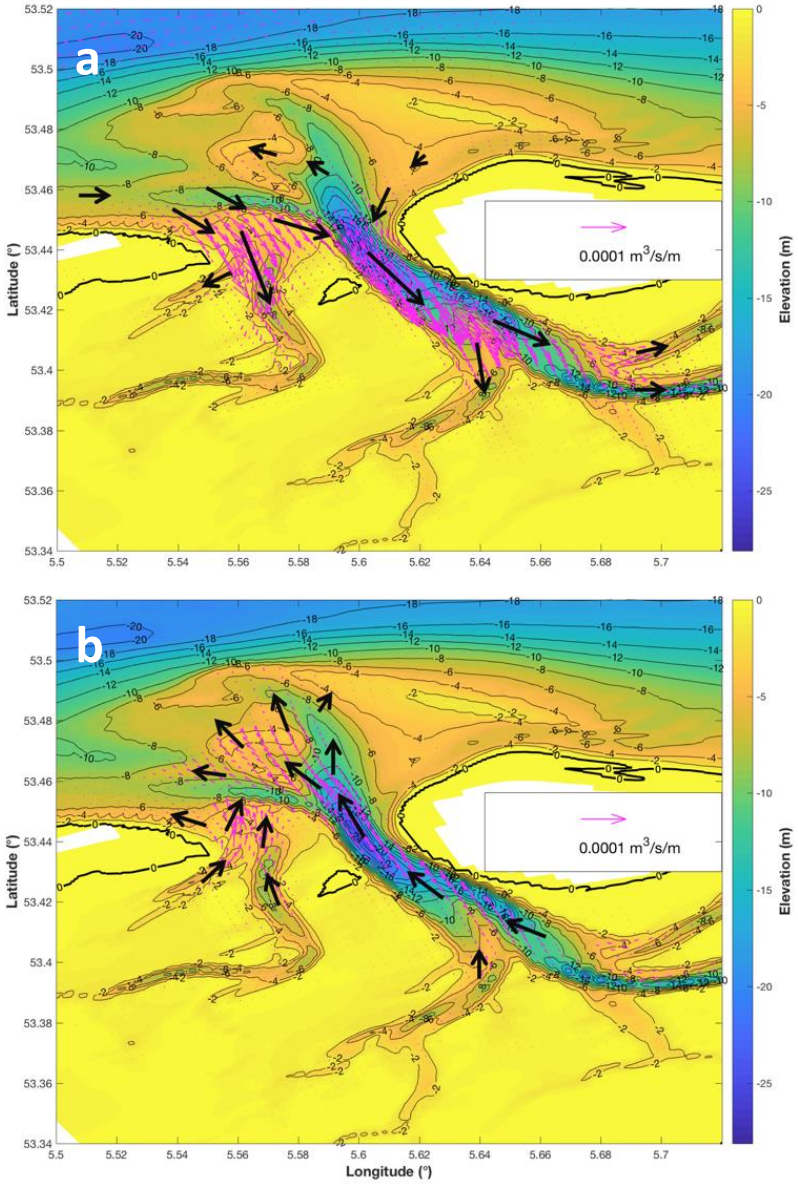

Figure 5.12 Residual sediment transport patterns of no-wind condition during: a) the uplifting phase, b) falling phase.

With regard to the sediment transport, it experiences the similar pattern as residual flows, see Figure 5.12. Unlike the situation of the model run EXT03 (closing off of watersheds), sediment is imported through the Westgat and the Borndiep. Due to the absence of winds,

no clear sediment transport activities occur at the ebb-tidal delta but only a small amount of north-westward transport through the seaward end of the main ebb channel Akkepollegat, to the west of the ebb0tidal delta. When the water level drops, the Ameland system exhibits the same pattern as that of previous conditions: functioning as the sediment drainage. However, the channel Westgat also flushes the sediment out of the system instead of importing sediment of previous conditions.

5.1.4.3 Water and mass balance in the Ameland system

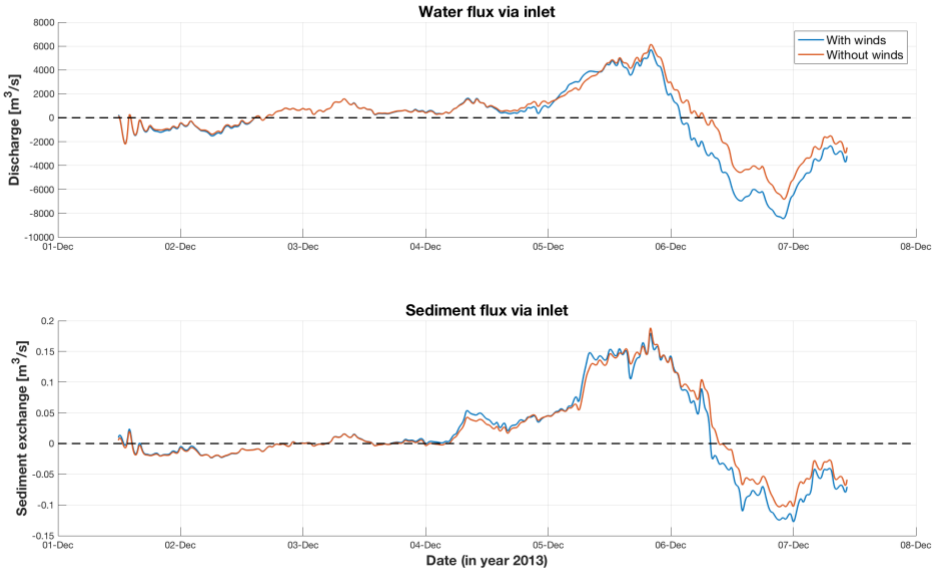

Figure 5.13 Time-series from 1st Dec to 8th Dec in 2013 of water (top) and sediment (bottom) discharge through cross-sections via the Ameland Inlet during watersheds closing off condition (blue) condition no-wind and no exchange over watersheds condition (red). The positive values mean mass import into the system while negative for export.

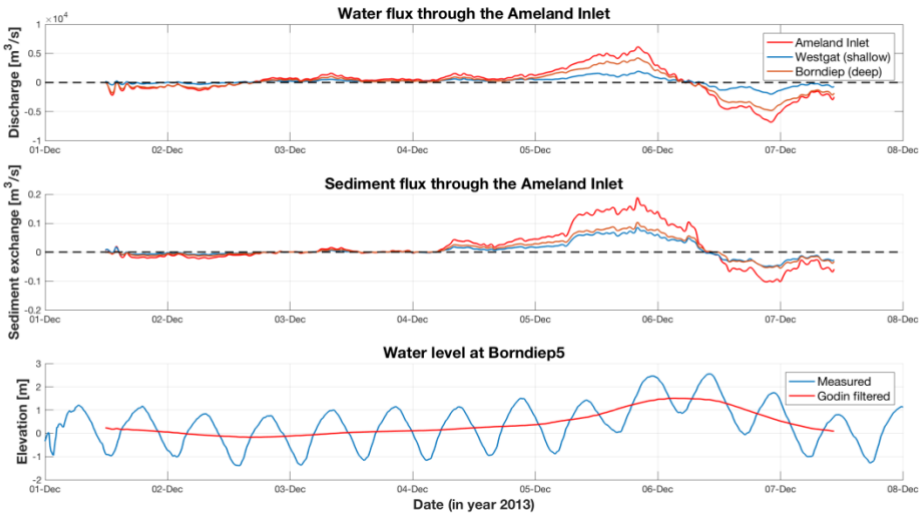

Figure 5.14 Time-series from 1st Dec to 8th Dec in 2013 of water (top) and sediment (middle) discharge through Ameland inlet during no-wind and no exchange over watersheds condition in which positive means mass import into the system. The whole inlet, shallow part (Westgat) and deep channel (Borndiep) are marked in red, blue and yellow respectively. The bottom plot shows the water level change in the same period where measured water levels are marked in blue while Godin filtered (mean water level) in red.

The time-series changes of water and sediment exchanges are indicated in comparison with those of model run EXT03, see Figure 5.13. Generally, these two experience the similar patterns. Before the storm, same amounts of water and sediment are imported for both conditions. During the surge rising, similar amounts of water and sediment are imported. However, as the water level drops the inlet is expected to flush less water and sediment out for no-wind condition with the peak output discharge of 6000 m^3/s (water) and 0.1 m^3/s (sediment).

Figure 5.14 again differentiates the Westgat and Borndiep. They have the same functions at each phase: 1) before surge rising: water and sediment input, 2) surge rising: larger water and sediment input, 3) water level decreasing: water and sediment output. Besides, two-thirds of water exchange takes place through the Borndiep while these two channels make the same contribution with regard to sediment exchange.

5.1.5 Constant surge height condition

This section corresponds to the model result of RIF401 where tides, winds and constant surge heights are applied. In this model run, storm surge has come but not left, resulting in a constant increase of 1.745 m of the mean water level.

5.1.5.1 Residual flow

Figure 5.15 shows the residual flow pattern for constant surge height condition. Local winds result in a small surge rising and falling. For both rising and falling phase, residual flow patterns do not vary too much at the ebb-delta and the sea. Offshore mean currents flow from the Ameland Island, over the ebb-tidal delta and to the Terschelling coast with decreasing magnitudes. During the uplifting phase, inflows can be found in both main and secondary channels (Borndiep and Westgat, respectively), which means water is imported into the basin via the whole inlet. Besides, the flow magnitude in the Westgat (0.6 m/s) is much larger than that in the Borndiep (0.2 m/s). However, during the falling phase, water is exported through Borndiep with the mean flow velocity of 0.5 m/s. With regard to the channel Westgat, residual currents from the longshore currents at the Ameland Island discharge into the basin, but then encounter with outflows from the basin channels Boschgat. As a result, the overall water exchange in Westgat is small and depends on relative magnitudes of longshore currents and basin outflows.

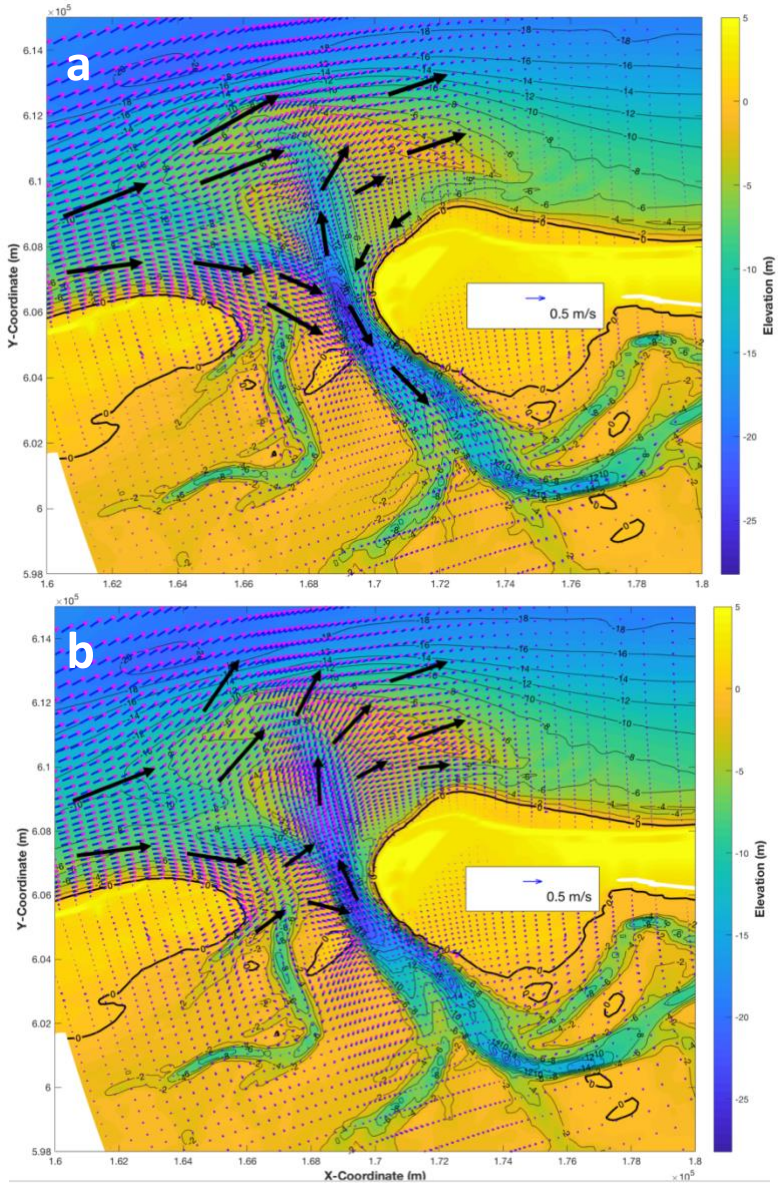

Figure 5.15 The residual flow pattern during a) rising phase, b) falling phase for constant surge height condition.

5.1.5.2 Residual sediment transport

Figure 5.16 shows the residual sediment transport pattern of constant surge height condition. At the basin, sediment is imported through the whole inlet during both wind-driven surge rising and falling phases with similar sediment transport magnitudes. The main pathway for sediment import is through the Borndiep (around 0.0008 $m^3/s/m$) whiles only a small sediment input takes place through the Westgat (0.0002 $m^3/s/m$). Compared to closing off watersheds condition (EXT03), it experiences an opposite case with the majority of sediment import occurring through the Westgat. However, during the falling, a small amount of sediment is exported seaward to the ebb-tidal delta through the Akkepollegat while no clear sediment transport can be found at the same location during rising phase.

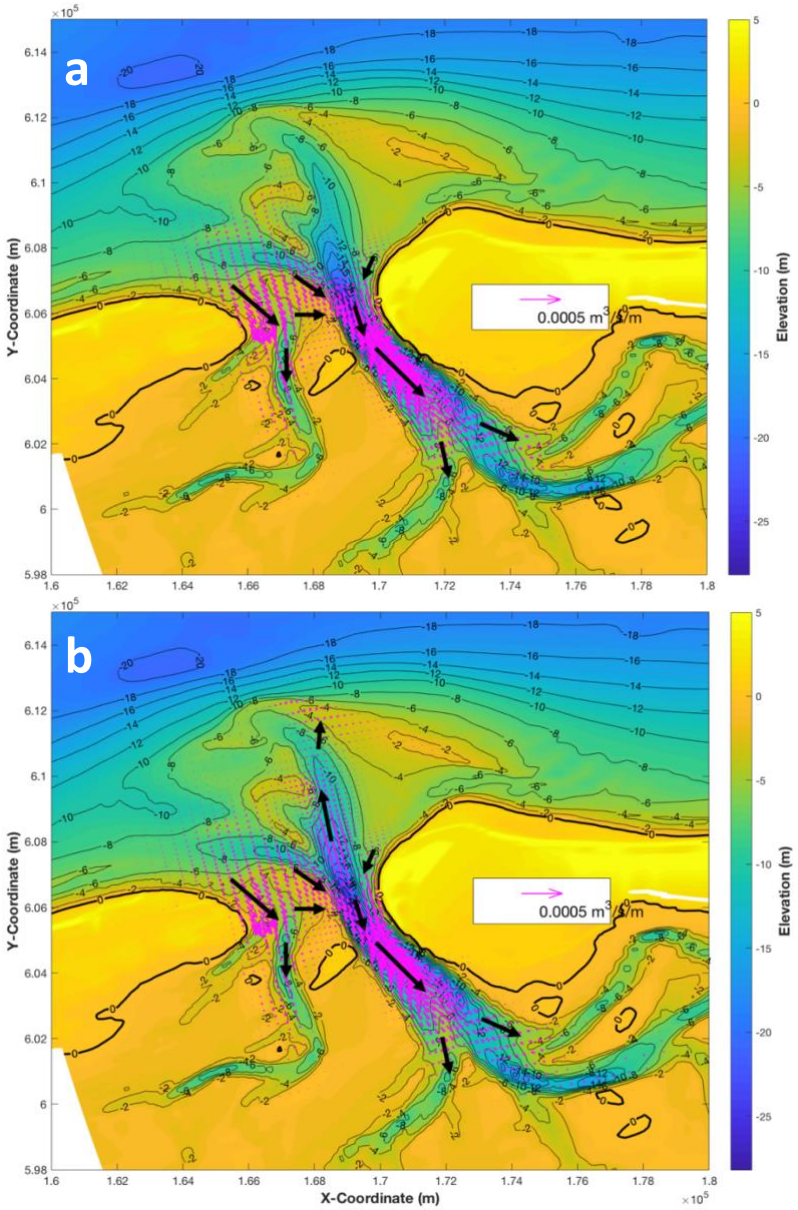

Figure 5.16 The residual sediment transport pattern during a) rising phase, b) falling phase for constant surge height condition.

5.1.5.3 Water and mass balance in the Ameland system

Figure 5.17 shows the time-series changes of water and sediment exchange as well as the mean water level at Borndiep for constant surge height condition. It can be observed that local winds impose a surge rising of around 0.2 m from the mid-day of Dec 5th till the early morning of Dec 6th. Then, the water level decreases back to the value before the surge rising on Dec 7th. In the meantime, water is imported when surge is rising but exported when falling. However, sediment is always imported into the system with equal contribution from the Westgat and the Borndiep. This sediment flux (around 0.4 to 0.6 m^3/s) is much stronger than previous conditions.

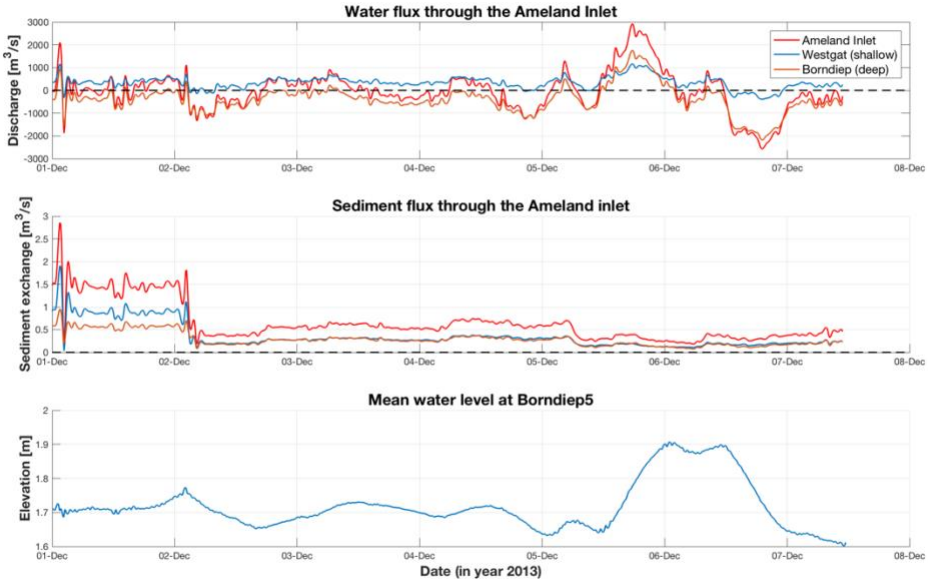

Figure 5.17 Time-series from 2nd Dec to 8th Dec in 2013 of water (top) and sediment (middle) discharge through Ameland inlet during constant surge height condition in which positive means mass import into the system. The whole inlet, Westgat and Borndiep are marked in red, blue and yellow respectively. The bottom plot shows the time-series mean water level at Borndiep.

5.2 Overall statistics for water balance and sediment budget

5.2.1 Integration period

In order to calculate the water balance and sediment budget in the Ameland system for each condition, the integration period should be firstly determined. It is defined by the duration between two times steps of model runs when the water level is zero during the surge rising and falling phases. Given that the water level is highly time and spatial dependent, it is not accurate to study the mean water level changes at one location for different conditions. Alternatively, in order to determine a proper integration period, the starting time step is selected during the rising phase while the ending time step is chosen during the falling phase with both cumulative Godin-filtered discharges through the entire basin are close to 0. Regarding to the max surge phase, the time step is corresponding to the maximum discharge during the storm, which indicates the transition from increasing to decreasing in water levels.

Figure 5.18 shows the cumulative Godin-filtered discharges for model run EXT02, EXT03 and EXT04. Since the mean values of the second half of the last tidal cycle cannot be derived when applying Godin-tidal filter, the last effective time step (928) was chosen as the ending time step for EXT04. Therefore, the starting time step (579) was selected with the same discharge as that of the ending time. For the constant surge height condition (RIF402), the surge changes are caused by local winds. It was shown in previous figures that winds generate the rise in the mean water level up to 0.32 m, which are much smaller than tidal driven (1.5 m). As a result, the integration period of model run RIF402 is determined by choosing two time steps with the same mean water levels during the surge changes.

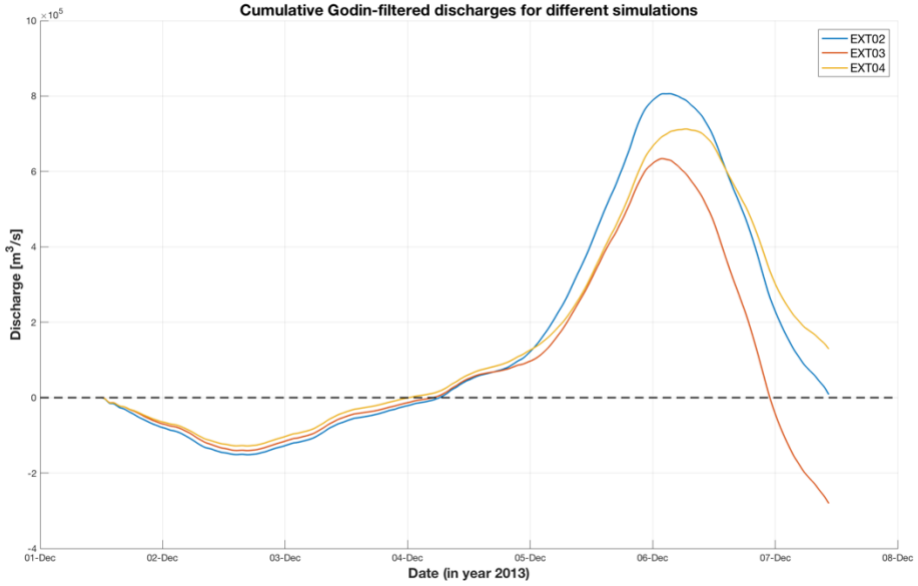

Figure 5.18 Cumulative Godin-filtered discharges for model run EXT02, EXT03 and EXT04.

Table 5.1 Integration period of water balance indicating the time steps and corresponding cumulative discharges through the whole system of surge rising, max surge and surge falling phases with the interval of time step of 10 minutes. Simulations of EXT02, EXT03, EXT04 and RIF401 correspond to the patterns during storms, watersheds closing off, no-wind and no exchange over watersheds and constant surge height conditions, respectively. For RIF401, the integration period is chosen by two time steps of the same water levels during the surge changes.

	Surge rising		Max surge		Surge falling	
Simulations	Starting time step	Cumulative discharge (m^2/s)	Time step	Cumulative discharge (m^2/s)	Ending time step	Cumulative discharge (m^2/s)
EXT02	470	-294.6	741	8.06E+05	928	8.45E+03
EXT03	463	-101.3	732	6.34E+05	859	-2.69E+03
EXT04	579	1.29E+05	760	7.13E+05	928	1.29E+05
RIF401	643	1.64	792	1.90	884	1.64

Table 5.1 shows integration periods with time steps and corresponding cumulative discharges. By comparing values for first two simulations, the surge rising periods are similar while the falling period for EXT02 is 13 hours (78 time steps) longer than that for EXT03. This means flooding of watersheds results in longer surge falling. A likely reason for this is during the falling phase water is still imported over the west watershed but less water is exported over the east watershed, causing more water would be flushed out via the inlet. Figure 5.18 indicates that it takes much more time for the inlet to drain the water without NW winds (the falling period is much longer). When it comes to the last simulation, RIF401, the period is different from previous since the local surge is only driven by local winds (constant surge height). Besides, NW wind can generate time dependent surge rise up to 0.32 m. Statistics of the model run RIF401 indicate that NW wind starts to cause surge rising at time step of 643 (around the mid-day of Dec 5th) which is quite later than previous conditions. Moreover, the period of surge changes is shorter for both rising and falling phases.

5.2.2 Water balance and sediment budget

Table 5.2 The amount of water and sediment importing into the Ameland system through the inlet, west watershed and east watershed during each condition where positive values means importing.

Inlet					
Mass	Simulations	Before storm (per tidal cycle)	Surge rising	Surge falling	Total
Water (Mm^3)	EXT02	16.14	7.89	-527.49	-519.60
	EXT03	8.91	380.87	-382.11	-1.24
	EXT04	7.10	323.74	-319.69	4.05
	RIF401	7.12	84.22	-83.05	0.72
Sediment (m^3)	EXT02	147.43	10,002.50	252.71	10,252.21
	EXT03	174.27	13,669.41	-2,821.92	10,847.49
	EXT04	133.25	12,365.00	-4,632.60	7,732.40
	RIF401	40,876.1	27,031.20	18,421.70	45,452.90
West watershed					
Mass	Simulations	Before storm (per tidal cycle)	Surge rising	Surge falling	Total
Water (Mm^3)	EXT02	10.53	1,009.80	448.25	1,458.05
	EXT03	0.00	0.00	0.00	0.00
	EXT04	0.00	0.00	0.00	0.00
	RIF401	0.00	0.00	0.00	0.00
Sediment (m^3)	EXT02	3.76	3,573.80	47.96	3,621.76
	EXT03	0.00	0.00	0.00	0.00
	EXT04	0.00	0.00	0.00	0.00
	RIF401	0.00			
East watershed					
Mass	Simulations	Before storm (per tidal cycle)	Surge rising	Surge falling	Total
Water (Mm^3)	EXT02	-0.23	-517.54	-414.60	-932.14
	EXT03	0.00	0.00	0.00	0.00
	EXT04	0.00	0.00	0.00	0.00
	RIF401	0.00	0.00	0.00	0.00

Sediment (m^3)	EXT02	-0.42	-2,050.00	-461.62	-2,551.60
	EXT03	0.00	0.00	0.00	0.00
	EXT04	0.00	0.00	0.00	0.00
	RIF401	0.00			

The quantities of water and sediment import through the inlet, west watershed and east watershed during each condition are listed in Table 5.2 where the overall situation of water and sediment exchanges can be observed. Before the storm, these exchanges are calculated by averaging the summation of water and sediment fluxes of the last two tidal cycles before water level starts to increase at the inlet, west watershed and east watershed. Similarly, values of surge rising and falling phases are calculated by adding up these fluxes according to integration periods for different model runs.

Before the storm, tidal averaged prisms are 16.14 Mm^3, 8.91 Mm^3, 7.10 Mm^3 and 7.12 Mm^3 for EXT02, EXT03, EXT04 and RIF401, respectively. This indicates that flooding of watersheds results in higher tidal prism. Similarly, NW wind is able to increase the tidal prism slightly. However, the rising in the mean water level does not affect the tidal prism.

During the rising phase, flooding of watersheds causes that water enters into the system mainly over west watershed (99%) and via inlet (only 1%), and leaves entirely over east watershed. However, during surge falling, water enters into the basin only over the west watershed and leaves via inlet (54%) and over the east watershed (46%). Unlike flow pattern, 90% of the total sediment import takes place via inlet with the rest over the west watersheds while all sediment is exported over the east watersheds.

Table 5.3 The overall exchange of water and sediment for each run.

Model run	Water (Mm^3)	Sediment(m^3)
EXT02	6.31	11,365.57
EXT03	-1.24	10,847.49
EXT04	4.05	7,732.40
RIF401	0.72	45,452.90

Table 5.2 shows the overall exchange of water and sediment for different conditions. It can be found that flooding of watersheds leading to 4.8% more sediment (518 m^3) imported into the basin. NW wind has stronger impacts on sediment transport, which causes around 3,100 m^3 sediment imported into the system. Moreover, the constant surge height results in the largest sediment input (a factor of 4 as that of the storm condition).

6 Discussion

This chapter is intended to discuss the main outcomes of this research which are the effects of flooding watersheds and winds on the patterns of residual flow and sediment transport at the Ameland Inlet. Besides, the results are compared and evaluated with previous relevant literatures.

6.1 Water exchange

Results have shown that the patterns of residual flow vary under different conditions. During the calm weathers when tides are dominant, residual currents are more confined in the channels, which agrees with the results of Pluis (2016). Besides, it was indicated that per tidal cycle, around 10.53 Mm^3 water is imported into the basin over the Terschelling watershed and 16.14 Mm^3 imported via the inlet. However, according to the results of Duran-Matute et al. (2014), the Terschelling watershed experiences the residual tidal prism of 23 Mm^3 while an outflow exists at the inlet throat (around 12 Mm^3) computed by the average of every tidal period during 2009 and 2010. A likely reason for this difference could be wind effects as winds can render residual flows highly variable (Duran-Matute et al., 2014). During the model period of Duran-Matute et al. (2014), southwestern winds took place continuously for two weeks in November while northwestern winds are dominant in this research. Besides, the difference can also be explained by in this research, the tidal averaged water exchange was calculated based on four-day data before the storm event. As a result, results are less accurate compared to Duran-Matute et al. (2014).

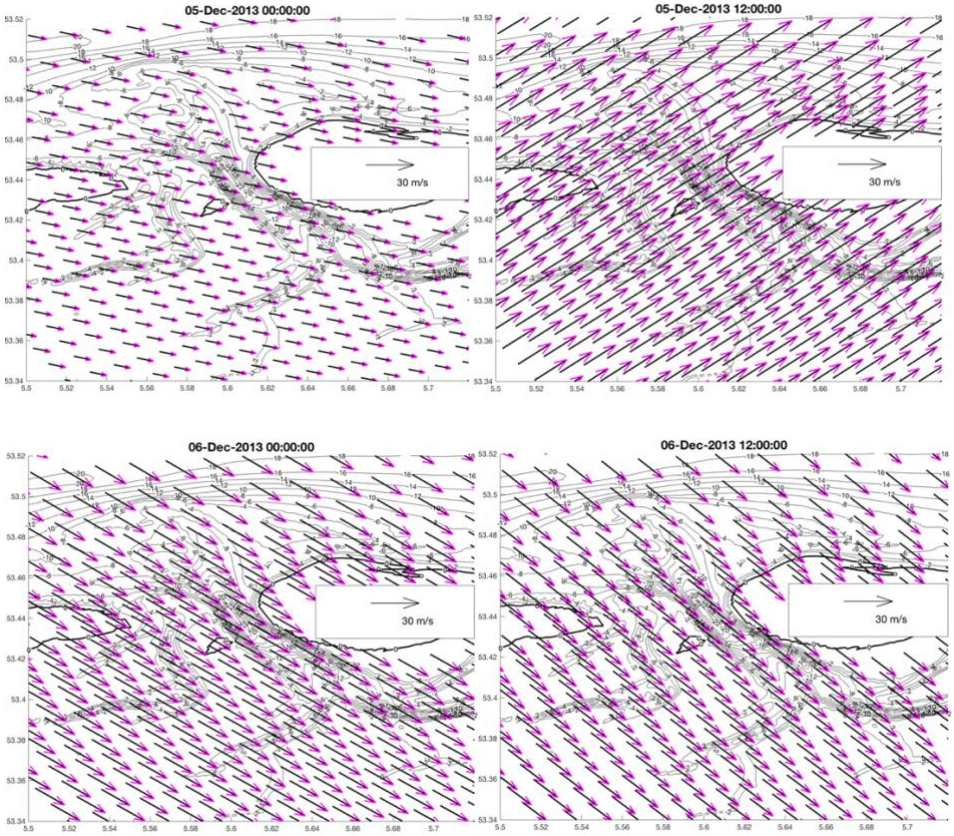

Figure 6.1 Wind data at 00:00 of Dec 5th (top left), 12:00 of Dec 5th (top right), Dec 5th (bottom left) and 12:00 of Dec 6th (bottom right) with the length of arrows indicating wind magnitude and pink headings for direction.

Figure 5.18 and Table 6.1 show that the time of surge falling (around 21 hours) for model run EXT03 is much shorter than that (around 34 hours) for EXT04. This could be explained by wind effects. By closely looking at the wind data, the wind direction is from west to southwest (5th Dec) and then to northwest (6th Dec), see Figure 6.1. As a result, in the first half of the storm, part of water is expected to be exported seaward out of the system due to southern and south-western winds, which decreases the time of falling phase for EXT04 compared to no-wind condition.

6.2 NW wind effects

Comparison between Figure 5.7 and 5.11 reveals how NW winds affect residual flow pattern. Firstly, it can be observed that winds generate residual currents that exceed tidal and surge driven, which is in accordance with results of Li (2013) and Duran-Matute et al. (2014). Besides, Duran-Matute et al. (2014) found that SW winds in excess of 15 m/s cause the inversion of the residual flow direction. Results in this research show that NW winds invert the residual flow direction in the main channel (the Borndiep) and along Ameland island from north-eastern (ebb) to south-western (flood). This research also indicates that the residual flow in the secondary channel (the Westgat) and along Terschelling island is strengthened by NW winds. Moreover, winds have more impacts at offshore region (the ebb-tidal delta and the sea).

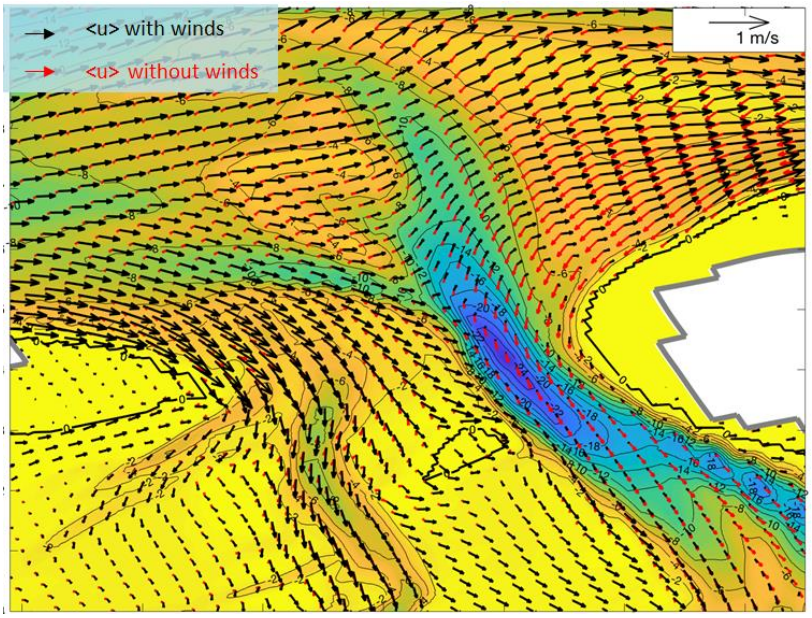

Figure 6.2 Comparison between depth averaged residual currents at the inlet with (black) and without NW winds (red).

6.3 Sediment exchange and changing tidal asymmetry

Results show that during the calm condition, the sediment transport is confined to channels where import occurs at the secondary channel Westgat and export takes place mainly through the main channel Borndiep. Compared with the results of Herrling & Winter (2014), the study area Otzumer Balje inlet system experiences the similar transport pattern. Besides, Table 5.1 indicates that sediment exchange takes place over watersheds with input over the west and output over the east.

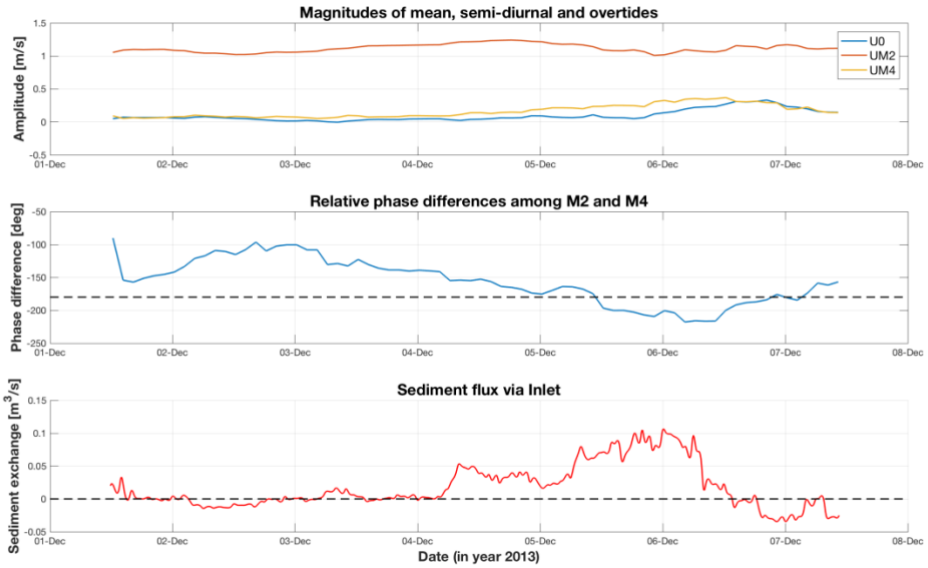

Figure 6.3 The tidal asymmetry in the main channel Borndiep during storms. Magnitudes of U_0, U_{M2} and U_{M4} are shown in the top figure while the relative phase difference ($(\varphi_{M_4} - 2\varphi_{M_2})$ is indicated in the middle figure. In the meanwhile, sediment flux changes via Inlet are shown at the bottom.

Storm is expected to result in landward sediment transport. From Table 5.2, it can be observed that model run RIF401 (constant surge height condition) experiences the largest amount of sediment input. Besides, the flooding watersheds result in more sediment imported into the basin. It is interesting to note that although outflows occur at the inlet, local sediment is still imported into the basin from time-series evolution figures (e.g. Figure 5.5 and 5.6). This could be explained by tidal asymmetry is excluded in flows by applying Godin tidal filter while sediment transport is as a result of tidal asymmetry and mean flows. According to Dronkers (1986), magnitudes of tidal constituents and their relative phase differences determine the bed-load transport. The suspended transport is caused by the duration asymmetry and spatial settling lag. Figure 6.3 shows the analysis of tidal asymmetry of changes in magnitudes of U_{M_0}, U_{M_2} and U_{M_4}, and in the phase difference $(\varphi_{M_4} - 2\varphi_{M_2})$ in the main channel Borndiep. It indicates that surge rising (from the mid-day of Dec 4th to mid-day of Dec 6th) results in the reduction of ebb dominance as the phase lag decreases from -180° to -220°. Although at this period the inlet exhibits ebb-dominance, the sediment is transported landward due to the increase in the magnitude of mean flows. As mean water level drops (from the mid-day of Dec 6th till the end of simulation), the phase difference goes back to -180°, leading to an increase of ebb dominance. In the meantime, the magnitude of mean currents decreases. As a result, the Ameland Inlet experiences sediment export when surge is falling. Lenstra (2018) investigated the effect of cyclic channel systems on the sediment transport in the Ameland Inlet. He found that rising in the mean water level decreases original ebb dominance and thus leads to flood-dominated tidal flows in the inlet. A likely explanation for this difference is that winds were not taken into consideration in his model simulations since winds can also induce surge rising. Besides, it was shown that winds generate residual currents that exceed tidal and surge driven.

A dynamic storm is expected to result in overall sediment import into the basin with balancing water. During the rising phase, a large amount of water enters into the system, leading to increases in the water level and residual flow velocity. It was shown that this reduces the ebb dominance in the inlet which therefore results in landward sediment transport associated with increasing mean flow magnitude. As surge is falling, water leaves

the basin with the water level back to its normal situation. Besides, it increases the ebb dominance but decreases the magnitude of mean flows. As a result, sediment is exported out of the basin. Overall, the amount of water is kept the same as storms come in and go out; however, sediment is imported because of the changing tidal asymmetry resulted from changing mean water levels.

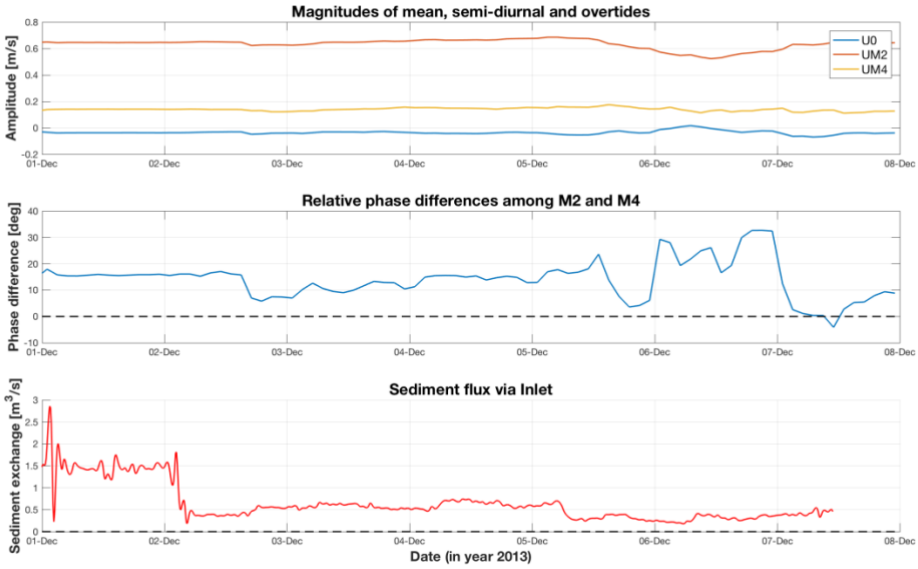

Figure 6.4 The tidal asymmetry in the main channel Borndiep for constant surge height condition. Magnitudes of U_0, U_{M2} and U_{M4} are shown in the top figure while the relative phase difference ($(\varphi_{M_4} - 2\varphi_{M_2})$ is indicated in the middle figure. In the meanwhile, sediment flux changes via Inlet are shown at the bottom.

In comparison, a constant surge height 1.745 m is added to the mean water level in the model run RIF401. Results of this run shows that 4 times larger of amount of sediment is imported per tidal cycle compared to the storm condition. Figure 6.4 shows the analysis of tidal asymmetry of changes in magnitudes of U_{M_0}, U_{M_2} and U_{M_4}, and in the phase difference ($\varphi_{M_4} - 2\varphi_{M_2}$) in the main channel Borndiep. It can be observed that the phase differences vary from 20° to 30°. As expected, sediment is always imported to the basin since the storm has come in but never gone out. Although it was shown that local winds result in a small surge of 0.2 m rising and falling (the phase difference fluctuates from the mid-day of Dec 5th to Dec 7th), the Ameland Inlet is still flood dominant. Unlike the default storm condition (EXT02), the Ameland Inlet experiences originally flood dominance. This could be explained by that in this model run an original mean water level of 1.745 m was applied in the whole basin while in the default storm run the water level starts from 0.

6.4 Limitations and further studies

This research gave an insight on how flooding watersheds and winds influence local flow and sediment transport patterns at the Ameland inlet system. As an import agent, waves are suggested to be considered in order to study these effects more accurately. Other literatures state that waves strongly affect offshore residual currents and sediment patterns especially during storms (e.g. Herrling & Winter, 2014). Besides, this research indicates the effects of flooding of watersheds during a large-scale storm, the Sinterklaas Storm. However, whether minor or moderate storms have similar impacts is not able to be shown. Thus, this research should be extended to more storms with different scales and winds directions.

7 Conclusion

In this master thesis, the patterns of flow and sediment transport during different conditions were examined using a series of model simulations in DELFT3D-FLOW. Results showed how flooding watersheds and winds affected these patterns by comparing the outcomes of each model run.

At the ebb-tidal delta, flooding of watersheds does not have too much influence. Residual flows and sediment transport are in the similar direction and magnitude. However, the NW wind has strong impacts at the ebb-tidal delta and more offshore region. Firstly, it generates much stronger residual currents than tides do, which shows a high agreement with the findings of Duran-Matute et al. (2014). Secondly, it inverts the residual flow direction along the Ameland Island from north-eastern (ebb-directed) to south-western (flood-directed). Besides, it strengths residual flows along Terschelling island. As a result, the NW winds leads to strong eastward mean currents at the ebb-tidal delta.

In the basin, flooding of watersheds has several effects. First, during surge rising, water enters into the system mainly over west watershed (99%) and via inlet (only 1%), and leaves entirely over east watershed. However, during surge falling, water enters into the basin only over the west watershed and leaves via inlet (54%) and over the east watershed (46%). 90% of the total sediment import takes place via inlet with the rest over the west watersheds while all sediment is exported over the east watersheds. Besides, around 4.8% more sediment (518 m^3) is imported owning to the connectivity of basins. Compared to flooding of watersheds, the NW wind is less significant in the basin. It inverts residual flow direction in the main channel (the Borndiep) and strengthens residual flows in the secondary channel (the Westgat). Besides, the NW wind has stronger impacts on sediment transport. It causes 43% more sediment (3,100 m^3) imported into the basin.

It was shown that a dynamic storm leads to sediment import when surge is rising but export when falling in the Ameland system. Moreover, the rising in the mean water level results in the reduction of ebb dominance. Together with the increase in the mean flow magnitude due to surge rising, it thus causes landward sediment transport. As surge is falling, both mean flow magnitude and mean water level decrease, leading to seaward sediment transport. In contrast, a passing storm with constant surge height (storm comes in but does not leave) results in all the time flood dominance, therefore leading to a factor of 4 more sediment import compared to a dynamic storm.

In conclusion, flooding of watersheds is more important on affecting flow and sediment transport patterns in the basin while the NW wind prevails at the ebb-tidal delta and more offshore region.

8 References

Arcadis (2017). *Plan van aanpak Meerjarige veldmetingen Eems-Dollard*. Retrieved Mar 1, 2018, from https://www.tenderned.nl/tenderned-web/.../1529436

Beets, D. J., & van der Spek, A. J. (2000). The Holocene evolution of the barrier and the back-barrier basins of Belgium and the Netherlands as a function of late Weichselian morphology, relative sea-level rise and sediment supply. *Netherlands Journal of Geosciences, 79*(1), 3-16.

Bertin, X., Fortunato, A. B., & Oliveira, A. (2009a). A modeling-based analysis of processes driving wave-dominated inlets. *Continental Shelf Research*, *29*(5-6), 819-834.

Bruun, P., & Gerritsen, F. (1959). Natural by-passing of sand at coastal inlets. *Journal of the Waterways and Harbors Division*, *85*(4), 75-108.

Buijsman, M. C., & Ridderinkhof, H. (2007). Long-term ferry-ADCP observations of tidal currents in the Marsdiep inlet. *Journal of Sea Research*, *57*(4), 237-256.

Carr-Betts, E., Beck, T.M., & Kraus, N.C. (2012). Tidal inlet morphology classification and empirical determination of seaward and down-drift extents of tidal inlets. *Journal of Coastal Research, 28*, 547-556.

Carrion Aretxabala, B. I. (2015). *Morphological impact of the Sinterklaas storm at Het Zwin: Numerical modelling with XBeach.* (Master's thesis). Delft University of Technology, Delft, The Netherlands.

Charnock, H. (1955). Wind stress on a water surface. *Quarterly Journal of the Royal Meteorological Society*, *81*(350), 639-640.

Cheung, K. F., Gerritsen, F., & Cleveringa, J. (2007). Morphodynamics and sand bypassing at Ameland inlet, the Netherlands. *Journal of Coastal Research*, 106-118.

Davies, J. L. (1964). A morphogenic approach to world shorelines. *Zeitschrift fur Geomorphologie, 8*, 127-142.

Davis R.A. & FitzGerald D.M. (2004). *Beaches and Coasts*. Oxford: Blackwell. pp. 419

deBeaumont, E. (1845). *Lemons de geologic*. Pratique: Paris, pp. 223-252.

De Fockert, A. (2008). *Impact of Relative Sea Level Rise on the Ameland Inlet Morphology* (Master's thesis). Delft University of Technology, Delft, The Netherlands.

Deltares (2014). *Delft3D-FLOW User Manual (Version 3.15.34158).* Delft, The Netherlands: Deltares.

Deltares (2014). *Regionale advisering Ameland Noordwest.* Retrieved May 1, 2018, from http://publications.deltares.nl/1209381_008d.pdf

De Swart, H. E., & Zimmerman, J. T. F. (2009). Morphodynamics of tidal inlet systems. *Annual review of fluid mechanics, 41*, 203-229.

Dissanayake, D. M. P. K., Roelvink, J. A., & Van der Wegen, M. (2009). Modelled channel patterns in a schematized tidal inlet. *Coastal Engineering*, *56*(11-12), 1069-1083.

Dissanayake, D. M. P. K., Ranasinghe, R. W. M. R. J. B., & Roelvink, J. A. (2012). The morphological response of large tidal inlet/basin systems to relative sea level rise. *Climatic change, 113*(2), 253-276.

Dronkers, J. (1986). Tidal asymmetry and estuarine morphology. *Netherlands Journal of Sea Research, 20(2-3), 117-131.*

Duran-Matute, M., Gerkema, T., De Boer, G. J., Nauw, J. J., & Gräwe, U. (2014). Residual circulation and freshwater transport in the Dutch Wadden Sea: a numerical modelling s tudy. *Ocean Science, 10*(4), 611-632.

EDMED (2009). *Netherlands National Monitoring of bathymetric data along the North Sea Coast (1965 -).* Retrieved Nov 18, 2017, from British Oceanographic Data Centre: https://www.bodc.ac.uk/resources/inventories/edmed/report/2954/

Engquist, B., & Majda, A. (1977). Absorbing boundary conditions for numerical simulation

of waves. *Proceedings of the National Academy of Sciences, 74(5),* 1765-1766.

Elias, E.P.L., & Bruens, A. (2013). Beheerbibliotheek Ameland–Feiten & cijfers *terondersteuning van de jaarlijkste toetsing van de kustlijn* (Project 1207724-004) (In Dutch). Delft, The Netherlands: Deltares.

Elias, E. P. L., Van der Spek, A. J. F., Wang, Z. B., & De Ronde, J. (2012). Morphodynamic development and sediment budget of the Dutch Wadden Sea over the last century. *Netherlands Journal of Geosciences, 91*(3), 293-310.

Elias, E.P.L., & Bruens, A. (2012). *Beheerbibliotheek Ameland – Feiten & cijfers ter ondersteuning van de jaarlijkste toetsing van de kustlijn* (Project 1207724- 004) (In Dutch). Delft, The Netherlands: Deltares.

Fisk, H. N. (1959). Padre Island and the Laguna Madre flats, coastal south Texas. *2nd Coastal Geography* (pp. 103-151). Conf., Louisiana State Univ., Baton Rouge, La.

Fitzgerald, D.M. (1982). Sediment bypassing at mixed energy tidal inlets. *Proceedings of 18th Coastal Engineering Conference*, 1094-1118.

Fitzgerald, D.M., Kraus, N.C., & Hands, E.B. (2000*). Natural Mechanisms of Sediment Bypassing at Tidal Inlets* (ERDC/CHL CHETN-IV-30). Vicksburg, MS, U.S.A.: US Army Corps of Engineers, Engineering Research and Development Center, Coastal and Hydraulics Laboratory.

Gerkema, T., Nauw, J. J., & van der Hout, C. M. (2014). Measurements on the transport of suspended particulate matter in the Vlie Inlet. *Netherlands Journal of Geosciences*, *93*(3), 95-105.

Giardino, A., Mulder, J., Ronde, J. D., & Stronkhorst, J. (2011). Sustainable development of the dutch coast: Present and future. *Journal of Coastal Research,* 166-172.

Hayes, M.O. (1975). Morphology of sand accumulation. In L.E. Cronin (Eds.), *Estuarine Research: Vol. 2* (pp. 3-22). New York, U.S.A.: Academic Press.

Hayes, M.O. (1979). Barrier island morphology as a function of tidal and wave regime. In S. Leatherman (Eds.), *Barrier Islands, from the Gulf of St. Lawrence to the Gulf of Mexico* (pp. 1-27). New York, U.S.A.: Academic Press.

Hayes, M.O. (1980). General morphology and sedimentpatterns in tidal inlets. *Sedimentary Geology, 26*, 139-156.

Hayes, M. O., & FitzGerald, D. M. (2013). Origin, evolution, and classification of tidal inlets. *Journal of Coastal Research, 69*(sp1), 14-33.

Herrling, G., & Winter, C. (2014). Morphological and sedimentological response of a mixed-energy barrier island tidal inlet to storm and fair-weather conditions. *Earth Surface Dynamics, 2*, 363-382.

Hoyt, J. H. (1967). Barrier island formation. *Geological Society of America Bulletin, 78*(9), 1125-1136.

Israël, C.G. (1998). *Morfologische ontwikkeling Amelander Zeegat* (Werkdocument RIKZ/OS-98.147X) (In Dutch). The Hague, The Netherlands: Rijkswaterstaat RIKZ. 95

Israël, C.G., & Dunsbergen, D.W. (1999). Cyclic morphological development of the Ameland Inlet, The Netherlands. *Proceedings of the Symposium on River, Coastal and Estuarine Morphodynamics (Genova, Italy), Vol. II*, 705–714.

Jiao, J. (2014). *Morphodynamics of Ameland Inlet: Medium-term Delft3D Modelling* (Master's thesis). Delft University of Technology, Delft, The Netherlands.

Kraus, N. C. (1998). Inlet cross-sectional area calculated by process-based model. *Coastal Engineering Proceedings, 1*(26).

Kraus, N. C. (2000). Reservoir model of ebb-tidal shoal evolution and sand bypassing. *Journal of Waterway, Port, Coastal, and Ocean Engineering, 126*(6), 305-313.

Lesser, G. R., Roelvink, J. V., Van Kester, J. A. T. M., & Stelling, G. S. (2004). Development and validation of a three-dimensional morphological model. *Coastal engineering, 51*(8-9), 883-915.

Li, C. (2013). Subtidal water flux through a multiple-inlet system: Observations before and during a cold front event and numerical experiments. *Journal of Geophysical Research: Oceans*, *118*(4), 1877-1892.

Nahon, A., Bertin, X., Fortunato, A. B., & Oliveira, A. (2012). Process-based 2DH morphodynamic modeling of tidal inlets: a comparison with empirical classifications and theories*. Marine Geology, 291*, 1-11.

Pluis, S. (2016*). Complex patterns of wave- and tide-driven flow and sediment transport on the cyclic ebb-tidal delta of the Ameland inlet – A short-term model study with a coupled Delft3D-model* (Master's thesis). Utrecht University, Utrecht, The Netherlands.

Price, W. A. (1962). Origin of barrier chain and beach ridge (abs.): Geol. *Soc. America Ann. Mtg. Program*, 119.

Oost, A. P., Hoekstra, P., Wiersma, A., Flemming, B., Lammerts, E. J., Pejrup, M., ... & Van der Berg, M. W. (2012). Barrier island management: Lessons from the past and directions for the future*. Ocean & coastal management, 68*, 18-38.

Ranasinghe, R., & Pattiaratchi, C. (2003). The seasonal closure of tidal inlets: causes and effects. *Coastal engineering journal*, *45*(4), 601-627.

Ridderinkhof, H. (1988a). Tidal and residual flows in the Western Dutch Wadden Sea I: numerical model results. *Netherlands Journal of Sea Research*, *22*(1), 1-21.

Ridderinkhof, W., Hoekstra, P., Van der Vegt, M., & De Swart, H.E. (2016). Cylic behaviour of sandy shoals on the Ebb-tidal deltas of the Wadden Sea. *Continental Shelf Research, 115*, 14-26.

Ridderinkhof, W., Swart, H. E., Vegt, M., & Hoekstra, P. (2016). Modeling the growth and migration of sandy shoals on ebb-tidal deltas. *Journal of Geophysical Research: Earth Surface*, *121*(7), 1351-1372.

Rusnak, G.A. (1960), *Sediments of Laguna Madre, Texas*. pp. 153-196.

Sha, L.P. (1989). Variation in ebb-delta morphologies along the West and East Frisian Islands, The Netherlands and Germany. *Marine Geology, 89*, 11–28.

Sha, L.P. (1990). *Sedimentological studies of the Ebb-tidal deltas along the West Frisian Islands, The Netherlands* (Published doctoral thesis). Utrecht University, Utrecht, The Netherlands: Geologica Ultraiectina.

Sha, L.P., & Van den Berg, J.H. (1993). Variation in ebb-tidal delta geometry along the coast of The Netherlands and the German Bight. *Journal of Coastal Research, 9*, 730–746.

Shepard, F. P., & Moore, D. G. (1955). Central Texas coast sedimentation: characteristics of sedimentary environment, recent history, and diagenesis: part 2. *AAPG Bulletin, 39*(8), 1463-1593.

Shepard, F.P. (1960). Recent sediments, northwest Gulf of Mexico: Tulsa, Okla., Am. *Assoc. Petroleum Geologists,* pp. 394.

Shirahata, K., Yoshimoto, S., Tsuchihara, T., & Ishida, S. (2016). Digital Filters to Eliminate or Separate Tidal Components in Groundwater Observation Time-Series Data. *Japan Agricultural Research Quarterly: JARQ*, *50*(3), 241-252.

Stronkhorst, J., Mulder, J.P.M., de Ronde, J, Huisman, B. & Sprengers, C. (2000) *LARGE-SCALE SAND NOURISHMENT STRATEGY OF THE DUTCH COAST; A SYSTEMS APPROACH.* Retrieved Dec 18, 2017, from www.vliz.be/imisdocs/publications/241293.pdf

Steetzel, H. (1995). *Voorspelling ontwikkeling kustlijn en buiten-delta's Waddenkust over de period 1990-2040* (WL rapport H1887) (in Dutch). The Netherlands: Waterloopkundig Laboratorium.

Stelling, G. S. (1983). On the construction of computational methods for shallow water flow problems.

Stutz, M. L., & Pilkey, O. H. (2011). Open-ocean barrier islands: global influence of climatic, oceanographic, and depositional settings. *Journal of Coastal Research*, *27*(2), 207-222.

Van de Kreeke, J., Brouwer, R. L., Zitman, T. J., & Schuttelaars, H. M. (2008). The effect of a topographic high on the morphological stability of a two-inlet bay system. *Coastal Engineering*, *55*(4), 319-332.

Van Rijn, L.C., Walstra, D.J.R., & Van Ormondt, M. (2004). *Description of TRANSPOR2004 and Implementation in DELFT3D-ONLINE* (Report Z3748.10). Delft, The Netherlands: Deltares.

Van Rijn, L.C. (2007a). Unified View of Sediment Transport by Currents and Waves. I: Initiation of Motion, Bed Roughness, and Bed-Load Transport. *Journal of Hydraulic Engineering, 133*, 649-667.

Van Rijn, L.C. (2007b). Unified View of Sediment Transport by Currents and Waves. II: Suspended Transport. *Journal of Hydraulic Engineering, 133*, 668-689.

Van Straaten, L. M. J. U. (1965). Coastal barrier deposits in south and north Holland. *Meded. Geol. Stichting, 17*, 41-87.

Van Straaten, L. M. J. U. (1961). Sedimentation in tidal flat areas. Bulletin of Canadian Petroleum Geology, 9(7), 203-226

Vroom, J. & Wang, Z.B. (2012). *Tidal divides.* Retrieved Feb 18, 2018, from Delft University of Technology, Faculty of Civil Engineering and Geosciences Repository: https://repository.tuDelft.nl/islandora/object/uuid:7384f3a7-cd04-4d7e-bf2a-6d116d2f9435/datastream/OBJ

Wang, Z. B., Hoekstra, P., Burchard, H., Ridderinkhof, H., De Swart, H. E., & Stive, M. J. F. (2012). Morphodynamics of the Wadden Sea and its barrier island system. *Ocean & coastal management*, *68*, 39-57.

Walters, R. A., & Heston, C. (1982). Removing tidal-period variations from time-series data using low-pass digital filters. *Journal of Physical Oceanography*, *12*(1), 112-115.

Woodroffe C.D. (2003). Coasts, Form, Process and Evolution. Cambridge: Cambridge Univ. Press.

Zenkovich, V. P. (1962). *Some new exploration results about sand shores development during the sea transgression.* NVA Oosthoek.

Zijl, F., Verlaan, M., & Gerritsen, H. (2013). Improved water-level forecasting for the Northwest European Shelf and North Sea through direct modelling of tide, surge and non-linear interaction. *Ocean Dynamics*, *63*(7), 823-847.

Zijl, F., Sumihar, J., & Verlaan, M. (2015). Application of data assimilation for improved operational water level forecasting on the northwest European shelf and North Sea. *Ocean Dynamics*, *65*(12), 1699-1716.